THE UNIVERSITY OF CHICAGO

ENDOCRINE THERAPY RESISTANCE-ASSOCIATED ERα-Y537S MUTATION ALTERS ERα/PR CROSSTALK IN BREAST CANCER

A DISSERTATION SUBMITTED TO

THE FACULTY OF THE DIVISION OF THE BIOLOGICAL SCIENCES

AND THE PRITZKER SCHOOL OF MEDICINE

IN CANDIDACY FOR THE DEGREE OF

DOCTOR OF PHILOSOPHY

COMMITTEE ON CANCER BIOLOGY

BY

ROSEMARY JOAN HUGGINS

CHICAGO, ILLINOIS

JUNE 2023

TABLE OF CONTENTS

LIST OF FIGURES

LIST OF TABLES

LIST OF ABBREVIATIONS

AF-1: activating function domain 1

AF-2: activating function domain 2

AI: aromatase inhibitor

Aldo: aldosterone

ANOVA: analysis of variance

AR: androgen receptor

ATCC: American Type Culture Collection

AXL: receptor tyrosine kinase

BRCA1/2: breast cancer type 1 and 2 susceptibility genes

cDNA: complementary deoxyribonucleic acid

ChIP: chromatin immunoprecipitation

ChIP-reChIP: sequential chromatin immunoprecipitation

CoIP: coimmunoprecipitation

CRISPR-Cas9: clustered regularly interspaced short palindromic repeats with caspase 9

CSS: charcoal-stripped fetal bovine serum

DAPI: 4′,6-diamidino-2-phenylindole

DBD: DNA binding domain

DCIS: ductal carcinoma *in situ*

DEGS2: delta-4-desaturase, sphingolipid 2

DHT: 5α-dihydrotestosterone

DMEM: Dulbecco's Modified Eagle Medium

DNA: deoxyribonucleic acid

E2: 17β-estradiol

EGFR: epidermal growth factor receptor

ERα: estrogen receptor alpha

ERβ: estrogen receptor beta

ERE: estrogen response element

***ESR1*:** estrogen receptor gene

ET: endocrine therapy

FBS: fetal bovine serum

FMN1: formin 1

FOXC1: forkhead box C1

Ful: fulvestrant

GFP: green fluorescent protein

GR: glucocorticoid receptor

HER2: human epidermal growth factor receptor 2

IDC: intraductal carcinoma

IGF-1R: insulin-like growth factor 1 receptor

IgG: immunoglobulin G

ILC: intralobular carcinoma

IR: insulin receptor

IRS1: insulin receptor substrate 1

KCNK15: potassium two pore domain channel subfamily K member 15

LBD: ligand binding domain

MEM: Modified Eagle Medium

MIND: mammary intraductal injection

NOS: not otherwise specified

NST: no special type

NT-157: small molecule inhibitor of IRS1

P4: progesterone

PBS: phosphate buffered saline

PCA: principal component analysis

PCR: polymerase chain reaction

PDX: patient-derived xenograft

PDxO: patient-derived organoids

Pen/Strep: penicillin and streptomycin

***PGR*:** progesterone receptor gene

PI3K: phosphoinositide 3-kinase

PICS III: protease inhibitor cocktail set 3

pIRS1: phosphorylated Serine 307 of IRS1

PLA: proximity ligation assay

PPAR-ɣ: peroxisome proliferator-activated receptor-ϒ

PR: progesterone receptor

PR-A: progesterone receptor, A isoform

PR-B: progesterone receptor, B isoform

PR-C: progesterone receptor, C isoform

PRE: progesterone response element

PTEN: phosphatase and tensin homolog

qPCR: quantitative polymerase chain reaction

R5020: promegestone

RNA: ribonucleic acid

RPMI: Roswell Park Memorial Institute 1640 cell line

RTK: receptor tyrosine kinase

RT-qPCR: reverse transcription-quantitative polymerase chain reaction

RXR: retinoid X receptor

SERDs: selective estrogen receptor degraders

SERMs: selective estrogen receptor modulators

SPRMs: selective progesterone receptor modulators

siRNA: small interfering RNA

TNBC: triple-negative breast cancer

TNM: tumor, lymph node, metastasis staging

TP53: tumor protein 53

TSS: transcription start site

Vehicle: ethanol, hormone-deprived condition

WT: wild type, referring to unmutated ERα

Y537S: tyrosine to serine mutation at position 537 of ERα

ACKNOWLEDGMENTS

I would first like to thank the University of Chicago Committee on Cancer Biology for giving me the opportunity to complete my Ph.D. training and Geoffrey Greene for the resources that allowed me to pursue my research interests. To all the lab members (past and present) who helped me grow as a scientist – thank you. To my committee members – Eileen Dolan, Lev Becker, and Russell Szmulewitz – for encouraging me and believing in me for the past five years. I am forever grateful to Eileen, Megan Mekinda, Michelle Domecki, and the rest of the UCCCC education and outreach teams, who gave me a sense of purpose and continuously reminded me of the "why?" behind our work.

I truly would not be here writing this if it were not for the endless support from my family and friends. To my parents, Kathleen O'Hara and Martin Huggins, who built a foundation from which I could grow to become the person I am today. To my brother, Harry Huggins, whose footsteps I followed as a child and from whom I have learned to set high expectations and goals for myself. To all my friends, who gave me a space to be more than just a scientist; reminding me who I am and what I value. And lastly, to my partner Scott Paloian, who held me up in the hardest parts of the last five years and helped me keep going. I can never thank you enough, but I hope this is a start. Thank you.

ABSTRACT

Background: Half of estrogen receptor (ERα)-positive breast cancer patients treated with endocrine therapies manifest intrinsic or acquired therapy resistance. One-third of these patients present with metastatic tumors containing ERα Y537S mutations. This constitutively activating ERα Y537S mutation is associated with endocrine therapy (ET) resistance and progression of metastatic breast cancer through its effects on ERα gene regulatory functions. However, the complex relationship between ERα and the progesterone receptor (PR), known as ERα/PR crosstalk, has yet to be characterized in the context of the ERα Y537S mutation. This study aimed to elucidate the effects of the ERα Y537S mutation on ERα/PR crosstalk and resultant transcriptional activity, and to identify potential therapeutic sensitivities that may offer novel treatment options to patients with ET-resistant breast cancer.

Methods: Proximity-based interactions of ERα and PR were assessed via NanoBRET assays, proximity ligation assays (PLAs), co-immunoprecipitation (CoIP), and sequential chromatin immunoprecipitation (ChIP-reChIP). Gene expression in MCF7 and T47D cells was assessed by RNA-seq analysis with comparison to publicly available patient tumor transcriptome data. siRNA knockdown of differentially regulated genes was used to confirm phenotypic relevance. Chromatin immunoprecipitation (ChIP)-qPCR and immunoblotting were used to assess ERα/PR-associated gene expression and protein expression, respectively. Data were analyzed by ordinary two-way ANOVA ($\alpha = 0.05$) with Tukey's multiple comparisons tests or nonlinear regression, where appropriate.

Results: Using a NanoBRET hormone receptor panel, I identified a particularly elevated interaction between ERα and PR, which was further increased in the context of the ERα Y537S mutation. Utilizing PLA, CoIP, and ChIP-reChIP assays, I further confirmed increased proximity-

based ERα/PR crosstalk in the context of the constitutively activating ERα Y537S mutation. Of note, ERα Y537S and PR co-occupancy at chromatin binding sites was increased (relative to ERα WT) at several genes implicated in breast cancer progression. Over 30 genes were differentially expressed in both patient tumor and cell line data (MCF7 and/or T47D cells) in the context of the ERα Y537S mutation. siRNA knockdown revealed an ERα Y537S-specific antiproliferative effect of depletion of several candidate genes. Of these, knockdown of the signaling adaptor protein IRS1 had a significant anti-proliferative effect on hormone-deprived MCF7 and T47D cells harboring either heterozygous or homozygous ERα Y537S mutations. Furthermore, ERα and PR occupancy at chromatin binding sites along *IRS1* were uniquely altered in the context of ERα Y537S in a cell line-dependent manner. Analysis of the IRS1 inhibitor NT-157 indicates an antiproliferative effect of the compound in ERα Y537S cell lines.

Conclusions: I identified a role of the ERα Y537S mutation beyond that of constitutive activity of the receptor; it also increases ERα/PR crosstalk through both physical interaction and gene regulatory functions. Previous research has characterized gene regulatory changes associated with the ERα Y537S mutation from the frame of ERα. Here, I identify consequential changes to both ERα and PR transcription factor activity, including at chromatin binding sites for the signaling adaptor protein IRS1. I identify a significant dependence of ERα Y537S-expressing cells on IRS1 for proliferation, indicating a potential therapeutic target for restoring treatment sensitivity to patients with breast cancers harboring ERα Y537S mutations.

CHAPTER I

INTRODUCTION AND BACKGROUND

Breast Cancer

Breast cancer has the highest incidence rate of any cancer in females in the United States. According to cancer statistics from the American Cancer Society, an estimated 290,560 people in the United States were diagnosed with invasive breast cancer in 2022. 43,780 Americans were projected to die from the disease in the same year [1]. Worldwide, 1 in 8 people assigned female at birth will be diagnosed with breast cancer in their lifetime, and roughly 685,000 deaths occur annually due to the disease [2-4]. Though considerable progress has been made in treating patients with breast cancer, it remains a leading cause of death and distress in the lives of millions.

The most significant risk factor for breast cancer (other than being born female) is simply age – the mean age of diagnosis in the United States is 61 [5]. Duration of hormone exposure in a female's life (age at menarche, age at first pregnancy, age at menopause, and use of oral contraceptives and/or hormone replacement therapy) also factors into breast cancer risk [5-8]. Longer exposure to endogenous estrogens, such as from early menarche and late menopause, correlates with increased breast cancer risk. Behavioral risk factors include alcohol consumption, a high-fat diet, and excess body weight [8-11]. Additionally, genetic predisposition may also contribute to breast cancer risk. Germline mutations in *BRCA1/2* account for the majority of known heritable risk, but patients with Li-Fraumeni syndrome (germline mutations in *TP53*) or Cowden syndrome (germline mutations in *PTEN*) are also at higher lifetime risk of developing breast cancer [12-14].

Most breast cancers fall into the category of breast carcinomas of lobular or ductal origin, with only about 1% of breast cancers categorized as breast sarcomas originating from connective

tissues of the breast [15, 16]. Breast carcinomas can be further classified as invasive or non-invasive (*in situ*), with ductal carcinoma *in situ* (DCIS) accounting for an estimated 51,400 diagnoses in the United States each year in addition to the numbers projected above [1]. Invasive carcinomas are generally what is thought of when considering breast cancer, as these cancers invade surrounding tissues and are at risk of metastasizing and compromising organ function.

Invasive carcinomas are further classified based on histopathology. Both invasive lobular carcinoma (ILC) and invasive ductal carcinoma (IDC) originate in the terminal duct lobular unit of the mammary gland [17]. ILC accounts for 10-15% of all breast cancers [16, 18-20]. The majority of ILCs lack E-cadherin expression, leading to reduced cell-cell adhesion properties and often the absence of a palpable mass [16, 18]. The majority of breast cancer cases (~80%) are classified as IDC, though IDC is quite morphologically diverse between patients. To account for variation in tumor grade, size, stromal proportions, and other characteristics, the majority of IDC is designated as IDC "not otherwise specified" (NOS) or "no special type" (NST) [5, 15-17, 21]. Both ILC and IDC are staged according to tumor size (T), lymph node involvement (N), and spread to metastatic sites (M) using the TNM system, developed by the American Joint Committee on Cancer and Union for International Cancer Control [22]. Histological grading of breast carcinomas varies depending on the institution but generally consists of scoring based on tubule formation, nuclear pleomorphism, and mitotic count to derive a grade of 1 to 3 [23, 24]. Grade 1 tumors are considered low-grade, highly differentiated, and less aggressive while grade 3 tumors are high-grade, poorly differentiated, and more likely to metastasize and/or recur [25, 26].

In addition to classification based on histopathological characteristics, ILCs and IDCs are further assessed for molecular biomarkers including expression of the estrogen receptor (ER), progesterone receptor (PR), and human epidermal growth factor receptor 2 (HER2). ER and PR

will be discussed in more detail in subsequent subsections. Based on ER, PR, and HER2 expression, breast cancer can be classified into four categories: luminal A (generally low grade, ER-positive, PR-positive, HER2-negative), luminal B (generally higher grade, ER-positive, PR-low/negative, HER2-negative), HER2-enriched (*HER2* gene amplification or overexpression), or triple-negative (TNBC, ER-negative, PR-negative, HER2-negative) [5, 27, 28]. TNBC is the most aggressive subtype due to limited options for targeted therapies [29, 30]. HER2-enriched breast cancers were previously considered to have an overall poor prognosis, but the development of anti-HER2 treatments has led to improved treatment efficacy and overall survival [31-34]. Approximately 80% of breast cancers are ER-positive and of these, 60% are also PR-positive [16, 28]. ER- and PR-positivity is associated with better prognosis and less aggressive cancers [30, 35].

Treatment of Breast Cancer

A mainstay of breast cancer treatment continues to be surgery, though mastectomies (removal of the breast) and lumpectomies (removal of the tumor alone) are far more conservative now than the initial radical mastectomies first performed by William Halsted in 1882, in which the breast, axillary nodes, and chest muscles were removed [3, 36]. In 1967, Bernard Fisher led a clinical trial that found that total mastectomy was just as effective as Halsted's radical mastectomy method, and was less disfiguring to patients [36]. The addition of radiation therapy in 1976 alongside lumpectomy or mastectomy, with the goal of reducing tumor burden (neoadjuvant radiation) and local recurrence (adjuvant radiation), led to further improvements in effective breast-conserving treatments that are still used today [36-40].

As with many cancers, the use of chemotherapeutics as systemic agents for killing breast cancer cells began in the 1970s, when several studies found an improvement in patient outcomes and a reduction in breast cancer mortality with adjuvant chemotherapy [41-45]. Chemotherapy as

a neoadjuvant treatment expanded the number of patients eligible for breast-conserving lumpectomy rather than total mastectomy but does not impact overall survival [46-48]. Due to the absence of targetable biomarkers in TNBC, chemotherapy – in particular, platinum-based chemotherapy – remains the most effective course of treatment for this breast cancer subtype [49, 50].

The development of biological and hormonal therapies beginning in the mid-20th century has led to invaluable targeted therapies for biomarker-positive breast cancers. HER2-targeted compounds, including the monoclonal antibody trastuzumab and several generations of tyrosine kinase inhibitors, reduce mortality and recurrence in HER2-positive breast cancers [31-34]. ERα-positive breast cancers benefit from hormone therapy, also known as endocrine therapy (ET), which will be a major consideration throughout this dissertation. The idea for ET began with George Beatson in 1895, who removed the ovaries of a breast cancer patient and observed shrinking of the tumor [3, 51-53]. It would be over fifty years later when Elwood Jensen identified the estrogen receptor, leading to the discovery of pro- and anti-estrogenic compounds and antibodies to facilitate further research [52, 54-59]. An early ET to show efficacy in treating ERα-positive breast cancers was tamoxifen, which is classified as a selective estrogen receptor modulator (SERM) and is still used clinically today [44, 60-64].

At present, tamoxifen is the dominant adjuvant ET treatment used in pre-menopausal patients due to abundant evidence that it improves survival rates significantly when given for 5 years post-surgery [44, 65-71]. It is also used as a neoadjuvant treatment to shrink tumors to facilitate breast-conserving surgery options [72, 73]. It is also used as a chemo-preventative to reduce the risk of invasive breast cancer in patients with DCIS or with a high risk of breast cancer due to family history and/or genetic predisposition [69, 70, 74]. Tamoxifen functions by competing

with estradiol for binding to the activating function 2 (AF2) domain of the estrogen receptor, thereby preventing E2-induced estrogen receptor activation. However, tamoxifen is considered a SERM and not a full antagonist due to its tissue-specific effects; while it inhibits ER function in the breast, it acts as a partial agonist in the uterus, leading to an increased risk of endometrial cancer in breast cancer patients with a uterus [75]. This is due to conformational changes to the receptor caused by SERM binding, which results in unique coregulator interactions in a cell type-dependent manner [76-79]. Other SERMs include raloxifene, which is also used clinically, and lasofoxifene, which has shown great promise in patients with advanced breast cancer [65, 77, 80]. Post-menopausal patients also benefit from neoadjuvant or adjuvant treatment with aromatase inhibitors (AIs). After menopause, ovarian tissues no longer produce estrogen and the majority of estrogen in the body is synthesized by the enzyme aromatase, including in breast tissue. By inhibiting aromatase function with AIs such as letrozole and anastrozole, the estrogen receptor is ligand-deprived, leading to improved disease-free survival in post-menopausal patients [73, 79, 81-84].

In addition to SERMs and AIs, which modulate estrogen receptor activity, selective estrogen receptor degraders (SERDs) function as complete antagonists. Fulvestrant (Ful) is a SERD that not only binds to and inhibits ER but promotes degradation of the receptor as well, making the receptor unavailable for further function [85-87]. Fulvestrant was initially approved for use in post-menopausal patients with advanced breast cancer with cancer progression after a first-line ET because it was found to extend progression-free survival somewhat [88-90]. It is now also used as a first-line ET, though some patients experience intolerable side effects from the drug [91-93].

In addition to endocrine therapies targeting the estrogen receptor, several compounds have

been developed as selective progesterone receptor modulators (SPRMs) including onapristone, telapristone (CDB4124), and PRA-027. These compounds have not been approved for clinical use in breast cancer, but both CDB4124 and PRA-027 have been assessed for safety and tolerability in phase 1 clinical trials [94-98]. Onapristone is in phase 1b-2 clinical trials that began in 2021 after evaluation for safety found the drug to be well-tolerated in patients with advanced, pre-treated breast, ovarian, or endometrial cancer [99-101]. Each of these aforementioned SPRMs has a unique mechanism of action: onapristone blocks PR dimerization, inhibits phosphorylation of the receptor, and prevents interaction with coactivators; PRA-027 prevents nuclear localization of PR; and CDB4124 is a potent PR antagonist and decreases PR expression [98, 102, 103]. Though not yet used clinically to treat breast cancer, SPRMs may become a mainstay of ET in the future.

Treatment Resistance

ET has led to significant improvement in post-surgical outcomes and relapse-free survival in patients with estrogen receptor-positive breast cancer [62]. Unfortunately, 15-20% of tumors predicted to respond to ET are intrinsically resistant, and 30-40% acquire resistance within 5-10 years [104, 105]. Paired with the high rate of diagnosis for ER-positive breast cancer, the high rate of treatment resistance (leading to more aggressive, metastatic disease) results in this seemingly treatable disease causing the most breast cancer-related deaths per year [1, 4, 106, 107]. Comparison of tumor genomes before and after treatment suggests that ET may drive selection of subclonal populations of tumor cells with mutations that promote tumor survival [104, 108, 109]. These resistance driver mutations include defects in components of DNA single-stranded break repair and *ESR1* (the gene coding for the estrogen receptor).

Previous widescale analysis of patient tumor genomes identified loss of function of the MutL complex, which is involved in mismatch repair in DNA single-stranded breaks, as a common

cause of ET resistance [110, 111]. Further investigation of the mechanism behind this resistance found that defective MutL results in loss of Chk2 cell cycle checkpoint activation, leading to uninhibited CDK4/6 activity which drives cell cycle progression [108, 110, 111]. Fortunately, CDK4/6 inhibitors can be used in combination with ET to restore sensitivity to these tumors with remarkable success [108, 112, 113].

A more challenging class of mutations associated with ET resistance is mutations arising in *ESR1*. The most commonly detected and well-characterized are point mutations arising around the region coding for the ligand-binding domain (LBD) of the estrogen receptor, though recently several *ESR1* fusion genes have also been identified in some patients. Such fusion proteins include ESR1-YAP1, ESR1-PCDH11X, ESR1-DAB2, and ESR1-GYG1, all of which are functional protein products containing the first six exons of *ESR1* fused with the C-terminal sequence of the associated protein [114-116]. Importantly, these fusions lack the ER LBD, leading to complete insensitivity to ET.

In terms of *ESR1* point mutations, 30-40% of patients with ET-resistant tumors present with mutations around the ER LBD [117-121]. *ESR1* Y537S is one of the most frequently identified ER mutations in patients, with the mutation appearing in 30% of circulating tumor cells from blood samples and at least 20% of metastatic tumors [116, 119, 120, 122]. Notably, *ESR1* Y537S is very rarely found in primary treatment-naïve tumors and is associated with tumor progression, suggesting that ET results in selective pressure toward more resistant and aggressive metastases [119]. Previous structural assessment in our lab demonstrated that *ESR1* Y537S stabilizes the activating function-2 (AF-2) cleft of the ERα LBD in the agonist-bound conformation, which facilitates constitutive activity of the LBD, even in the absence of ligand binding [123]. Conversely, *ESR1* Y537S alters the antagonist state of AF-2, resulting in reduced

affinity of antagonists for the receptor and resistance to inhibition by SERMs and SERDs [123].

Estrogen Receptor

As described previously, Elwood Jensen discovered estrogen receptors in 1958 [55, 57]. In the late 20th century, further characterization identified two distinct, yet homologically similar estrogen receptors known as ERα and ERβ [124-127]. Though the two receptors share 95% homology within the DNA binding domain (DBD) and 55% homology in the LBD, they are encoded by two separate genes on different chromosomes (*ESR1* on chromosome 6, and *ESR2* on chromosome 14) [128, 129]. ERα and ERβ also differ in their relative expression in different tissues – for example, ERα is dominant in the mammary gland, uterus, and bone while ERβ is prominent in the ovarian granulosa cells and immune system [77, 128]. ERβ in the breast is believed to have an antiproliferative effect, opposing the tumorigenic functions of ERα [130]. However, the relative expression of ERα compared to ERβ in the mammary gland is generally much higher in breast cancer, so researchers are typically referring to ERα in breast cancer unless specifically stated otherwise [128].

ERα is a transcription factor consisting of 2 transcriptional activation domains (ligand-independent AF-1 domain and ligand-dependent AF-2 domain), an LBD, as well as a core DBD and hinge region. As mentioned previously, the ET resistance-associated ERα Y537S mutation stabilizes the AF-2 cleft of the LBD in the agonist-bound conformation, which facilitates constitutive activity of the LBD, even in the absence of ligand binding [123]. In the absence of mutations, the natural ERα ligand, estradiol (E2), is responsible for ERα-associated gene regulation in both normal mammary tissue development and hormone-dependent tumor growth. Under classical ERα signaling, E2 binds to ERα and leads to ERα dimerization and the formation of a complex containing coactivators and corepressors. Upon dimerization, ERα translocates to the

nucleus and binds to estrogen response elements (EREs) to regulate expression of target genes [131]. Unliganded ERα is present in the nucleus as well.

Non-classical ERα signaling also occurs, where ERα complexes bind to other transcription factors, acting as a coregulator for factors such as NFkB and AP1. Many of these interactions occur in response to ERα activation by E2 binding, but E2-independent ERα activity is also known to occur. ERα engages in complex E2-independent signaling networks with many receptor tyrosine kinases (RTKs) including epidermal growth factor receptor 2 (EGFR), human epidermal growth factor receptor 2 (HER2), and insulin-like growth factor 1 receptor (IGF-1R). Gene expression regulation through these pathways is bidirectional – RTKs may regulate ERα transcription factor function independent of estradiol binding, and ERα may reciprocally regulate RTK expression and activity [131]. This complex network may contribute to estradiol-independent activation and reduce cell dependency on E2. Both E2-dependent and E2-independent mechanisms of ERα activity are associated with innumerable cell growth, proliferation, and survival functions associated with breast cancer.

Progesterone Receptor

Similar to the estrogen receptor, the progesterone receptor (PR) was first characterized and cloned in the late 20th century [132-134]. *PGR* on chromosome 11 codes for three distinct isoforms of PR (PR-A, PR-B, and PR-C), although only PR-A and PR-B contain DBDs and are transcriptionally active. Hereon, discussion of PR refers to both PR-A and PR-B, unless specifically stated otherwise.

In addition to DBDs, PR-A and PR-B contain an N-terminal transactivation domain, a hinge region, and an LBD. PR-B is considered the full-length isoform of PR and contains three activating function domains for coregulator interactions (AF1, AF2, and AF3) while PR-A is

truncated and contains only two (AF1 and AF2) [135, 136]. PR is located in both the cytoplasm and nucleus, as both ligand-bound and unbound receptors [102]. Similar to ERα, classical PR function consists of progestin binding to the receptor, resulting in homodimers or heterodimers of PR-A and PR-B and retention of the complex in the nucleus. In the nucleus, PR binds to DNA at progesterone response elements (PREs) and regulates target gene expression. Like ERα, PR can also function via non-classical signaling through tethering interactions with other transcription factors, linking PR with pathways such as SRC, MAPK, PI3K, and EGFR [102]. The cyclical regulation and potential for ligand-independent function observed with both ERα and PR suggest an important mechanism by which tumors survive and progress.

Hormone Receptor Crosstalk

Hormone receptor crosstalk can refer to reciprocal gene regulation by two different hormone receptors, hormone-independent activity of a receptor in response to activity by a different receptor, or physical interaction of two receptors in a regulatory complex. For example, ERα/PR crosstalk occurs via:

1) Liganded ERα regulates *PGR* gene transcription [137-141]
2) Liganded PR increases ERα target gene regulation through ERα phosphorylation [137]
3) PR-dependent chromatin remodeling facilitates ERα binding [142, 143]
4) ERα/PR physical interaction via regulatory complexes may contribute to ligand-independent target gene expression [137, 144, 145]

The clearest example of ERα/PR crosstalk is evidence of ERα/PR complex formation. Immunoprecipitation (IP) assays and ChIP-seq identified that ERα and PR physically interact and are recruited to genomic loci as a complex [146]. Additionally, long-distance chromatin looping between EREs and PREs facilitates ERα/PR interactions between proximal and distal DNA

regions [146]. This is closely related to the third mode of crosstalk, in which PR was found to bind more readily to DNA regions with high-nucleosome occupancy whereas ERα generally binds only to open chromatin regions. PR occupancy then facilitates chromatin remodeling, allowing for ERα to bind and regulate gene expression [143, 146].

The expression profile of each hormone receptor alone is very much context-dependent, and the intersection of the two seems to be as well. When treated with estradiol or progestin alone, ERα+/PR+ breast cancer tumor slices exhibited an 85% overlap in genes similarly up- or down-regulated [146]. When treated with both estradiol and progestin, there was a significant downregulation in many ERα-regulated genes, suggesting a unique transcription profile under combined receptor agonism [146]. Furthermore, PR-A seems to inhibit ERα binding while PR-B redistributes ERα binding [142]. Unliganded PR also binds to the *ESR1* promoter in the absence of estradiol, sustaining ERα expression in hormone-deprived conditions [147].

ERα/PR crosstalk is thought to play a role in breast cancer progression and may contribute to the altered gene expression profile of ET-resistant tumors [137, 142, 144]. The crosstalk of ERα and PR with growth factor signaling pathways (HER2, IGF1R, EGF, and MAPK) is extensive and overlapping and likely contributes to endocrine-resistant tumor progression. Rapid activation of MAPK/ERK and AKT by PR results in ERα and PR recruitment to chromatin, driving ERα-associated gene expression including further PR expression, which feeds the cyclical regulation of these key regulatory pathways [137]. Thus, it is likely that a constitutively active ERα, such as in the case of the ET resistance associated ERα Y537S mutation, contributes to an altered ERα/PR crosstalk phenotype.

Rationale for Studying the Effects of ERα Y537S on ERα/PR Crosstalk

Previous work by Hari Singhal in the laboratory of Geoffrey Greene found that co-

treatment with a SERM and SPRM (tamoxifen and CDB4124, respectively) led to tumor regression in T47D xenograft mice (Fig. 1.1) [146]. These results indicated potential therapeutic value in co-targeting ERα and PR with ET treatment, at least in the context of unmutated ERα.

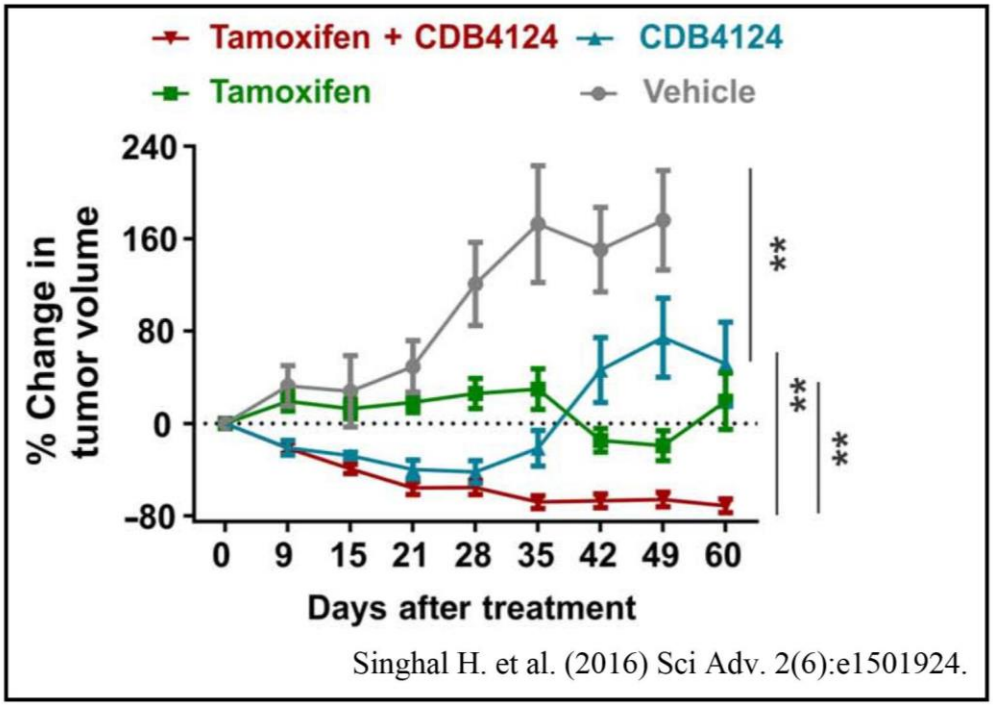

Figure 1.1: Combined SERM/SPRM therapy leads to tumor regression in T47D ERα WT xenograft mice. Figure originally published by Singhal et al. (2016) in Sci. Adv. Captioned: T47D xenografts were grown in ovariectomized nude mice containing estrogen silastic implants and were treated with placebo, tamoxifen, CDB4124, or tamoxifen plus CDB4124. The average tumor volume at the start of therapies was 125mm^3, and percentage change in tumor volume is shown (n = at least 7). P values are calculated using mixed linear modeling. Control group is plotted until day 49 because a significant number of mice in the control group died after day 49. Significant difference between treatments is indicated as ** $p < 0.005$.

Though these findings regarding combined SERM/SPRM therapy were interesting and may provide a promising therapeutic avenue for hormone receptor-positive breast cancers, further investigation was required. Hari Singhal's experimentation was limited to a T47D ERα WT xenograft model, with mammary fat pad injection of the cells into mice. Upon joining the lab, I repeated the *in vivo* SERM/SPRM treatment experiment in xenograft mice injected intraductally with GFP/luciferase-labeled MCF7 ERα WT and ERα Y537S cells. Whereas mammary fat pad

xenografts are historically more common, mammary intraductal (MIND) injections more closely represent the origins of invasive ductal carcinoma [148]. Analysis of the average radiance (p/s/cm²/sr) for each treatment group indicated significantly decreased tumor proliferation in the ERα WT group treated with combined ERα/PR modulation (tamoxifen+CDB4124), similar to Hari Singhal's findings (Fig. 1.2a) [142]. However, tumor proliferation significantly increased in response to combined ERα/PR modulation in the ERα Y537S group (Fig. 1.2b). These findings suggested that the relationship between ERα and PR may be altered in the context of the ERα Y537S mutation.

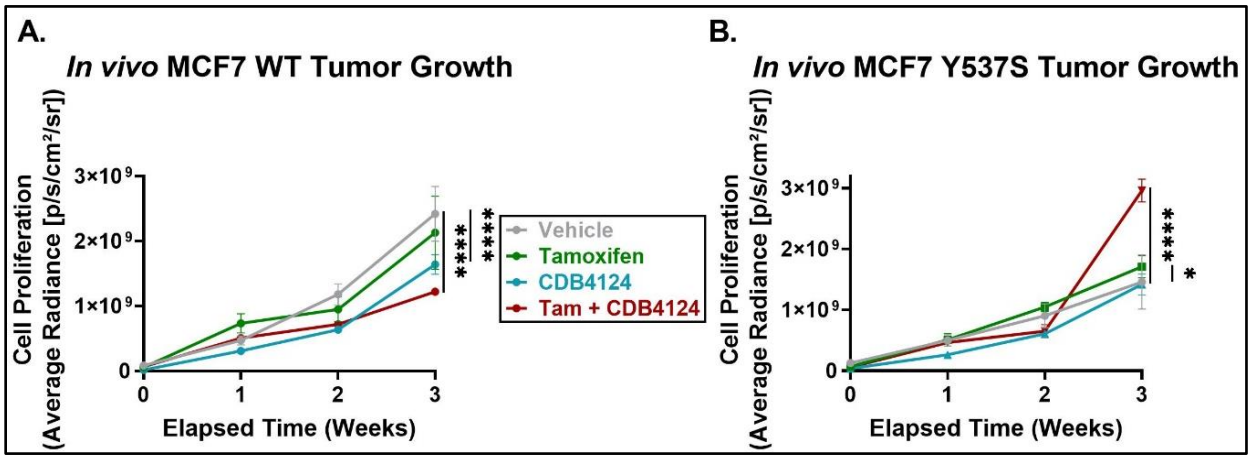

Figure 1.2: Combined SERM/SPRM therapy leads to reduced tumor proliferation in MCF7 ERα WT, but increased tumor proliferation in MCF7 ERα Y537S xenograft mice. Average radiance (p/s/cm²/sr) upon luciferin injection in MIND mouse models with GFP/luciferase-labeled A) MCF7 ERα WT or B) MCF7 ERα Y537S xenografts. Mice were treated 5 days per week for 3 weeks with vehicle (ethanol), tamoxifen, CDB4124, or combined tamoxifen and CDB4124. Significant difference between treatments is indicated as * $p < 0.05$ or **** $p < 0.0001$.

Given the multimodal nature of ERα/PR crosstalk involving both physical interaction of the receptors through regulatory complexes as well as reciprocal regulation of transcription factor activity, I hypothesized that the functional effects of ERα Y537S are not limited to ERα, but also affect the activity of PR. Elucidating the extent to which ERα Y537S alters ERα/PR crosstalk will further our understanding of how this activating mutation contributes to ET resistance and may offer alternative targets for treating resistant disease.

CHAPTER II

MATERIALS AND METHODS

Mammary Intraductal (MIND) Mouse Model

MCF7 ERα WT and ERα Y537S cells were labeled with GFP/luciferase dual reporter lentiviral transduction and injected intraductally into the mammary glands of mice. Mammary intraductal injections closely represent the most common form of breast cancer, invasive ductal carcinoma. Mice were treated intraperitoneally with vehicle (ethanol+oil), tamoxifen (10mg/kg in ethanol+oil), CDB4124 (10mg/kg in DMSO+oil), or a combination of tamoxifen and CDB4124 (10mg/kg of each). Mice were treated for 3 weeks, receiving 15 treatments in total. Tumors were visualized and quantitatively measured using the IVIS Spectrum fluorescent imaging system approximately one week after the initial intraductal cell injection but before beginning drug treatment. Subsequent images were taken each week during drug treatment.

Cell Lines and Growth Conditions

HEK293 cells were obtained from the ATCC and maintained in phenol red-free DMEM containing 5% fetal bovine serum (FBS), 1% Pen/Strep, and 1% L-Glutamine. Before NanoBRET assays, HEK293 cells were cultured in phenol red-free DMEM containing 10% charcoal-stripped serum (CSS), 1% Pen/Strep, and 1% L-Glutamine.

MCF7 and T47D cells (originally obtained from ATCC) were previously edited using CRISPR-Cas9 technology to express the heterozygous or homozygous *ESR1* mutation known as ERα Y537S. MCF7 parent cells (MCF7 ERα WT) and MCF7 ERα Y537S-heterozygous cells (MCF7 ERα Y537S-het) were generated and gifted by Ben Ho Park, originally at Johns Hopkins University and now at Vanderbilt University. MCF7 ERα Y537S-homozygous cells (MCF7 ERα Y537S-hom) were generated and gifted by Sarat Chandarlapaty at Memorial Sloan Kettering

Cancer Center. All MCF7 cell variants were maintained in phenol red-free DMEM containing 5% FBS, 1% Pen/Strep, and 1% L-Glutamine. Before experimentation, MCF7 cell variants were cultured in phenol red-free DMEM containing 10% CSS, 1% Pen/Strep, and 1% L-Glutamine.

T47D parent cells (T47D ERα WT) and T47D ERα Y537S-het cells were generated and gifted by Steffi Oesterreich at the University of Pittsburgh. Both T47D ERα WT and ERα Y537S-het cell lines were maintained in phenol red-free RPMI media containing 10% FBS and 1% Pen/Strep. T47D ERα Y537S-homozygous (T47D ERα Y537S-hom) were generated by David Shapiro at the University of Illinois at Urbana-Champaign originally and were gifted from Carol Lange at the University of Minnesota with the modification of shGFP. T47D Y537S-hom cells were maintained in phenol red-free MEM containing 10% CSS, 1% Pen/Strep, and 0.2ug/uL puromycin for continuous selection. Before experimentation, all T47D cell variants were cultured in phenol red-free RPMI containing 10% CSS, and 1% Pen/Strep for 48 hours.

Plasmids, Compounds, and Antibodies

pCDNA3.1-based plasmids containing the complete coding sequences for the steroid receptor genes were provided by David Hosfield at the University of Chicago. Briefly, N- and C-terminal fusion of the NanoLuc and HaloTag reporters were appended to the steroid receptor genes using Gibson Assembly with primers designed using the assembly tools within SnapGene (Insightful Science; available at snapgene.com). Briefly, PCR was used to amplify the coding regions of the steroid receptor genes and to linearize the expression plasmids pHTN HaloTag CMV Neo or pFLN-1 NanoLuc (Promega #N1811, see table 1 for primers). PCR products were isolated via gel electrophoresis and assembled using HiFi assembly mix (NEB #E2621L). Plasmids were verified by DNA sequencing. NanoBRET Nano-Glo Substrate (Promega #N1571) and HaloTag NanoBRET 618 Ligand (Promega #G9801) were used in NanoBRET assays.

Gene	Plasmid	Tag Position (relative to receptor)	Primer Name	Sequence (5' – 3')
ESR1 (ER)	NanoLuc	N-terminal	NLERa_ERa_f	AGCTCTTAAGGCTAGAGTATTAATACGACTCACTATAGGGATGACCATGACCCTCCACAC
ESR1 (ER)	NanoLuc	N-terminal	NLERa_ERa_r	TCTTCGAGTGTGAAGACCATTCCTGATCCAACGACCGTGGCAGGG
ESR1 (ER)	NanoLuc	C-terminal	NLERa_NL_f	GTTTCCCTGCCACGGTCGTTGGATCAGGAATGGTCTTCACACTCGAAGATTTCG
ESR1 (ER)	NanoLuc	C-terminal	NLERa_NL_r	TAGTTATTGCTCAGCGGTGGCAGCAGCCAACTCAGCAAGCTCACGCCAGAATGCGTTCG
PGR (PR)	NanoLuc	N-terminal	NLPR_PR_f	GTTTCCCTGCCACGGTCGTTGGATCAGGAATGGTCTTCACACTCGAAGATTTCG
PGR (PR)	NanoLuc	N-terminal	NLPR_PR_r	TAGTTATTGCTCAGCGGTGGCAGCAGCCAACTCAGCAAGCTCACGCCAGAATGCGTTCG
PGR (PR)	NanoLuc	C-terminal	NLPR_NL_f	AGCTCTTAAGGCTAGAGTATTAATACGACTCACTATAGGGATGGAAGTGCAGTTAGGGCT
PGR (PR)	NanoLuc	C-terminal	NLPR_NL_r	CCAGTACCGATTTCTGCCATTCCTGATCCCTGGGTGTGGAAATAGATGGGC
ESR1 (ER)	HaloTag	N-terminal	HTERa_ERa_f	AGCTCTTAAGGCTAGAGTATTAATACGACTCACTATAGGGATGACCATGACCCTCCACAC
ESR1 (ER)	HaloTag	N-terminal	HTERa_ERa_r	CCAGTACCGATTTCTGCCATTCCTGATCCAACGACCGTGGCAGGG
ESR1 (ER)	HaloTag	C-terminal	HTERa_HT_f	GTTTCCCTGCCACGGTCGTTGGATCAGGAATGGCAGAAATCGGTACTGGC
ESR1 (ER)	HaloTag	C-terminal	HTERa_HT_r	TAGTTATTGCTCAGCGGTGGCAGCAGCCAACTCAGCAAGCGCCGGAAATCTCGAGC
PGR (PR)	HaloTag	N-terminal	HTPR_PR_f	AGCTCTTAAGGCTAGAGTATTAATACGACTCACTATAGGGATGACTGAGCTGAAGGCAAAGG
PGR (PR)	HaloTag	N-terminal	HTPR_PR_r	CCAGTACCGATTTCTGCCATTCCTGATCCCTTTTTATGAAAGAGAAGGGGTTTCACCATCCCT
PGR (PR)	HaloTag	C-terminal	HTPR_HT_f	CCCTTCTCTTTCATAAAAAGGGATCAGGAATGGCAGAAA TCGGTACTGGC
PGR (PR)	HaloTag	C-terminal	HTPR_HT_r	TAGTTATTGCTCAGCGGTGGCAGCAGCCAACTCAGCAAGCGCCGGAAATCTCGAGC

Table 1: Steroid receptor gene primer sequences for plasmid construction

Aldosterone (Aldo, Sigma #A9477), 5α-dihydrotestosterone (DHT, Sigma #D-073), progesterone (P4, Sigma #P0130), and 17β-estradiol (E2, Sigma #E2758) were used in NanoBRET assays. Promegestone (R5020, Perkin Elmer #NLP004005MG) was used in place of P4 for all assays in MCF7 and T47D cells. NT-157 (Selleck Chemical #S8228), 4-hydroxytamoxifen (4OHT, Sigma #94873), lasofoxifene (Laso, Sermonix Pharmaceuticals), fulvestrant (Ful, Selleck Chemical #S1191), CDB4124 (Repros Therapeutics), and PRA-027 (Pfizer, formerly Wyeth Pharmaceuticals) were used for confluence-based drug screen assays. Structures for all compounds used are shown in figure 2.1. Vehicle (ethanol) was used as a control for all experiments.

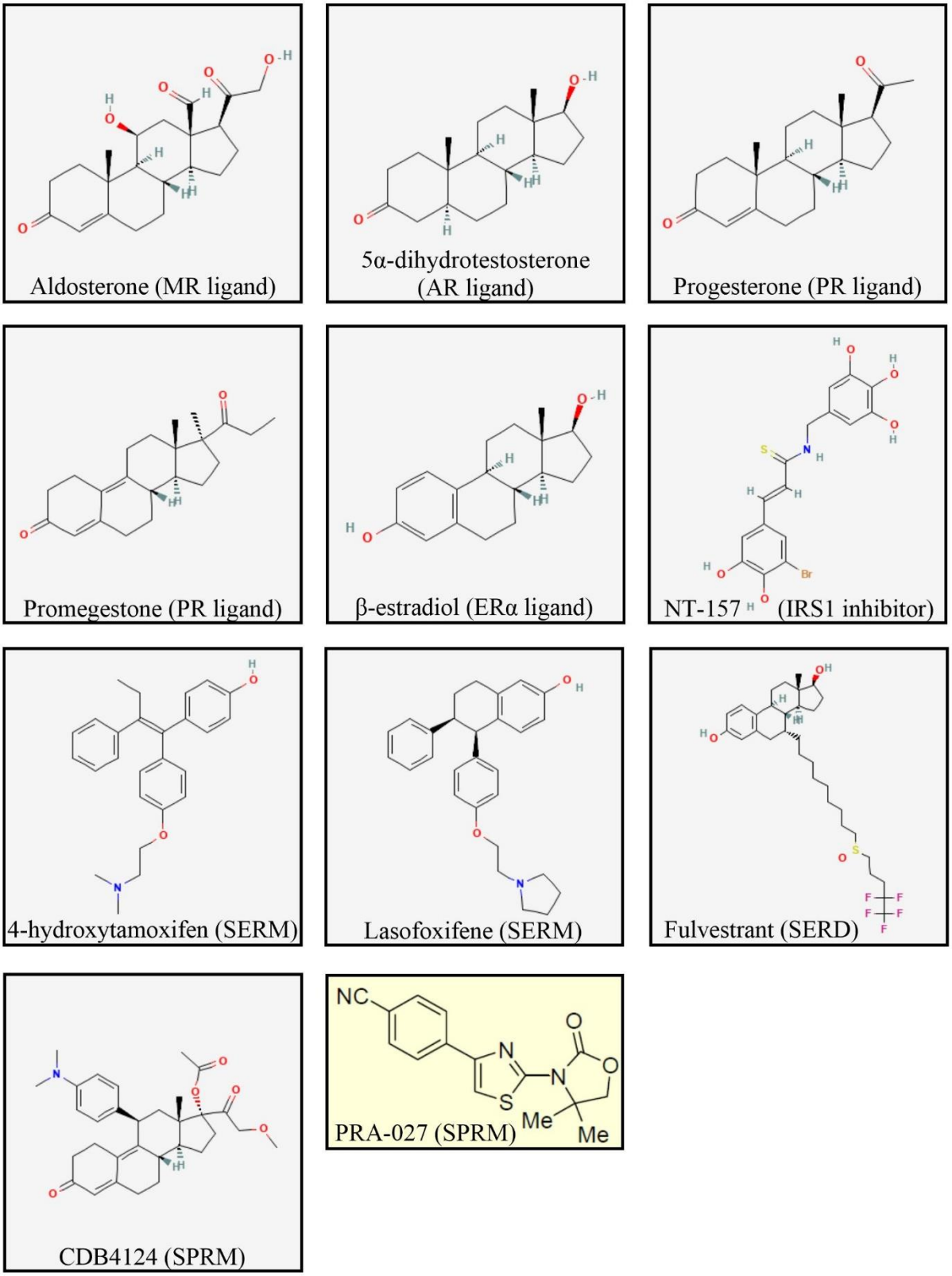

Figure 2.1: Chemical structures of compounds used. Structures were obtained from the National Center for Biotechnology Information PubChem database, except PRA-027. The structure of PRA-027 was obtained from Wyeth Research (2009)[98].

D8Q2J rabbit monoclonal antibody (Cell Signaling #8757) was used for the detection of PR-A and PR-B in proximity ligation assays (PLA). F10 mouse monoclonal antibody (Santa Cruz Biotechnology #sc-8002) was used for the detection of ERα in PLA. Normal rabbit IgG (Santa Cruz Biotechnology #sc-2027) and normal mouse IgG (Santa Cruz Biotechnology #sc-2025) were used as negative control antibodies for D8Q2J and F10, respectively. D8Q2J was also used for immunoprecipitation of PR-A and PR-B in coimmunoprecipitation (CoIP) assays. The rabbit polyclonal antibody ab75635 (Abcam) was used for immunoprecipitation of ERα in CoIP assays. KD68 rat monoclonal antibody (originally generated by Greene et al. [149] and produced and purified by the University of Chicago Flow Cytometry Core) was used for single and sequential chromatin immunoprecipitation (ChIP and ChIP-reChIP, respectively) to immunoprecipitate chromatin to which PR-A or PR-B was bound. The ERα C-terminal antibody from Epicypher (#13-2012) was used for ERα immunoprecipitation in ChIP and ChIP-reChIP. Normal rabbit IgG and normal rat IgG (Santa Cruz Biotechnology #sc-2026) were used as negative control antibodies for Epicypher ERα C-terminal and KD68, respectively.

F10 and KD68 were used for immunoblot detection of ERα and PR-A/PR-B, respectively. Anti-IRS1 rabbit polyclonal antibody (Abcam #ab52167) was used for the detection of pan-IRS1. Phospho-IRS1 (Ser302) rabbit polyclonal antibody (Cell Signaling #2384S) was used for the detection of phospho-Serine307 (pSer307) IRS1 (the antibody detects pSer302 of mouse IRS1, but pSer307 of human IRS1). AC-15 mouse monoclonal antibody (Santa Cruz Biotechnology #sc-69879) and Histone H3 (D1H2) rabbit monoclonal antibody (Cell Signaling #4499S) were used for the detection of β-actin and Histone H3, respectively, as loading controls in immunoblot detection.

NanoBRET Assay

After culturing HEK293 cells in charcoal-stripped media (DMEM containing 10% CSS) for 48 hours, cells were trypsinized and collected. Using a Countess cell counter and trypan blue staining at a 1:1 ratio of stain to cell solution, the number of live cells was calculated, and the cell solution was diluted to 1e6 cells/mL in stripped media. Using a multichannel pipette, 100uL of cell solution was dispersed into each well of a 96-well plate (black, clear-bottomed plate) for 1e5 cells/well. After 24 hours, cells were co-transfected with the appropriate HaloTag and NanoLuc plasmids (experimental or control plasmids, at concentrations optimized by preliminary experiments – generally 250ng/uL for HaloTag plasmids and 50ng/uL for NanoLuc plasmids) plus transfection reagent (20uL Lipofectamine 2000 + 800uL PBS) followed by incubation for 24hrs at 37°C and 5% CO_2. The following day, cells were treated with the appropriate compounds and 10uL of 500nM HaloTag ligand (G618) for 3 hours. Just before assay quantification in a luminometer, NanoLuc substrate was added to each well, followed by brief shaking to mix. Assays were quantified using the NanoBRET protocol on the TECAN Synergy Neo plate reader in the University of Chicago Cellular Screening Center. This protocol measures total donor luminescence at 450nm (indicative of NanoLuc expression) and total acceptor fluorescence at 610nm (indicative of HaloTag expression). Data is analyzed as the ratio of acceptor fluorescence to donor luminescence (fluorescence/luminescence) as described by Machleidt and colleagues [150].

Proximity Ligation Assay (PLA)

After culturing MCF7 and T47D cells in stripped media for 48 hours, 5,000 cells/well were plated into each well of an 8-well glass bottom chamber slide. Cells were then treated with the appropriate compounds for ERα and/or PR stimulation for 24 hours. Cells were fixed using 37% formaldehyde, followed by permeabilization with 100% methanol. Proximity ligation was

performed according to the Millipore Sigma Duolink® PLA Fluorescence Protocol using the Duolink® Anti-rabbit PLUS probe (#DUO92002, to detect PR through a 1:1000 dilution of D8Q2J antibody), Duolink® Anti-mouse MINUS probe (#DUO92004, to detect ERα through a 1:1000 dilution of F10 antibody), Duolink® Red Fluorescence Detection Reagents (#DUO92008), Duolink® Wash Buffers (#DUO82049), and Invitrogen SlowFade™ Gold antifade mounting reagent (#S36940). Image acquisition was completed by the University of Chicago Integrated Light Microscopy Core with a Leica SP8 3D STED laser scanning confocal microscope (Leica Microsystems, Inc., Buffalo Grove, IL).

Coimmunoprecipitation (CoIP)

After culturing MCF7 and T47D cells in stripped media for 48 hours and treating with the appropriate compounds for ERα and/or PR stimulation for 24 hours, ~10e6 cells per sample were harvested in ice-cold PBS. Cells were lysed using the Thermo Scientific™ NE-PER™ Nuclear and Cytoplasmic Extraction Reagents (#78833) with Protease Inhibitor Cocktail Set III (PICS III, Calbiochem # 535140) according to the manufacturer's protocol to collect cytoplasmic and nuclear extracts from cells. Isolated nuclear and cytoplasmic extract concentrations were measured using the Protein A280 program of a Nanodrop. 5% of each sample was reserved as input, mixed with 5X Laemmli sample buffer, and stored at -20°C. The remaining lysates were divided into aliquots containing 2mg lysate each, and the appropriate antibody for immunoprecipitation was added to each (4uL D8Q2J for PR, 5uL ab75635 for ERα, and 1uL rabbit IgG as negative control). After rotating at 4°C overnight, 30uL of Protein G Mag Sepharose (Cytiva #28951379) magnetic beads in the appropriate lysis buffer (CER I for cytoplasmic lysates, NER for nuclear lysates) plus PICS III was added to each sample and rotated at 4°C for an hour. Samples were then washed in lysis buffer, eluted in 2X Laemmli Sample Buffer (BioRad #161-0737), boiled, and run on a 4-20%

Mini-PROTEAN® TGX Protein Gel (BioRad #4568096). After transferring the protein onto a nitrocellulose membrane, ERα and PR were detected with F10 and KD68, respectively.

Chromatin Immunoprecipitation (ChIP)

After culturing MCF7 and T47D cells in stripped media for 48 hours and treating with vehicle, 10nM E2, 10nM R5020, or 10nM E2+10nM R5020 for 1 hour, ~10e6 cells were harvested in ice-cold PBS. Cells were crosslinked in 1% formaldehyde in PBS. Crosslinking was quenched by the addition of glycine at a final concentration of 125mM. Crosslinked cell pellets were snap frozen and stored at -80°C.

For each ChIP experimental replicate, ~20e6 crosslinked cells (from 2 crosslinked aliquots) were lysed in lysis buffer with PICS III using sonication (high, 30 seconds on/off, for 5 intervals of 10 minutes). 5% of lysate was reserved for input control and snap frozen to store at -80°C. Lysates were diluted to 1ug/uL protein based on Nanodrop A280 concentrations and divided into 1mL aliquots. Five micrograms of the appropriate antibodies (KD68 for PR ChIP, Epicypher ERα C-terminal for ERα ChIP, rat IgG for PR negative control, and rabbit IgG for ERα negative control) were added to the appropriate lysate aliquots and rotated at 4°C overnight. Protein-chromatin was isolated and eluted using protein G beads. Eluted ChIP samples were incubated with RNAse A and Proteinase K to reverse the crosslinked protein-chromatin. Input samples and ChIP DNA was purified using a Qiagen QIAquick PCR Purification Kit, and purified DNA samples were eluted in 30uL nuclease-free water.

Sequential Chromatin Immunoprecipitation (ChIP-reChIP)

ChIP-reChIP experimental methods were adapted from the chapter "Sequential Chromatin Immunoprecipitation Protocol: ChIP-reChIP" in *Methods in Molecular Biology, DNA-Protein Interactions* by Furlan-Magaril et al. [151]. After culturing MCF7 and T47D cells in stripped

media for 48 hours and treating with the appropriate compounds for ERα and/or PR stimulation for one hour, ~20e6 cells were harvested in ice-cold PBS. Cells were crosslinked in 1% formaldehyde in PBS. Crosslinking was quenched by the addition of glycine at a final concentration of 125mM. Crosslinked cell pellets were snap frozen and stored at -80°C.

For each ChIP-reChIP experimental replicate, ~80e6 crosslinked cells (from 4 crosslinked aliquots) were lysed in lysis buffer with PICS III using sonication (high, 30 seconds on/off, for two intervals of 15 minutes). 5% of lysate was reserved for input control and snap frozen to store at -80°C. Lysates were diluted to 1ug/uL protein based on Nanodrop A280 concentrations and divided into 1mL aliquots. Five micrograms of the appropriate antibodies (KD68 for PR ChIP, Epicypher ERα C-terminal for ERα ChIP, rat IgG for PR negative control, and rabbit IgG for ERα negative control) were added to the appropriate lysate aliquots and rotated at 4°C overnight. Protein-chromatin was eluted from the primary immunoprecipitation samples using protein G beads, after which a secondary immunoprecipitation using the reciprocal ERα or PR antibody was completed.

Eluted ChIP-reChIP samples, as well as single antibody ChIP samples, were incubated with RNAse A and Proteinase K to reverse the crosslinked protein-chromatin. DNA was purified using a Qiagen QIAquick PCR Purification Kit, and purified DNA samples were eluted in 30uL nuclease-free water.

ChIP and ChIP-reChIP Quantitative Polymerase Chain Reaction (qPCR)

Input and ChIP (or ChIP-reChIP) purified DNA was quantified using IDT primers specific for probable regions of shared chromatin binding by ERα and PR, as identified by Khushi et al. (2014) and consistent with candidate genes identified from RNA-seq and siRNA knockdown experiments [152]. Primer sequences are available in table 2. Quantabio PerfeCta® SYBR® Green

FastMix Reaction Mix with ROX™ was used for qPCR reactions using a Roche Step-One Real-Time PCR machine. Reactions were run in triplicate, with 3 biological replicates per sample. qPCR Ct results were averaged and normalized to the endogenous control R18S (ΔCt_{mean}). Input ΔCt_{mean} values were adjusted to consider the percent of the sample taken for input (5%), calculated as $\Delta Ct_{mean(input)}$ - $\log_2(20)$. $\Delta\Delta Ct_{mean}$ for each ChIP or ChIP-reChIP condition was calculated as the difference between the corresponding adjusted $\Delta Ct_{mean(input)}$ and the $\Delta Ct_{mean(ChIP/ChIP\text{-}reChIP)}$. Percent input was then calculated as $100(2^{\Delta\Delta Ct})$.

Primer Name	Primer Sequence (5' - 3')
DEGS2 ChIP 1 FWD	TTACCAGCAGGCTCACATTC
DEGS2 ChIP 1 REV	AACCTGGCACCTTGTTCTC
DEGS2 ChIP 2 FWD	CCTCACTCCTGCCTCTTCTAT
DEGS2 ChIP 2 REV	CTTCCTCCATGCCTATGCTATTC
FMN1 ChIP 1 FWD	GGATCTCAGAAGCTTGGCTATT
FMN1 ChIP 1 REV	CCTGGACACCTGTGCTAATC
FOXC1 ChIP 3 FWD	TCTGCTGCTCAAGGCATTAC
FOXC1 ChIP 3 REV	AGGGAGAGAGAAGAGGGATAGA
FOXC1 ChIP4 FWD	GACCCTCAGGCACATTAATCA
FOXC1 ChIP4 REV	CTTCTCTGGAAGTCACTGACAC
IRS1 ChIP 2 FWD	CCATTCATGCTTCTGCTCAAAT
IRS1 ChIP 2 REV	TGTGTTTCCCTGTGGTGTAG
IRS1 ChIP 3 FWD	ACATCCAAGAACTCTAGCAACAA
IRS1 ChIP 3 REV	GCTAGGTCATTGTCACCTCAAA
IRS1 TSS FWD	CTGGAAGGAACAGAGGGACG
IRS1 TSS REV	GGACGTGAGACACTTCCTGG
IRS1 Protein Coding FWD	AGCTGTAGGAGAGCCTGGTA
IRS1 Protein Coding REV	CAACATCAACAAGCGGGCTG
R18S FWD	GAGTGTTCAAAGCAGGTCCAA
R18S REV	CCTCTAGCGGTGCAATACAAA

Table 2: Primers for ChIP and ChIP-reChIP qPCR

RNA Extraction and Sequencing (RNA-seq)

MCF7 and T47D cell variants were plated at 2e5 cells per well of a 6-well plate in stripped media. After 48 hours, cells were treated with vehicle, 10nM E2, 10nM R5020, or 10nM E2+10nM R5020 and collected via trypsinization after 2 hours of treatment. RNA was extracted using the

Qiagen RNeasy Plus kit (#74104) according to the manufacturer's protocol. RNA concentrations were quantified by Nanodrop nucleic acid measurement.

Quantitative reverse transcription polymerase chain reaction (RT-qPCR) was used to quantify RNA expression at known ERα target genes and to ensure high-quality RNA for library preparation and sequencing. cDNA was synthesized from 1ug RNA using 5X Quanta Bio qScript Mastermix (#95048) according to the Quanta Bio qScript protocol. Applied Biosystems™ TaqMan™ Fast Advanced Master Mix (#4444557) and Human Beta-2-Microglobulin endogenous control (B2M, #4326319E) were used for RT-qPCR using a Roche Step-One Real-Time PCR machine. Primers used for RT-qPCR of select ERα target genes are available in table 3. Reactions were run in triplicate, with 3 biological replicates per sample. qPCR Ct results were averaged and normalized to the endogenous control R18S (ΔCt_{mean}). $\Delta\Delta Ct_{mean}$ for each ChIP condition was calculated as the difference between the corresponding adjusted $\Delta Ct_{mean(input)}$ and the $\Delta Ct_{mean(ChIP)}$. Fold change was then calculated as $2^{-\Delta\Delta Ct}$.

IDT RT-qPCR Primers		
Gene	**Primer ID**	**Ref Seq**
PGR	Hs.PT.58.50458902	NR_073143(7)
SGK1	Hs.PT.58.19153459.gs	NM_001143676(4)

Table 3: IDT RT-qPCR primers for RNA quality control

RNA library preparation for sequencing was completed using the KAPA mRNA HyperPrep Kit (#KR1352) according to the manufacturer's protocol. Sequencing was completed on the Illumina NovaSeq 6000 by the University of Chicago Functional Genomics core (RRID: SCR_019196).

RNA-seq Analysis

RNA-seq data were uploaded to the Galaxy platform and analyzed using the public server at usegalaxy.org [153]. Sequencing files were mapped to the hg19 human reference genome using

Bowtie2 and read counts per gene were generated from the aligned sequences using HTSeq-Count. DESeq2 was used to determine differentially expressed genes between each cell variant and between each treatment.

Analyzed MCF7 and T47D RNA-seq data were compared to de-identified patient tumor RNA-seq data obtained from the publicly available MET500 and Personal Oncogenomics 570 (POG570) datasets [154, 155]. Specific dataset IDs can be found in table 4. DESeq2 was used to compare differential gene expression between patient tumors harboring ERα Y537S mutations (4 from MET500 and 6 from POG570) and those with ERα WT (31 from MET500 and 32 from POG570).

Patient Tumor RNAseq Dataset IDs	
ERα Y537S	
MET500 ERα Y537S	**POG570 ERα Y537S**
MO_1129-capt-SI_6222-D1RWDACXX	18625_P00041
MO_1185-capt-SI_6794-H77P5ADXX	19512_P00060
MO_1305-capt-SI_7919-C4CRJACXX	26054_P00903
MO_1355-capt-SI_8457-C4L7VACXX	27329_P01026
	27765_P01093
	33154_P01932
ERα WT	
MET500 ERα WT	**POG570 ERα WT**
MO_1051-capt-SI_5093-D0VCEACXX	27216_P00991
MO_1090-capt-SI_5612-D18NCACXX	27219_P01009
MO_1107-capt-SI_5841-C19M0ACXX	27328_P01031
MO_1126-capt-SI_6287-D1RTCACXX	27503_P01044
MO_1159-capt-SI_6477-C1M1KACXX	28325_P01202
MO_1213-capt-SI_7016-C26CMACXX	30248_P01421
MO_1237-capt-SI_7190-C245WACXX	30487_P01486
MO_1239-capt-SI_7209-C245WACXX	30902_P01592
MO_1247-capt-SI_7265-C25YAACXX	31042_P01615
MO_1288-capt-SI_7733-C32VAACXX	31043_P01614
MO_1289-capt-SI_7734-C32VAACXX	31185_P01639
MO_1292-capt-SI_7736-C32VAACXX	31190_P01643
MO_1298-capt-SI_7847-C3Y81ACXX	32274_P01772
MO_1324-capt-SI_8129-C4E6CACXX	32571_P01850
MO_1335-capt-SI_8245-C471RANXX	36621_P02129
MO_1359-capt-SI_8460-C4L7VACXX	37312_P02235
MO_1364-capt-SI_8599-HAABDADXX	37365_P02247
MO_1411-capt-SI_9312-C5N2AANXX	38250_P02390
MO_1424-capt-SI_9381-C5N1GANXX	25483_P00631
MO_1427-capt-SI_9477-C5N19ANXX	25662_P00719
MO_1439-capt-SI_9741-C5N0KANXX	14231_A10982
MO_1454-capt-SI_9940-C6EJUANXX	15122_P00038
MO_1495-capt-SI_11221-C6UTYANXX	15227_T00056
MO_1515-capt-SI_11438-HV7JNADXX	20115_P00085
MO_1521-capt-SI_11539-C7GBMANXX	21347_P00125
MO_1528-capt-SI_11541-C7GBMANXX	21720_P02357
MO_1534-capt-SI_11904-C7F4VANXX	22499_P00168
MO_1536-capt-SI_11944-C7G8DANXX	22597_P00199
MO_1551-capt-SI_12338-C7FN8ANXX	23736_P00305
TP_2025-capt-SI_6023-D1EBEACXX	25962_P00850
TP_2141-capt-SI_12056-H53C5ADXX	25984_P00893
	27034_P00971

Table 4: Publicly available patient tumor RNAseq dataset IDs

siRNA Knockdown Screen

Dharmacon™ custom siRNA libraries were used for siRNA knockdown experiments (Table 5). MCF7 and T47D cell variants were treated and transfected using Lipofectamine™ RNAiMAX (#13778150) after 48 hours of hormone starvation in stripped media. YOYO™-1 Iodide (491/509) (#Y3601) was added at a final concentration of 10nM to quantify cell death over time, as well as proliferation, using the Incucyte S3. siRNA screens were conducted at the University of Chicago Cell Screening Center (CSC, RRID: SCR_017914).

Catalog Number	Gene Symbol	Gene ID	Catalog Number	Gene Symbol	Gene ID
M-014568-01	CCDC170	80129	M-003610-02	LRPAP1	4043
M-017182-00	CCDC185	164127	M-019107-02	NCOA6	23054
M-022265-01	CT62	196993	M-015805-01	PHC3	80012
M-010296-01	DEGS2	123099	M-030782-01	PTX4	390667
M-012425-02	FBXL6	26233	M-012137-00	RBBP4	5928
M-004451-01	FCMR	9214	M-032290-02	RNF169	254225
M-030385-01	FMN1	342184	M-027174-01	SBK1	388228
M-009318-01	FOXC1	2296	M-009097-01	SDR42E1	93517
M-008672-01	GNPDA2	132789	M-015832-01	SERPINA5	5104
M-012583-01	IGFBP4	3487	M-006998-01	SETD4	54093
M-003994-00	INO80E	283899	M-012990-00	SIN3A	25942
M-003015-01	IRS1	3667	M-017827-00	SMIM14	201895
M-006258-00	KCNK15	60598	M-023035-01	TBC1D28	254272
M-006265-00	KCNK6	9424	M-017531-01	WDR90	197335
M-032906-00	KRTAP5-10	387273	M-025859-01	ZNF517	340385

Table 5: Dharmacon siGENOME SMARTpool library

Immunoblotting

Cells were lysed using NE-PER™ Nuclear and Cytoplasmic Extraction Reagents (Thermo Scientific #78835) containing cOmplete™ EDTA-free Protease Inhibitor Cocktail (Roche #04693159001) and PhosSTOP™ (Roche #4906845001) to isolate cytoplasmic and nuclear extracts separately. Protein concentrations were quantified using the A280 Nanodrop program. Lysates were prepared with SDS-containing sample buffer such that 100ug of cytoplasmic protein

and 30ug nuclear protein would be loaded per well of a 4-20% polyacrylamide gel (Bio-Rad #4568096) for electrophoresis, followed by membrane transfer.

NT-157 Drug Screen

NT-157, an IRS1 inhibitor, was prepared at a stock concentration of 100mM in ethanol. MCF7 and T47D cell variants were hormone starved in charcoal-stripped media for 48 hours followed by treatment with 5uM NT-157, alone or in combination with a) 100nM 4OHT, b) 100nM lasofoxifene (laso), c) 1uM fulvestrant (ful), d) 100nM CDB4124 or e) 100nM PRA-027 (Table 6). Proliferation was measured over 5 days using the Incucyte S3 platform. Compound screens were conducted at the University of Chicago Cell Screening Center (CSC, RRID: SCR_017914).

Vehicle	Vehicle + 5uM NT-157	100nM 4OHT	100nM 4OHT + 5uM NT-157
100nM Laso	100nM Laso + 5uM NT-157	1uM Ful	1uM Ful + 5uM NT-157
100nM CDB4124	100nM CDB4124 + 5uM NT-157	100nM PRA-027	100nM PRA-027 + 5uM NT-157

Table 6: Treatments used in NT-157 combination drug screen

Statistical Analysis

Data (except dose-response curves for NanoBRET assays) were analyzed by ordinary two-way ANOVA ($\alpha = 0.05$) with Tukey's multiple comparisons tests to compare between treatments within each cell line, as well as between cell lines for each treatment. Dose-response curves were analyzed with nonlinear regression for log(treatment) vs. response to calculate log(IC50) values. Ordinary one-way ANOVA ($\alpha = 0.05$) with Tukey's multiple comparisons tests were used to compare IC50 values between each treatment. For all analyses: **** p-value < 0.0001, *** p-value < 0.001, ** p-value < 0.01, * p-value < 0.05.

CHAPTER III

ENDOCRINE THERAPY RESISTANCE-ASSOCIATED ERα-Y537S MUTATION RESULTS IN INCREASED ERα-PR INTERACTION

Background

Steroid hormone receptors are type I nuclear receptors that are implicated in the progression of endocrine-associated cancers, including breast cancer. Approximately 75% of breast cancer cases are characterized as hormone receptor-positive in terms of estrogen receptor (ERα) and/or progesterone receptor (PR) [156]. Dimerization is a key step in mediating the function of all hormone receptors. Though homodimers form more readily than heterodimers due to high binding affinity between receptors of shared structure, physical interactions between different hormone receptors play an important role in cell function [157-159]. Such physical interactions may occur through a variety of structurally diverse mechanisms that bring different hormone receptors in proximity, including:

1. Heterodimerization, such as the three-point interaction between peroxisome proliferator-activated receptor-ϒ (PPAR-ϒ) and retinoid X receptor (RXR) [160]
2. Allosteric modulation of hormone receptor binding to DNA via DNA binding domain (DBD) interactions [158]
3. Formation of complexes of hormone receptors with shared co-regulators, which are expressed in a temporal and cell-dependent manner [157, 158, 161]

Regardless of the method by which physical interactions between different hormone receptors occur, such interactions play a key role in what is known as hormone receptor crosstalk. Receptor crosstalk can refer to reciprocal gene regulation by two different hormone receptors, hormone-independent activity of a receptor in response to activity by a different receptor, or physical

interaction of two receptors in a regulatory complex. For example, ERα/PR crosstalk occurs via:

1) Liganded ERα regulating *PGR* gene transcription [137-141]
2) Liganded PR increasing ERα target gene regulation through ERα phosphorylation [137]
3) PR-dependent chromatin remodeling to facilitate ERα binding [142, 143]
4) ERα/PR physical interaction via regulatory complexes contributing to ligand-independent target gene expression [137, 144, 145]

ERα/PR crosstalk is thought to play a role in breast cancer progression and may contribute to the altered gene expression profile of ET-resistant tumors [137, 142, 144]. Endocrine therapies such as aromatase inhibitors (AI) or tamoxifen are often the first-line therapy for patients with hormone-sensitive breast cancers and have improved post-surgery outcomes and relapse-free survival [62]. Despite its benefits, ~25% of patients treated with adjuvant ET for five years or more develop ERα point mutations that drive treatment resistance and contribute to the progression of metastatic breast cancer [118, 120, 121]. ERα Y537S is one of the most frequently identified ERα mutations in patients, with the mutation appearing in one-third of circulating tumor cells from blood samples and at least 20% of metastatic tumors [116, 119, 120, 122, 162]. Notably, while ERα Y537S is very rarely found in primary treatment-naïve tumors, it is associated with tumor progression, especially in response to aromatase inhibitors, suggesting that ET results in selective pressure toward more resistant and aggressive metastases [62].

ERα Y537S stabilizes the activating function-2 (AF-2) cleft of the ERα ligand binding domain (LBD) in the agonist-bound conformation, which facilitates constitutive activity of the LBD, even in the absence of ligand binding [123]. Inversely, ERα Y537S alters the antagonist state of AF-2 by reducing the affinity of antagonists for the receptor, thereby increasing resistance to inhibition by selective estrogen receptor modulators and degraders (SERMS and SERDS) [123].

Further investigation into the effects of ERα Y537S on the transcription factor activity of ERα identified ~900 genes that were significantly induced in ERα Y537S, including several genes that were uniquely bound by ERα Y537S compared to ERα WT [62].

Given the multimodal nature of ERα/PR crosstalk involving both physical interaction of the receptors through regulatory complexes as well as reciprocal regulation of transcription factor activity, we hypothesized that the functional effects of ERα Y537S are not limited to ERα, but also affect the activity of PR. Here, I focus on the effects of ERα Y537S on the physical interaction of ERα and PR, utilizing the informative NanoBRET assay [150] for live-cell analysis of such interactions alongside validation of the model using proximity ligation (PLA), coimmunoprecipitation (CoIP), and sequential chromatin immunoprecipitation assays (ChIP-reChIP). I identify an increased physical interaction between ERα and PR in the context of the ERα Y537S mutation, including an increase in ERα/PR co-occupancy at integral chromatin binding sites. Elucidating the extent to which ERα Y537S alters ERα/PR crosstalk will further our understanding of how this activating mutation contributes to ET resistance and may offer alternative targets for treating resistant disease.

Results

Optimization and validation of nuclear receptor expression plasmids for NanoBRET assays

Prior to utilizing NanoBRET assays to experimentally investigate the effects of various manipulations (ligand treatment, receptor mutations, etc.), the optimal NanoLuc and HaloTag positions were determined through a complete comparison of quantified fluorescence/luminescence ratio for each possible arrangement of C-terminal and N-terminal tag positions (Fig. 3.1). The assays presented in this subsection were conducted by David Hosfield and Amira Ishag-Osman but are presented to support the validity of the NanoBRET system for

assessing nuclear receptor interactions.

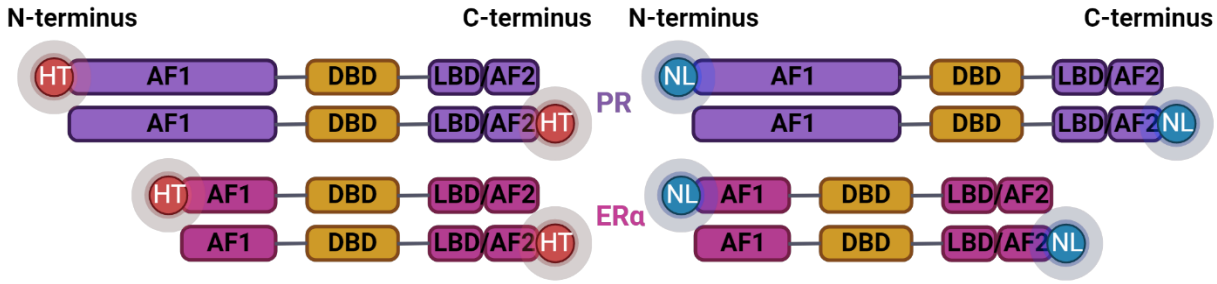

Figure 3.1: Diagram depicting possible combinations of HaloTag and NanoLuc conformations for ERα and PR. Graphic created with BioRender.com.

For each nuclear receptor (ERα and PR-B), NanoLuc and HaloTag relative positions were considered optimal based on the ability of the nuclear receptors to homodimerize in response to the receptor's native ligand without interference from the position of the NanoBRET tags (Fig. 3.2a-b). C-terminal HaloTag and NanoLuc positioning was optimal for both ERα and PR (Table 7).

ERα and PR-B homodimerization was specifically induced in response to E2 and P4 only (respectively); even at artificially high concentrations of ligand, ERα and PR-B only formed significant proximity-based interactions in response to their own native ligands (Fig. 3.2c,d). To further confirm that receptor homodimerization was not affected by NanoBRET tagging of the receptors, the native ligand of each receptor (as described above) was titrated to assess dose-dependent, ligand-induced nuclear receptor homodimerization. ERα and PR-B homodimerization in response to E2 and P4 (respectively) were strongly dose-dependent, with IC50 values in the nanomolar range (Fig. 3.3, Table 8). In total, these data highlight the NanoBRET assay as a biologically relevant, live-cell method to quantify proximity-based interactions among ERα and PR hormone receptors.

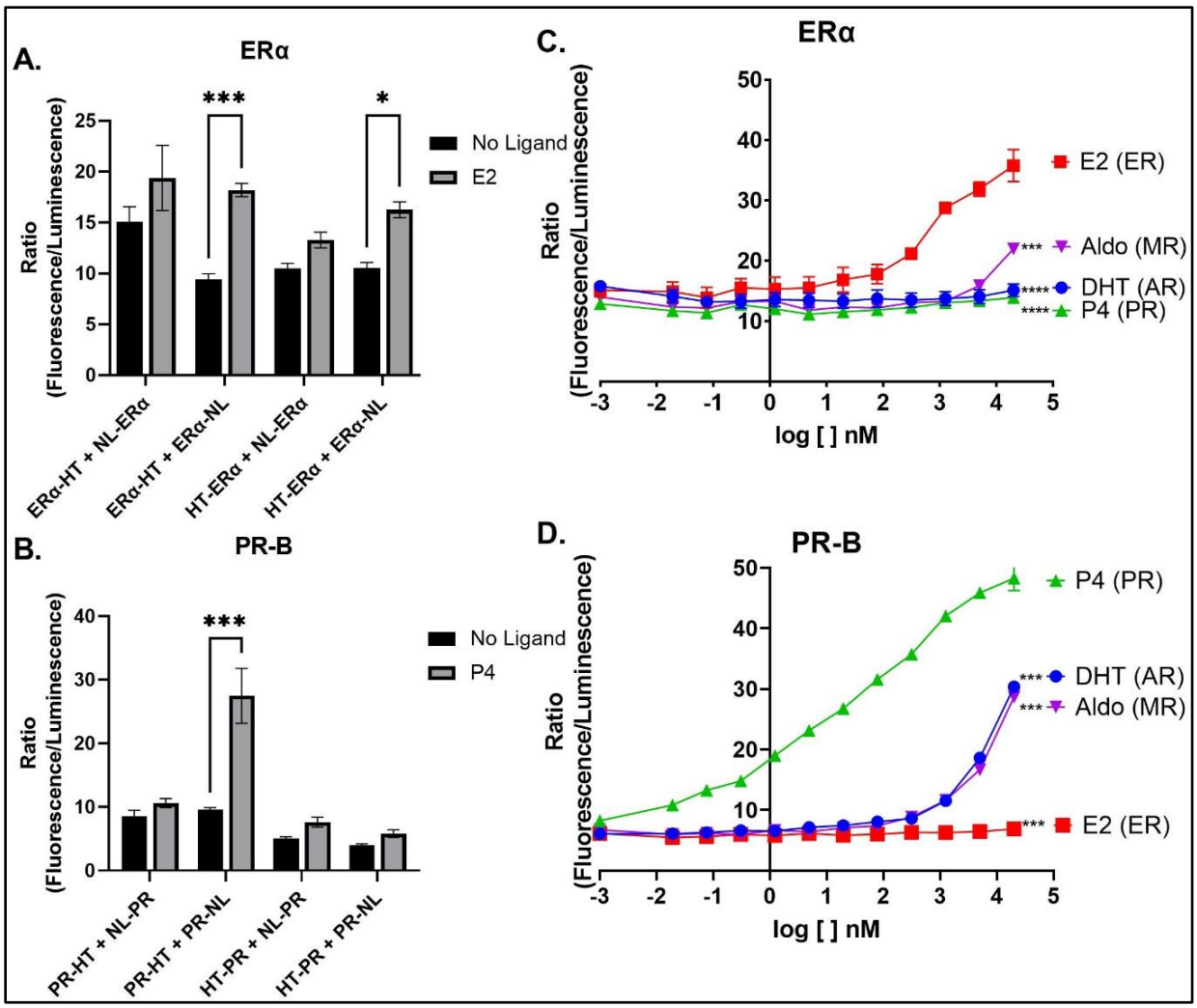

Figure 3.2: Optimal HaloTag and NanoLuc position allows for ligand-induced homodimerization of nuclear receptors. A-B. NanoBRET ratios of fluorescent to luminescent signal quantified upon addition of the NanoLuc substrate to cells treated with vehicle or the native receptor ligand for **A)** ERα and **B)** PR-B homodimers. **C-D.** NanoBRET dose-response curves of **C)** ERα and **D)** PR-B homodimer formation in response to non-native hormones, relative to formation in response to native ligand. Significant difference between NanoBRET ratios is indicated as * $p < 0.05$, ** $p < 0.005$, *** $p < 0.0005$, or **** $p < 0.0001$. Data represents minimum 3 biological replicates.

Receptor	HaloTag	NanoLuc
ERα	C-terminus	C-terminus
PR	C-terminus	C-terminus

Table 7: Optimal NanoBRET tag positions

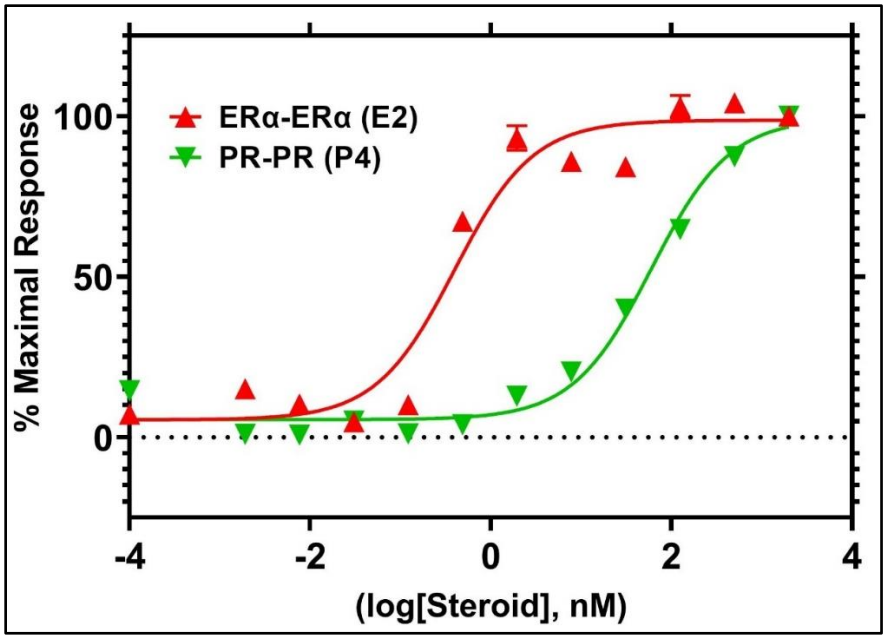

Figure 3.3: NanoBRET dose-response curves of ERα and PR-B homodimer pairs in response to treatment with their native ligands. IC50 values calculated from these curves are listed in table 8.

Homodimer	Ligand	IC50 (nM)	95% CI (nM)
ERα-ERα	E2	0.3971	(0.2727 – 0.5829)
PR-PR	P4	60.02	(45.82 – 78.50)

Table 8: IC50 values of homodimerization in response to native ligands

Upon optimization of the NanoBRET assay for quantifying hormone receptor homodimerization, the method was applied to investigate the proximity-based interaction of ERα with PR-B. As noted previously, physical interaction of ERα and PR-B and occupation at shared transcription start sites are key components of ERα/PR crosstalk [137, 144]. Similar to the optimization of HaloTag and NanoLuc configurations for homodimer formation of each nuclear receptor (Fig. 3.1, Fig. 3.2a,b), a methodical approach was taken to determine the optimal configuration of NanoBRET tag positions for assessing proximity-based interactions of ERα and PR-B (Fig. 3.4a,b). As with homodimer formation, C-terminal configuration of the NanoBRET tags was optimal, with ERα-HaloTag and PR-B-NanoLuc proximity increasing significantly in response to P4 treatment (Fig. 3.4b).

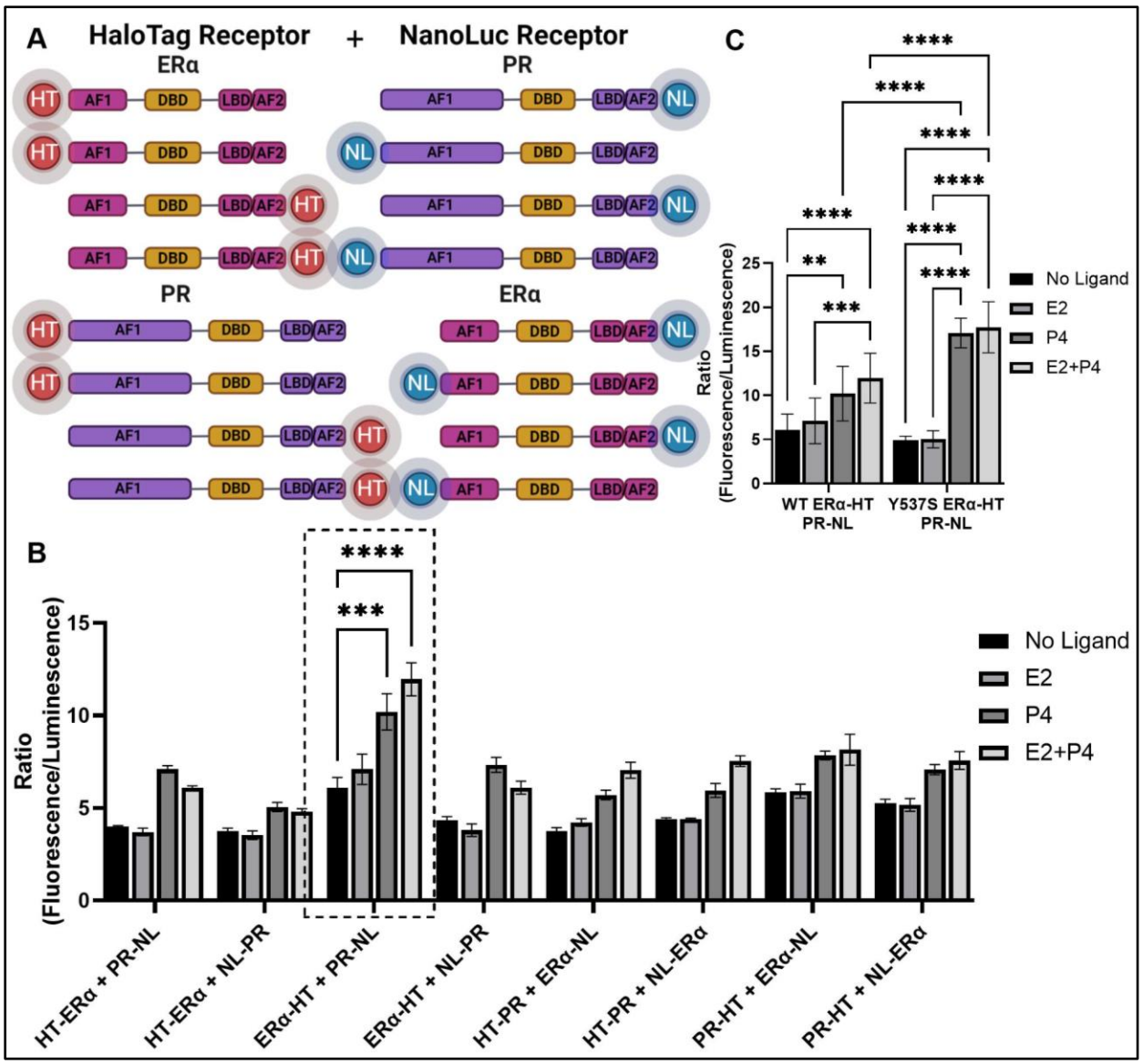

Figure 3.4: Optimized HaloTag and NanoLuc positioning allows for analysis of ERα and PR proximity-based interaction via NanoBRET assays. **A.** Diagram depicting possible combinations of HaloTag and NanoLuc conformations with ERα and PR. Graphic created with BioRender.com. **B.** NanoBRET ratios of fluorescence to luminescence for each combination of HaloTag and NanoLuc conformations depicted in A, in response to vehicle, E2 (ERα native ligand) and P4 (PR native ligand), alone or in combination. Optimal tag positioning based on responsiveness of the receptor proximity to ligand treatment is outlined with a dashed line. **C.** Using optimal NanoLuc/HaloTag positioning, graph shows NanoBRET ratios of ERα WT or ERα Y537S in proximity with PR-B in response to vehicle, E2 (ERα native ligand), and P4 (PR native ligand), alone or in combination. Data represents minimum 3 biological replicates. Significant difference in NanoBRET ratios is indicated as ** $p < 0.005$, *** $p < 0.0005$, or **** $p < 0.0001$.

ERα/PR proximity increases in the context of the ERα Y537S mutation

The ERα Y537S mutation is often found in treatment-resistant metastatic breast cancers, and thus it is of significant interest to fully characterize the phenotypic effects of the mutation as well as how it may be targeted. Given the reported role of ERα/PR crosstalk in breast cancer progression and the apparent value of the NanoBRET method for assessing ERα and PR-B proximity-based interactions, we introduced the specific TAT>TCT point mutation in exon 8 of the *ESR1* plasmid to create the ERα Y537S tyrosine to serine amino acid substitution. ERα proximity to PR-B increased significantly in response to R5020, and this increase was nearly two-fold greater in the context of the ERα Y537S mutation (Fig. 3.4c).

PR agonism contributes to increased ERα/PR proximity in the context of the ERα Y537S mutation

To confirm the increased ERα/PR proximity observed in the context of the ERα Y537S mutation using the NanoBRET method, we utilized three proximity-based methods to assess ERα/PR co-localization in MCF7 and T47D breast cancer cell lines. Importantly, experiments were completed in MCF7 and T47D cells expressing either unmutated ERα (ERα WT), heterozygous ERα WT/Y537S (ERα Y537S-het), or homozygous ERα Y537S/Y537S (ERα Y537S-hom). Though patient tumors tend to harbor heterozygous ERα mutations [163], assessing the mutation in isolation (as with ERα Y537S-hom) is critical to understanding the phenotypic effects of the mutation without interference of the unmutated receptor.

Proximity ligation assays (PLA) against probed antibodies for ERα and PR identified significantly greater puncta formation per cell in MCF7 and T47D cells expressing ERα Y537S-hom, indicating increased ERα/PR proximity compared to ERα WT or ERα Y537S-het cells (Fig. 3.5, Fig. 3.6, Fig. 3.7). Though the majority of PLA puncta were detected outside the nucleus in all cell variants, nuclear PLA puncta were significantly increased in the context of ERα Y537S-

hom relative to ERα WT or ERα Y537S-het, suggesting an elevated role of ERα/PR proximity-based interaction at chromatin (Fig. 3.7c,d). Interestingly, only cells expressing ERα Y537S showed treatment-dependent effects on PLA-based proximity; in MCF7 ERα Y537S-hom, R5020 significantly increased ERα/PR nuclear proximity while proximity was decreased slightly in T47D ERα Y537S-het and -hom in response to R5020 treatment relative to vehicle (Fig. 3.7).

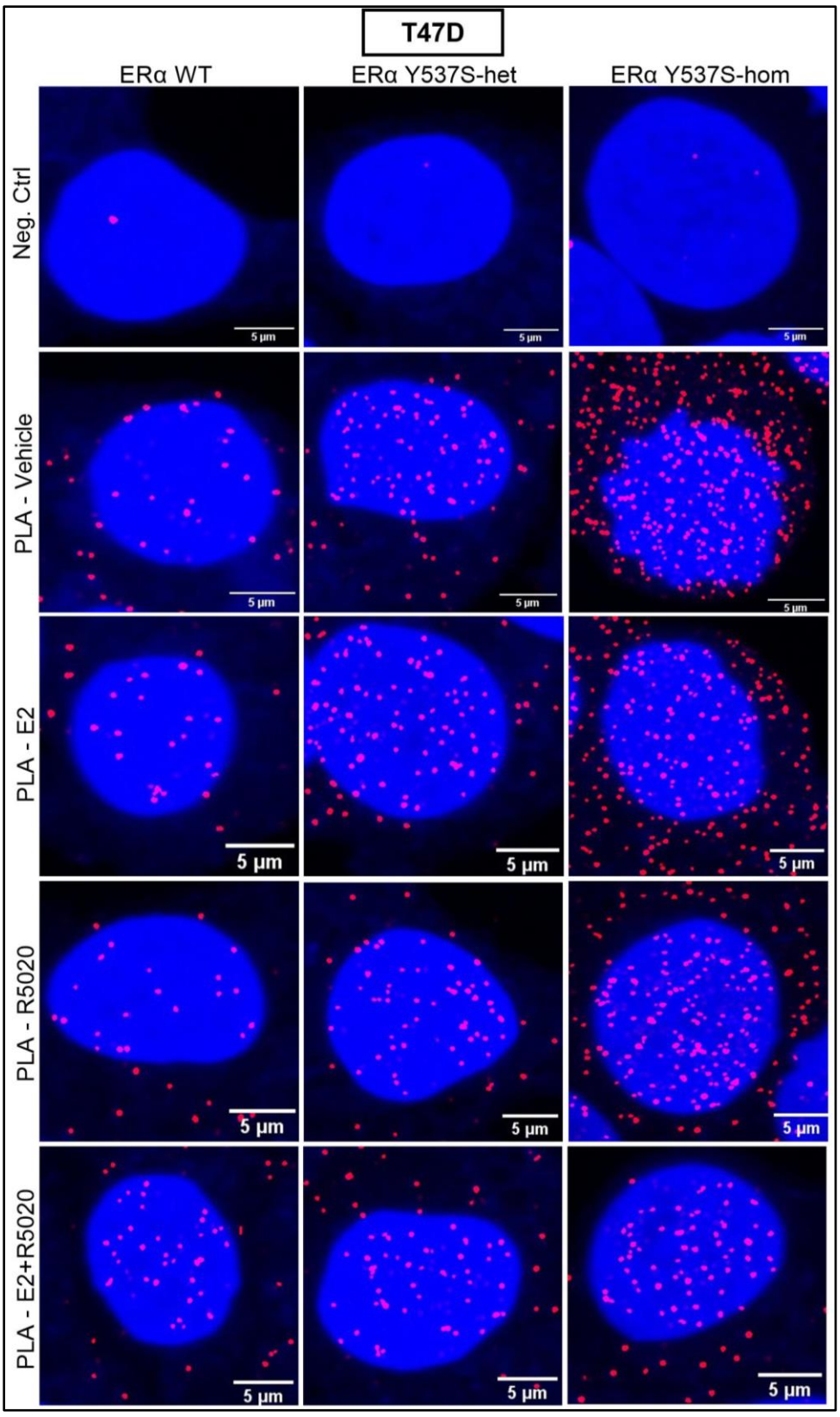

Figure 3.5: Representative confocal images of PLA (red puncta) and DAPI (blue nuclei)-stained cells after vehicle, E2, R5020, or combined treatment in T47D cells.

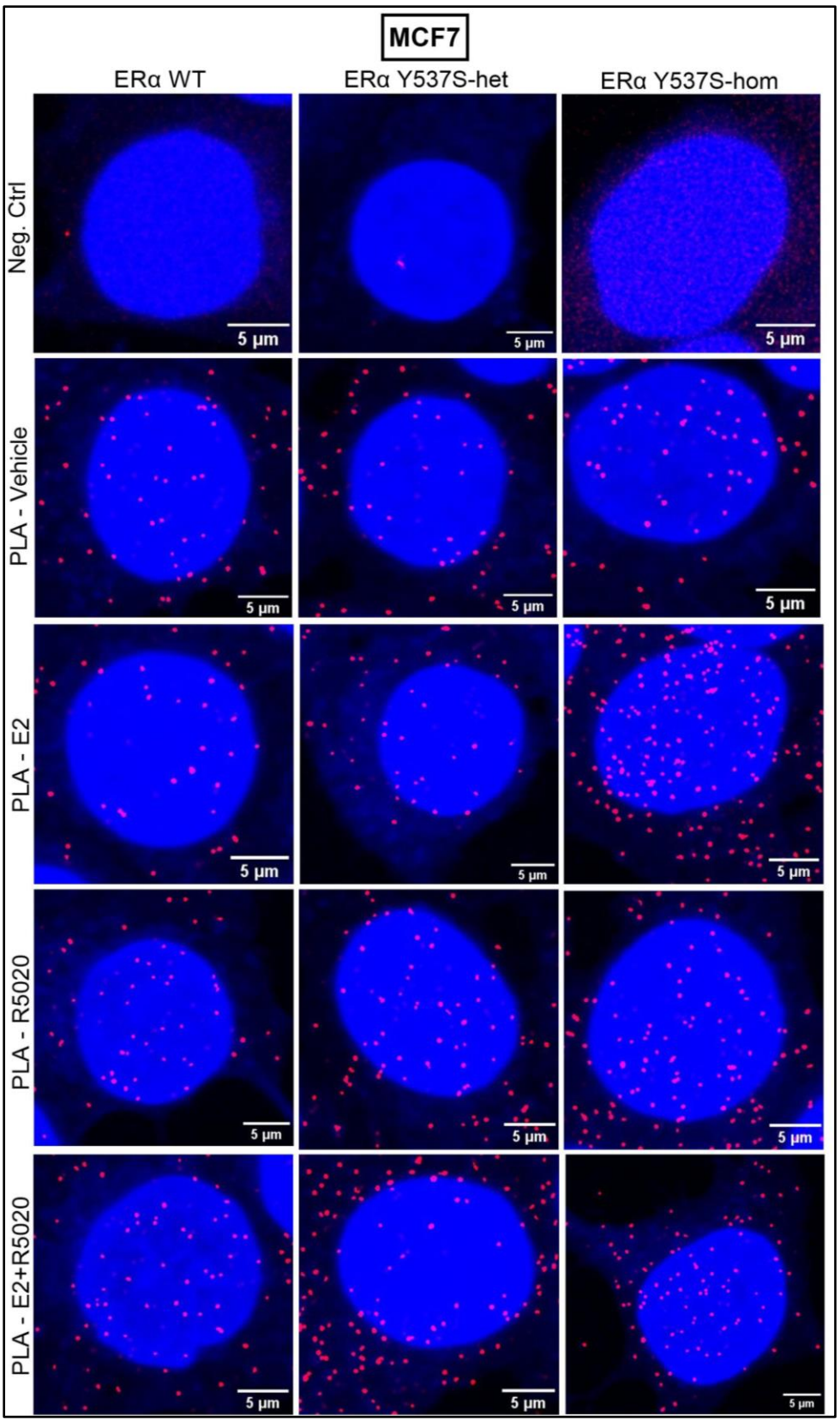

Figure 3.6: Representative confocal images of PLA (red puncta) and DAPI (blue nuclei)-stained cells after vehicle, E2, R5020, or combined treatment in MCF7 cells.

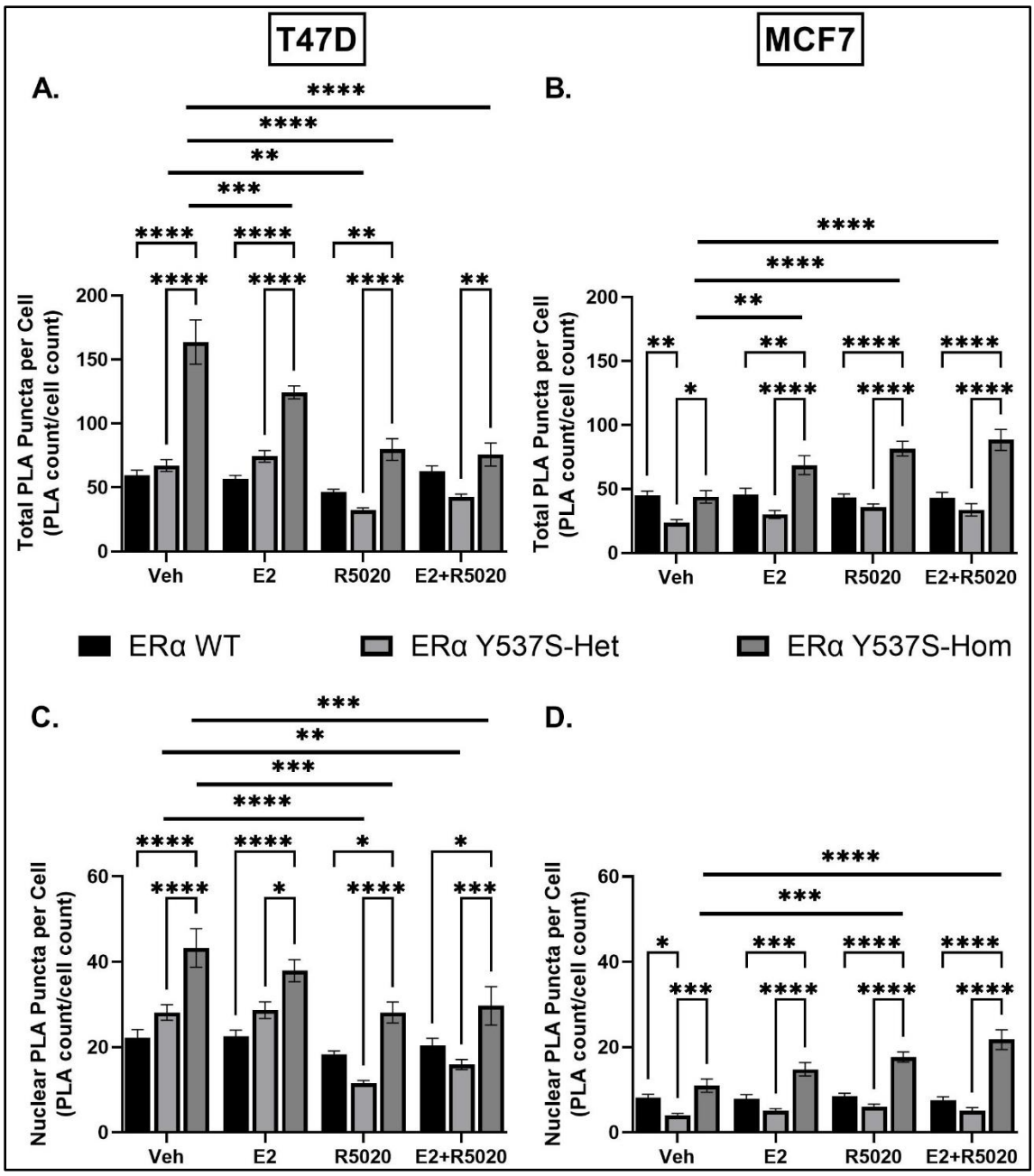

Figure 3.7: ERα/PR proximity-based interaction is increased in the context of ERα Y537S-hom relative to ERα WT or Y537S-het. A-B. Quantification of average total PLA puncta counts per cell for **A)** T47D and **B)** MCF7 cells. **C-D.** Quantification of average nuclear PLA puncta counts per cell for **C)** T47D and **D)** MCF7 cells. Data represents 3 replicates. Significant difference is indicated as * $p < 0.05$, ** $p < 0.005$, *** $p < 0.0005$, or **** $p < 0.0001$.

To further confirm these results, we detected PR in cytoplasmic and nuclear extracts from MCF7 and T47D cells after ERα immunoprecipitation. Coimmunoprecipitation (CoIP) again identified significantly increased ERα/PR proximity-based interaction in the context of ERα

Y537S-hom, though the extent of this difference relative to ERα WT was context-dependent (Fig. 3.8a,b). PR pulldown with ERα was significantly greater in the context of ERα Y537S-hom for both MCF7 and T47D cytoplasmic extracts after vehicle treatment (Fig. 3.8c,d). Similar to the PLA results, nuclear ERα/PR CoIP was significantly increased in the context of ERα Y537S-hom relative to either ERα WT or ERα Y537S-het (Fig. 3.8e,f). Though nuclear ERα/PR proximity-based interaction was only significantly increased after combined E2 and R5020 treatment in MCF7 ERα Y537S-hom cells relative to ERα WT, T47D ERα Y537S-hom cells showed ligand-independent (vehicle) and R5020-dependent increases in ERα/PR CoIP (Fig. 3.8e,f).

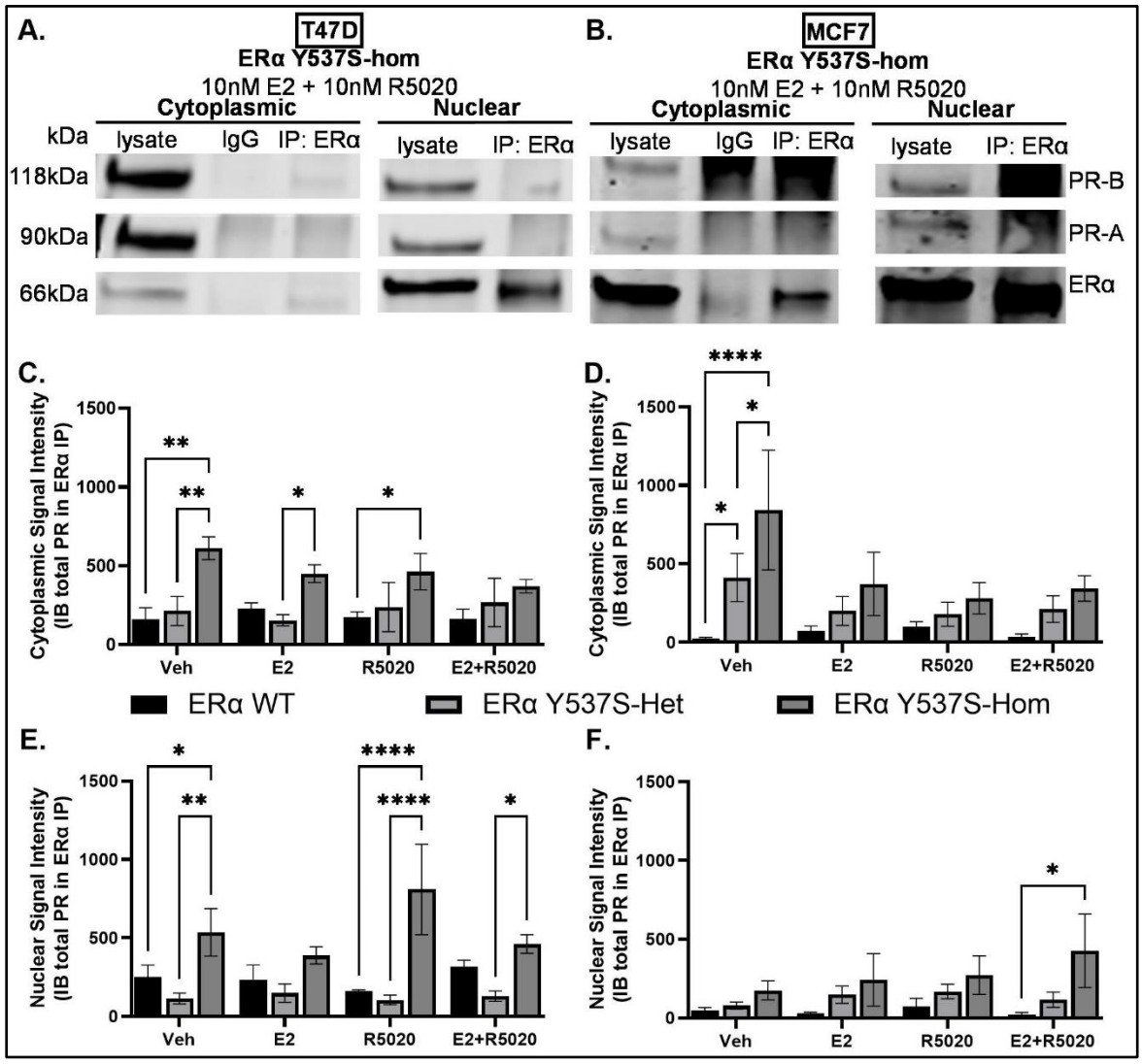

Figure 3.8: ERα/PR proximity-based interaction is increased in the context of ERα Y537S in

a partially R5020-dependent manner. A-B. Representative immunoblot images of ERα-immunoprecipitated lysates from **A)** T47D ERα Y537S-homozygous or **B)** MCF7 ERα Y537S-homozygous cells treated with 10nM E2 and 10nM R5020. **C-F.** Average quantified signal intensity of ERα immunoprecipitants with immunoblotting for PR from **C)** T47D cytoplasmic extracts, **D)** MCF7 cytoplasmic extracts, **E)** T47D nuclear extracts, and **F)** MCF7 nuclear extracts after treatment with vehicle, E2, and R5020, alone or in combination. Data represents 3 biological replicates. Significant difference is indicated as * $p < 0.05$, ** $p < 0.005$, or **** $p < 0.0001$.

ERα Y537S contributes to a unique pattern of ERα/PR co-occupancy at chromatin binding sites

Given the abundant evidence of significant ERα/PR proximity-based nuclear interaction from PLA and CoIP assays, we next investigated the active binding of ERα and PR simultaneously at specific chromatin sites through sequential chromatin immunoprecipitation (ChIP-reChIP). Primers for ChIP-reChIP qPCR of *FOXC1*, *IRS1*, and *FMN1* were designed based on previous research by Khushi et al. (2014) which identified chromatin sequences of potential overlapping ERα and PR binding [152]. These genes in particular were selected based on RNA-seq analyses in our lab (see chapter IV). In T47D ERα Y537S-hom, co-binding of ERα and PR at *FOXC1* and *IRS1* was increased more than two-fold compared to ERα WT or ERα Y537S-het in a ligand-independent manner (Fig. 3.9a-b). Interestingly, co-occupancy of ERα and PR at *FMN1* increased only in the context of ERα Y537S-het in both MCF7 and T47D cells, and this response was R5020-dependent in T47D cells and E2-dependent in MCF7 cells (Fig. 3.9c,f). This opposing ligand dependence may be attributed to differing reliance of the two cell lines on ERα and PR; T47D cells express more PR than MCF7 cells and MCF7 cells express more ERα (Fig. 3.8a-b). Following this trend, ERα and PR co-occupancy at *FOXC1* and *IRS1* was increased in an E2-dependent manner in MCF7 cells expressing ERα Y537S compared to ERα WT (Fig. 3.9d-e). Interestingly, this increase was most prominent in ERα Y537S-het apart from a significant increase of ERα/PR co-occupancy at *IRS1* in the context of ERα Y537S-hom treated with E2 and R5020 (Fig. 3.9e). In total, these data highlight a unique relationship between ERα and PR in the context of the ERα Y537S mutation.

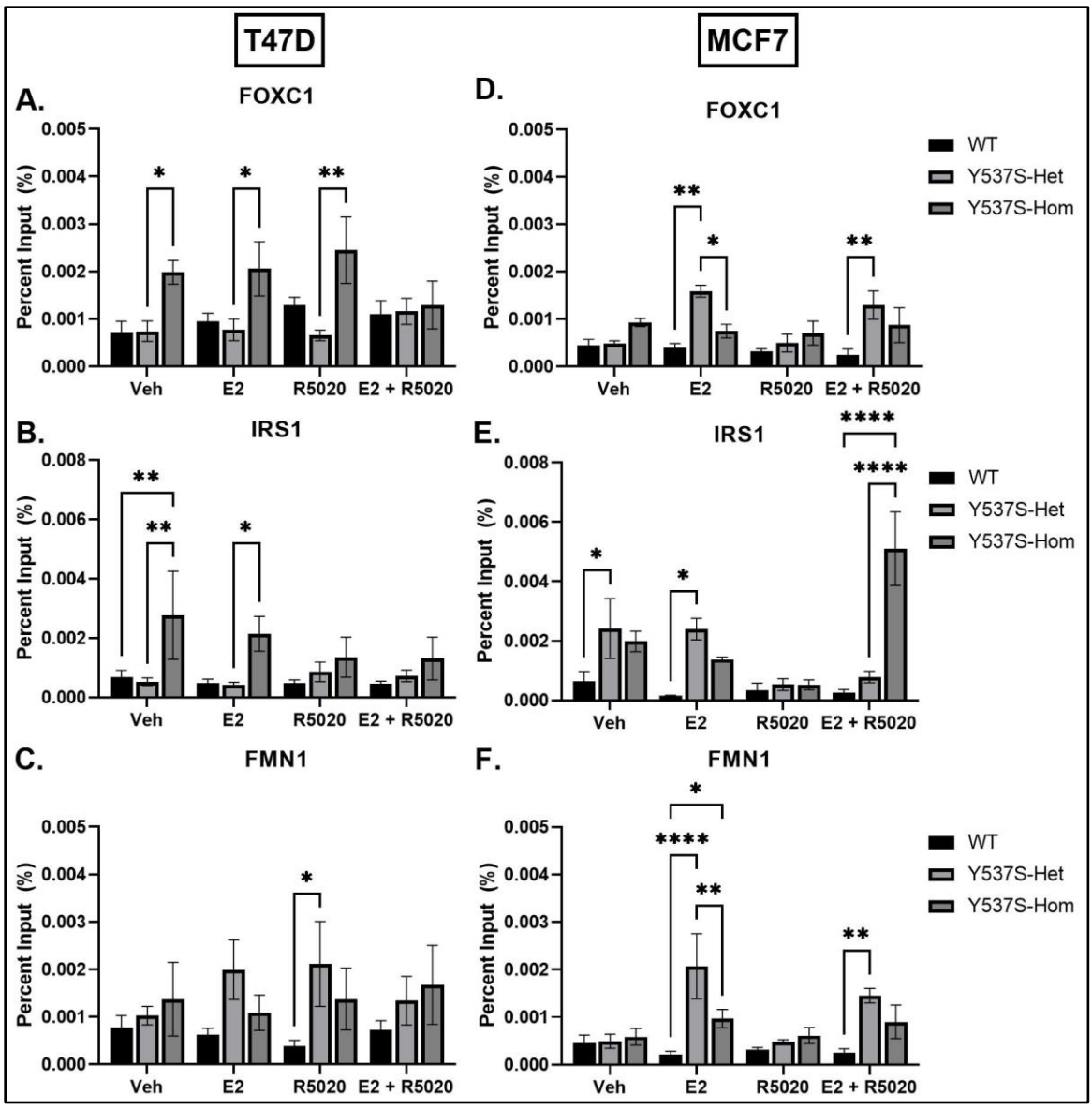

Figure 3.9: ERα/PR co-occupancy at shared, overlapping chromatin binding sites increases in the context of ERα Y537S. A-F. Quantification of ChIP-reChIP assays as a percent of corresponding input chromatin after 1hr treatment with vehicle, E2, and R5020, alone or in combination. Quantification of ERα/PR co-occupancy in T47D cells at **A)** *FOXC1*, **B)** *IRS1*, **C)** *FMN1*, and in MCF7 cells at **D)** *FOXC1*, **E)** *IRS1*, and **F)** *FMN1*. Data represents 3 biological replicates, each with 3 technical replicates. Significant difference is indicated as * $p < 0.05$, ** $p < 0.005$, or **** $p < 0.0001$.

Discussion

Although nuclear receptors canonically function through homodimerization, recent research has suggested that receptor crosstalk may amplify or dampen the activities of nuclear receptors, including those highly implicated in breast cancer [137, 143, 146, 157-161]. However,

these interactions have not previously been studied in all possible combinations of steroid hormone receptor crosstalk, leaving interactions of potential clinical consequence unexplored. Here, we developed a panel of optimized steroid hormone receptor-expressing plasmids for use in NanoBRET assays to rapidly quantify receptor homo- and heterodimerization in a live-cell, scalable setting.

Using the NanoBRET platform, we identified a PR ligand-responsive, proximity-based interaction between ERα and PR, potentially indicative of heterodimer formation. Given previous research investigating the role of ERα/PR crosstalk in breast cancer [137, 142, 146], we created an ERα NanoBRET plasmid harboring the ET resistance-associated ERα Y537S mutation to determine if ERα/PR proximity-based interaction is altered in the context of ERα Y537S. ERα Y537S and PR proximity-based interaction was significantly induced by PR stimulation with R5020, and to a much greater extent than with ERα WT and PR. These findings not only supported the value of the NanoBRET method for investigating nuclear receptor heterodimerization but also indicated a potential PR-driven ERα/PR heterodimerization that is enhanced by the ERα Y537S mutation.

Given the lack of ample literature on functional nuclear receptor heterodimers, reliance on the NanoBRET results alone would be insufficient to conclude that ERα/PR heterodimerization is increased in the context of ERα Y537S. Thus, I further assessed proximity-based interactions of ERα and PR three-fold using PLA, CoIP, and ChIP-reChIP analyses in both T47D and MCF7 breast cancer cell lines. Across both cell lines and all treatments, ERα Y537S-hom cells had significantly greater PLA puncta in both the cytoplasm and the nucleus than either ERα WT or ERα Y537S-het cells, indicating more ERα/PR proximity-based interactions in the context of ERα Y537S than when ERα WT is present. CoIP analyses indicated comparable results, though

interestingly only the CoIP analysis replicated the R5020-induced increase in ERα/PR interaction observed by NanoBRET. This may be due to the different ERα antibodies used in the two assays.

Of particular interest in the CoIP and PLA results is the observation that ERα/PR proximity-based interaction increases significantly in the nucleus in the context of the isolated ERα Y537S mutation represented by the ERα Y537S-hom cells. Though steroid hormone receptors, including ERα and PR, perform functions related to signaling pathways in the cytoplasm, their canonical transcription factor role is to enter the nucleus to modulate transcription at corresponding response elements [137, 164]. Thus, increased ERα/PR heterodimerization in the nucleus suggests a potential effect of the ERα Y537S mutation on ERα/PR-driven transcription. I, therefore, performed sequential ChIP for ERα and PR to isolate chromatin at which both ERα and PR were bound. I chose chromatin sites to sequence based on the 2014 publication by Khushi et al. which identified DNA sequences that contained potential shared, overlapping ERα and PR binding sites.

Though the ChIP-reChIP qPCR results indicated a less consistent pattern of ERα Y537S-associated changes to ERα/PR co-occupancy than any of the previous methods used in this study, this is expected. As previously published, ERα and PR cistromes are uniquely characterized in the context of ERα Y537S; some binding sites are lost, others are gained, and some are amplified [119, 146]. Despite observed differences between cell lines and treatments, the overwhelming pattern is that ERα/PR co-occupancy at chromatin binding sites for *FOXC1*, *IRS1*, and *FMN1* are significantly increased in the context of ERα Y537S, at both the heterozygous and homozygous expression level. These particular genes are significant because they contain potential overlapping binding sites for ERα and PR as identified by Khushi et al. (2014). Of note, *FOXC1* codes for a pioneer transcription factor that has been implicated in the progression of numerous cancers, including basal-like breast cancer and triple-negative breast cancer [165, 166]. IRS1 is a

component of the insulin receptor tyrosine kinase signaling pathway and contributes to ET resistance in ERα-positive breast cancers [167]. *FMN1* is an E2-responsive ERα target gene [168]. In total, these findings support a reprogramming of ERα/PR crosstalk through receptor heterodimerization and genomic co-occupancy that likely drives downstream transcriptional changes associated with the ERα Y537S mutation. Further experiments will assess the cistromic and transcriptomic effects of the ERα Y537S mutation on ERα and PR nuclear receptor functions.

CHAPTER IV

ERα/PR-ASSOCIATED TRANSCRIPTIONAL REGULATION IS ALTERED IN THE CONTEXT OF THE ERα-Y537S MUTATION AND CONTRIBUTES TO ENDOCRINE THERAPY-RESISTANT TUMOR PROLIFERATION

Background

The use of endocrine adjuvant therapy (ET) in hormone-sensitive ERα-positive breast cancers has led to a significant improvement in outcome and relapse-free survival [62]. Unfortunately, ~25% of patients who are treated with ET for 5 years develop somatic *ESR1* point mutations that drive therapy resistance and contribute to the progression of metastatic breast cancer. ERα Y537S is one of the most frequently identified ERα mutations in patients, with the mutation appearing in ~30% of circulating tumor cells from blood samples and at least 20% of metastatic tumors [116, 118-120, 122].

Notably, ERα Y537S is very rarely found in primary treatment-naïve tumors and is associated with tumor progression, suggesting that ET results in selective pressure toward more resistant and aggressive metastases [119]. Previous structural assessment in our lab demonstrated that ERα Y537S stabilizes the activating function-2 (AF-2) cleft of the ERα ligand binding domain (LBD) in the agonist-bound conformation, which facilitates constitutive activity of the LBD, even in the absence of estradiol [123]. Conversely, ERα Y537S interferes with the antagonist state of AF-2, resulting in reduced affinity of antagonists for the receptor and resistance to inhibition by selective estrogen receptor modulators and degraders (SERMs and SERDs) [123]. Further investigation into the effects of ERα Y537S on the transcription factor activity of ERα identified ~900 genes that were significantly induced in MCF7 and T47D ERα Y537S cell lines, including several genes that were uniquely bound by ERα Y537S as compared to ERα WT [119].

While gene expression changes associated specifically with mutant ERα have understandably been the main focus in terms of assessing the effects of ERα Y537S, there are alterations to PR-mediated gene expression as well. Previous research in our lab and others has assessed ERα/PR crosstalk and found that, in ERα+/PR+ treatment-naïve cells, combined modulation of both receptors promoted tumor regression, and chromatin binding profiles indicated that PR alters ERα-associated gene expression in the ERα WT context [137, 142, 143, 146]. However, the effect of ERα Y537S on ERα/PR crosstalk has not been thoroughly investigated. Given that liganded ERα regulates *PGR* (PR gene) transcription, it is highly likely that the constitutively active ERα Y537S mutation results in altered PR expression and activity [137-141]. In this chapter, I aim to determine the effects of the ERα Y537S mutation on ERα/PR crosstalk and resulting transcriptional activity and to elucidate how this unique interaction leads to ET resistance in ERα-positive breast cancer. I identified a unique transcriptome associated with the ERα Y537S mutation at shared regulatory binding sites of ERα and PR, including near *IRS1*. Our results suggest that inhibition of insulin receptor substrate-1 (IRS1) might restore therapeutic sensitivity to patients with ET-resistant breast cancer.

Results

Homozygous expression of the ERα Y537S mutation results in a distinct transcriptome in MCF7 and T47D cell lines

To assess transcriptomal changes associated with the ERα Y537S mutation, RNA-seq was completed in MCF7 and T47D breast cancer cell lines with endogenous expression of ERα wild-type (ERα WT), heterozygous ERα Y537S (ERα Y537S-het), or homozygous ERα Y537S (ERα Y537S-hom). Both heterozygous and homozygous ERα Y537S cells were included in all experiments. Although ERα Y537S typically presents clinically as a heterozygous mutation,

determining the function of the mutated receptor in the homozygous context is necessary to characterize the interaction of ERα Y537S in the absence of ERα WT with other cellular components including PR.

Triplicate RNA-seq data clustered tightly for each cell line variant and treatment: hormone depleted (vehicle), E2 (ERα ligand), R5020 (PR ligand), or combined E2 and R5020 (Fig. 4.1, Fig. 4.2). Though overall gene expression differed between MCF7 and T47D cells, a similar pattern emerged in cluster 10, highlighting a pattern of genes differentially expressed in the context of the ERα Y537S mutation (Fig. 4.3). In both MCF7 and T47D cells and regardless of treatment, ERα Y537S-hom cells differentially expressed significantly more genes than ERα Y537S-het cells when each was compared to ERα WT (Fig. 4.4, Fig. 4.5). Notably, hormone-depleted MCF7 ERα Y537S-hom cells differentially expressed 789 transcripts compared to 85 in MCF7 ERα Y537S-het (Fig. 4.4a,b).

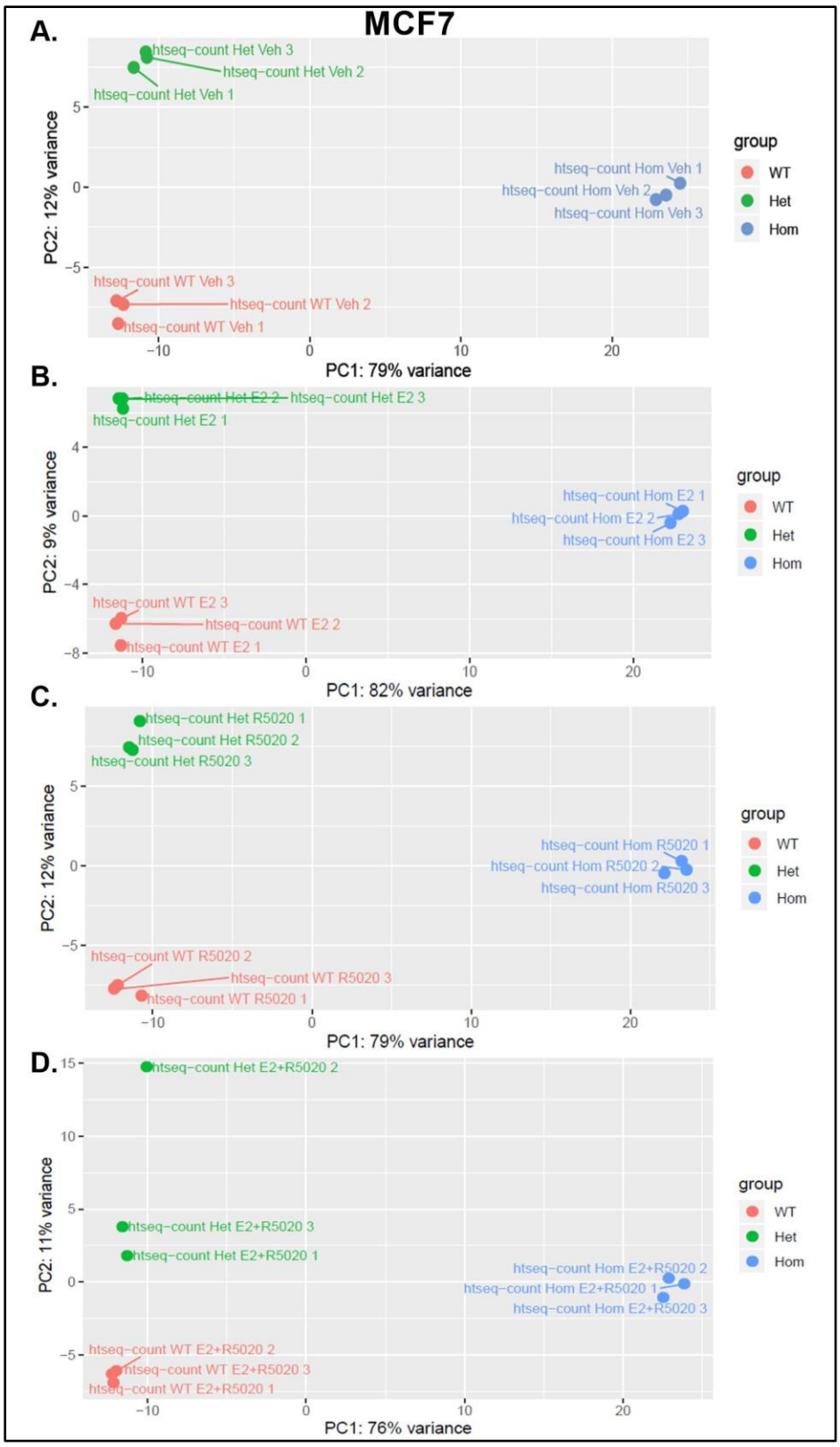

Figure 4.1: PCA plots of MCF7 RNA-seq data show close clustering of biological replicates. PCA plots of RNA-seq replicates of MCF7 ERα WT, ERα Y537S-het, and ERα Y537S-hom cells treated with A) vehicle, B) E2, C) R5020, or D) E2 + R5020.

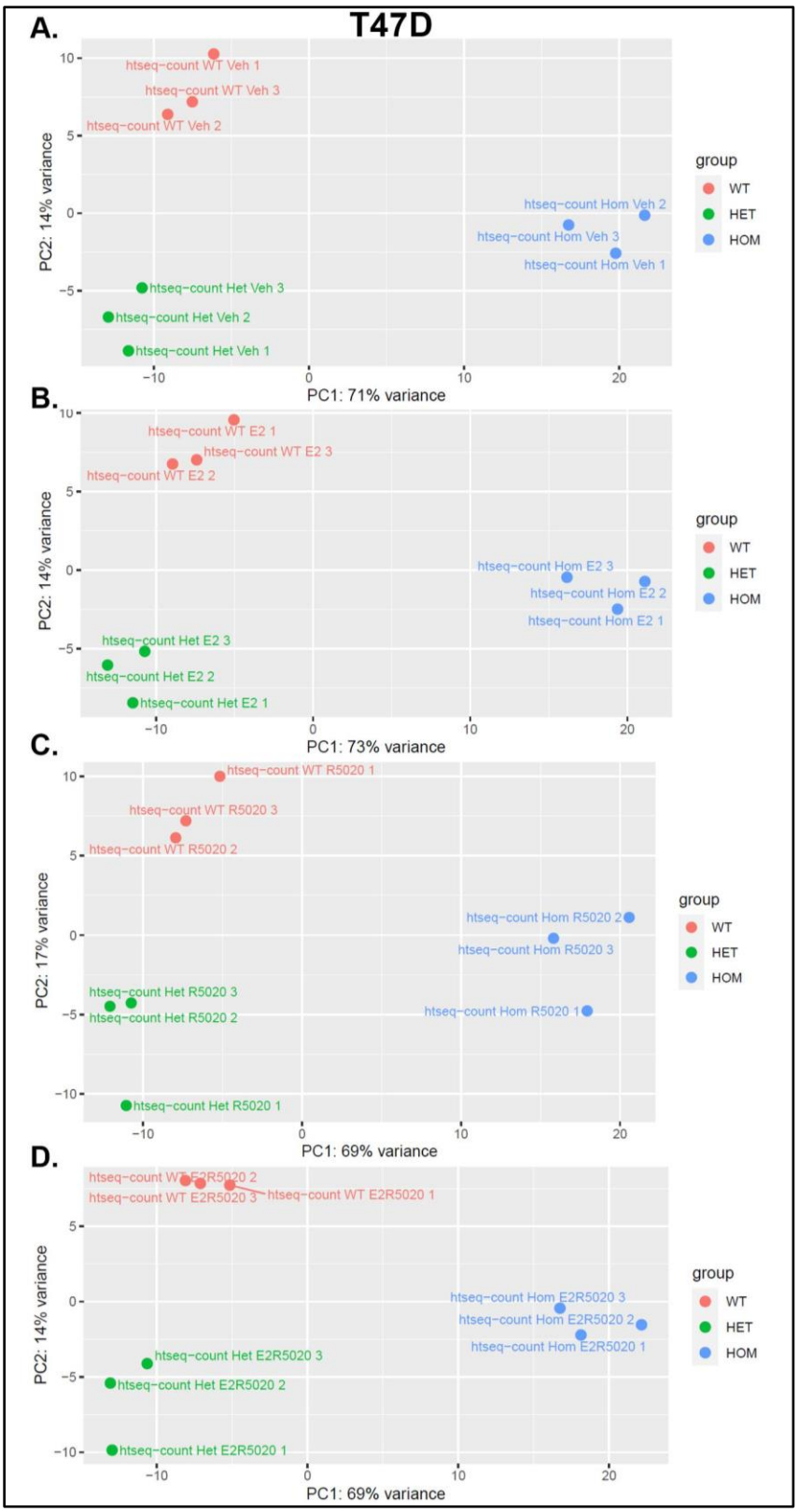

Figure 4.2: PCA plots of T47D RNA-seq data show close clustering of biological replicates. PCA plots of RNA-seq replicates of T47D ERα WT, ERα Y537S-het, and ERα Y537S-hom cells treated with A) vehicle, B) E2, C) R5020, or D) E2 + R5020.

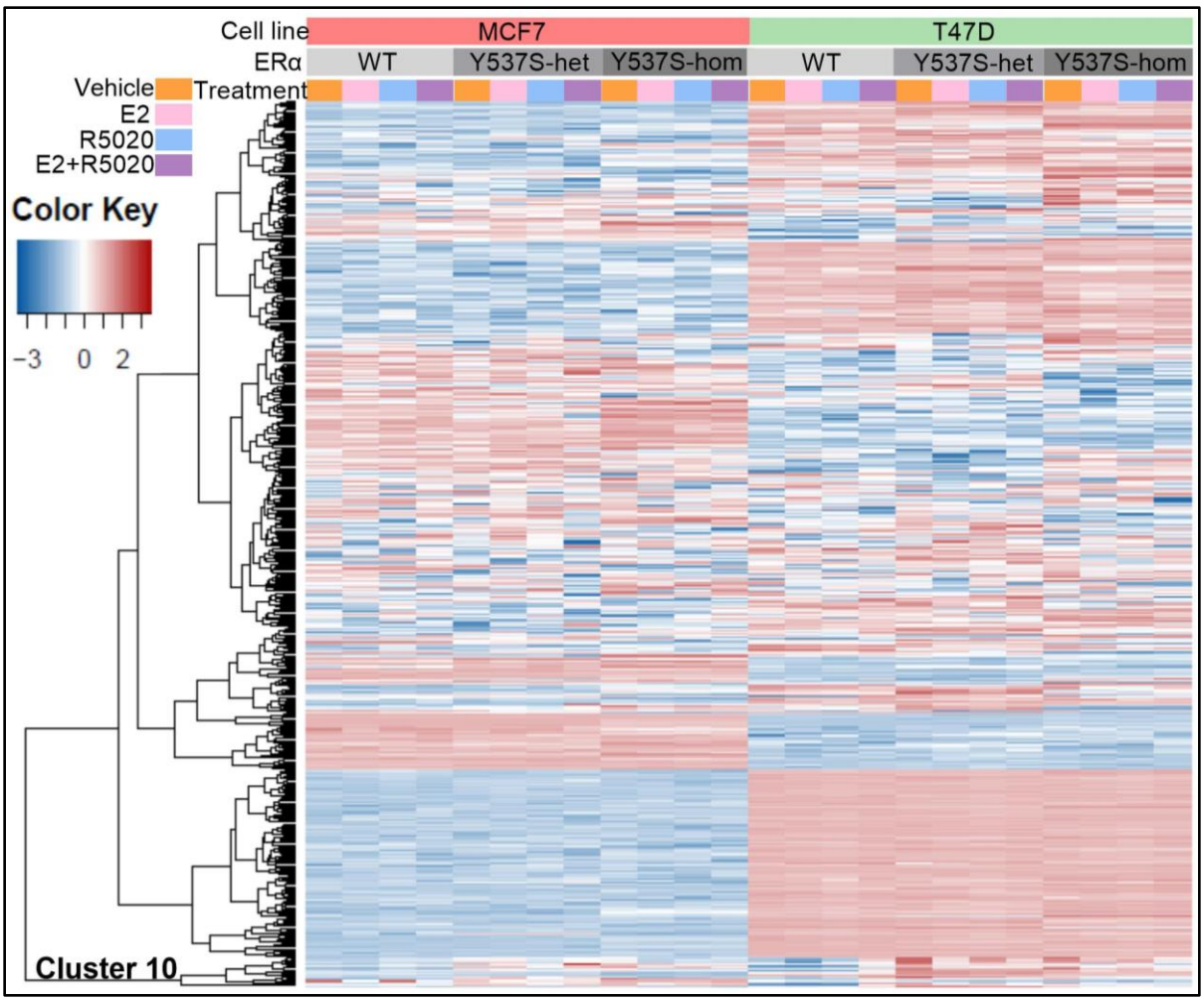

Figure 4.3: MCF7 and T47D cells have distinct transcriptomes but share a pattern of differential expression in cells expressing ERα Y537S. Heatmap of $\log_2$-transformed read counts from RNA-seq data of MCF7 and T47D cell lines, each expressing ERα WT, ERα Y537S-het, or ERα Y537S-hom. Each cell line variant was treated with vehicle (hormone-deprived), 10nM E2, 10nM R5020, or both. Gradient indicates low (blue) to high (red) read counts for each transcript, clustered by row. Cluster 10 indicates a transcript cluster with a shared pattern of gene expression in both MCF7 and T47D cells expressing ERα Y537S. Data for each column represents the average of 3 biological replicates.

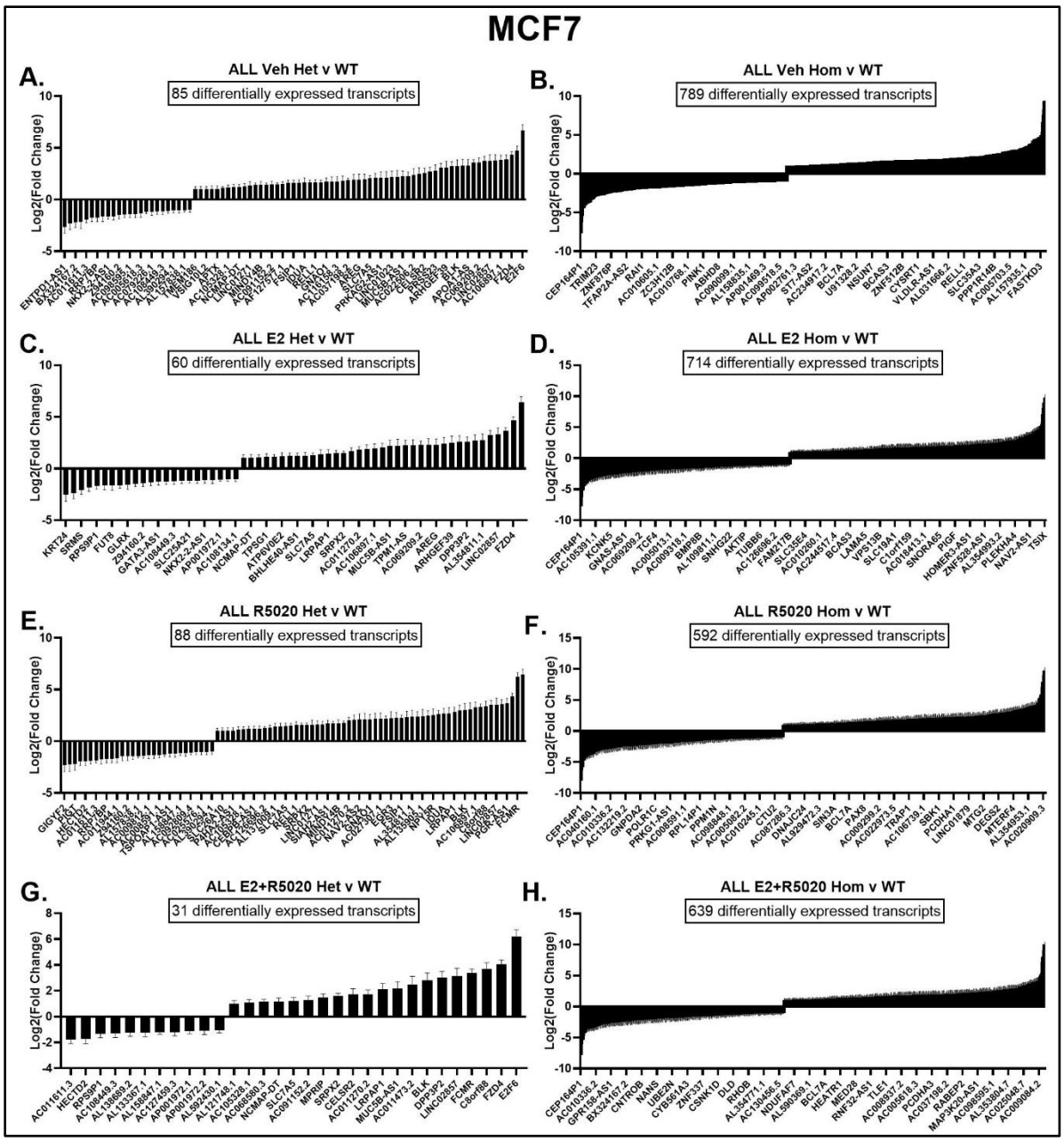

Figure 4.4: MCF7 ERα Y537S-hom cells differentially expressed significantly more genes than ERα Y537S-het cells when each was compared to ERα WT. Plot of log2(fold change) for differentially expressed transcripts ($|\log2(FC)| > 1$, p-adj < 0.05) in MCF7 cells expressing ERα Y537S-het (A, C, E, G) or ERα Y537S-hom (B, D, F, H), relative to ERα WT, after treatment with A,B) vehicle, C,D) E2, E,F) R5020, or G,H) E2+R5020.

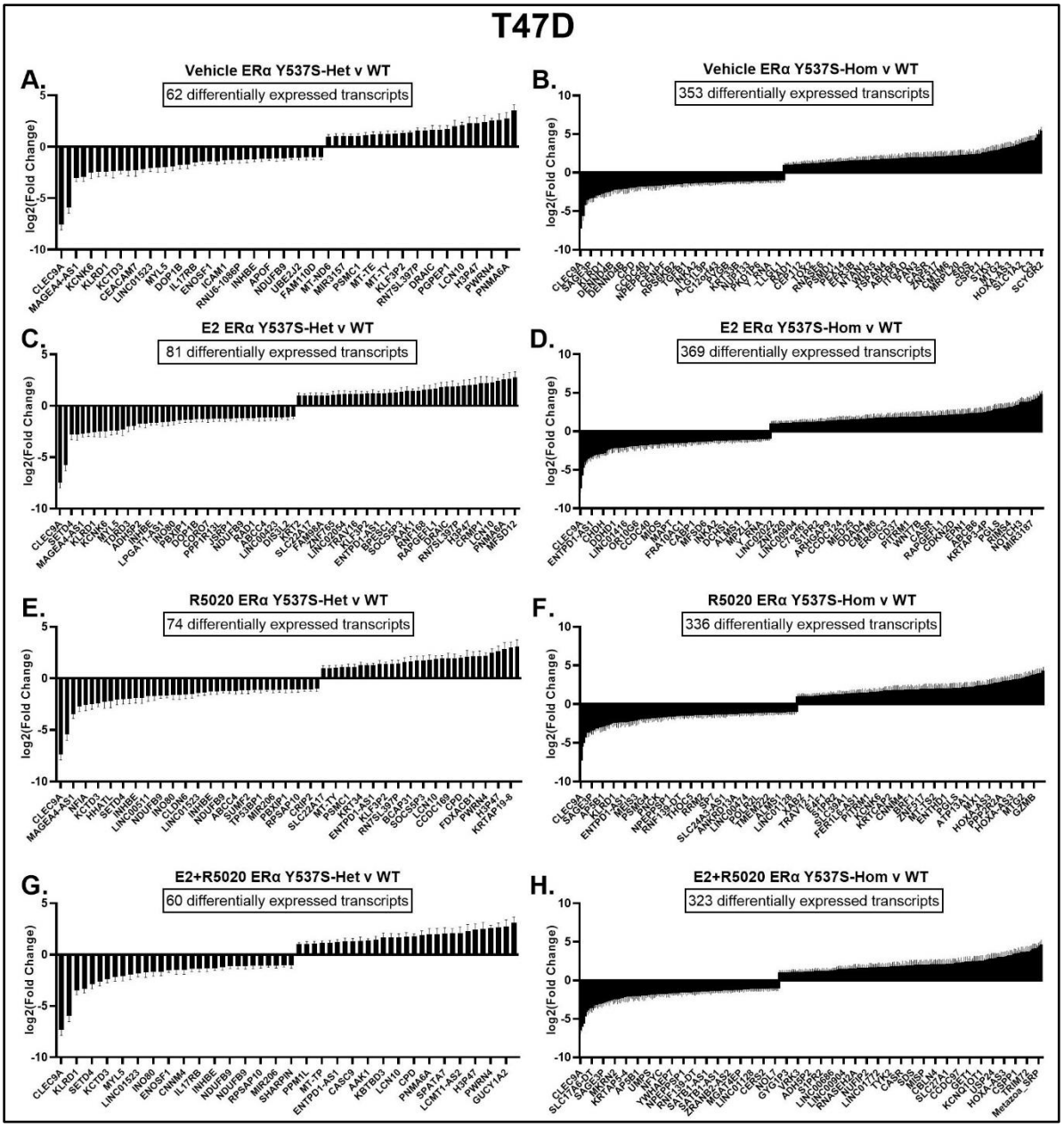

Figure 4.5: T47D ERα Y537S-hom cells differentially expressed significantly more genes than ERα Y537S-het cells when each was compared to ERα WT. Plot of log2(fold change) for differentially expressed transcripts (|log2(FC)| > 1, p-adj < 0.05) in T47D cells expressing ERα Y537S-het (A, C, E, G) or ERα Y537S-hom (B, D, F, H), relative to ERα WT, after treatment with A,B) vehicle, C,D) E2, E,F) R5020, or G,H) E2+R5020.

In total, over 600 genes and 350 genes were found to be differentially expressed in the context of the ERα Y537S mutation (heterozygous and homozygous, compared to ERα WT) in MCF7 and T47D, respectively (Fig. 4.6a). These findings are in line with previous studies on the

effect of the Y537S mutation on ERα-driven gene expression [119, 163]. I next filtered these data to include only genes containing potential shared cis-regulatory regions of ERα and PR binding identified by Khushi et al. (2014) (Fig. 4.6a). This allowed us to focus on gene expression changes that might be a direct result of altered ERα/PR crosstalk, whereas previous research investigated transcriptomal changes correlated with ERα Y537S more generally.

Similar to the pre-filtered data, MCF7 and T47D ERα Y537S-hom cells differentially expressed significantly more overlapping ERα/PR-shared regulatory genes than their respective ERα Y537S-het counterparts (Fig. 4.6b,c). These findings uncovered a distinct transcriptome associated with ERα Y537S in a context without clouding of data by the presence of ERα WT. However, without further analyses, these data are largely correlative and do not offer insight into the clinical significance or mechanism by which ERα Y537S alters ERα/PR-shared regulatory gene expression.

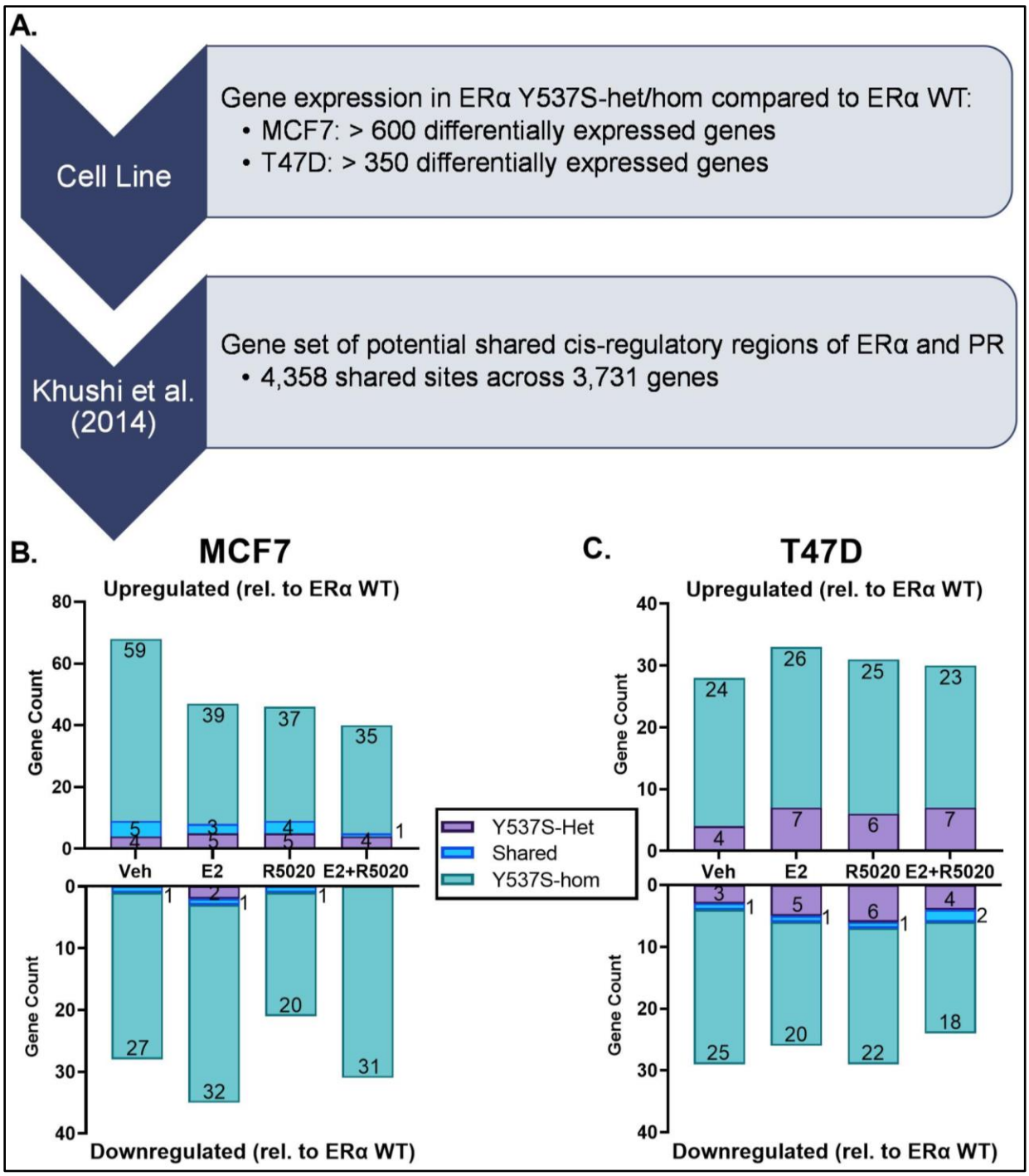

Figure 4.6: Genes with potential shared ERα/PR regulatory binding sites are differentially expressed in the context of ERα Y537S-hom. A) Flowchart depicting the filtering of RNA-seq data of all genes differentially expressed in the context of ERα Y537S to obtain data only for genes represented in the Khushi et al. (2014) dataset of potential shared ERα/PR binding sites. Upregulated and downregulated mRNA transcript counts from genes matching these criteria are shown for B) MCF7 and C) T47D cell variants.

Differentially expressed genes are conserved between MCF7, T47D, and patient tumors expressing ERα Y537S mutations

To determine the clinical relevance of the transcriptional changes observed in MCF7 and T47D cell lines, I analyzed de-identified hormone receptor-positive breast cancer patient tumor RNA-seq data obtained from the publicly available MET500 and Personal Oncogenomics 570 (POG570) datasets [154, 155]. Ten datasets from tumors containing ERα Y537S mutations were analyzed for differential gene expression relative to site-matched ERα WT tumor datasets, which identified 2,406 differentially expressed genes in the context of ERα Y537S (Fig. 4.7). Of these, 26 genes were also differentially expressed in MCF7, and 17 in T47D cells expressing ERα Y537S (Fig. 4.8a,b). Notably, most of the differentially expressed genes were upregulated (as opposed to downregulated) in both patient tumors and cell line data, and this upregulation occurred independent of ERα and/or PR hormone stimulation (Fig. 4.8a,b). This highlights the known ligand-independent activity of ERα Y537S.

Of the genes differentially expressed in both cell lines and patient tumors containing ERα Y537S mutations, only four contained potential ERα-PR shared regulatory binding sites, as identified by Khushi et al. (2014). These were *DEGS2* (Delta-4-Desaturase, Sphingolipid 2), *FMN1* (Formin 1), *IRS1* (Insulin Receptor Substrate 1), and *KCNK15* (Potassium Two Pore Domain Channel Subfamily K Member 15), all of which were expressed ~2- to 4-fold more in MCF7 ERα Y537S-hom cells (independent of hormone stimulation) and patient tumors than their respective ERα WT counterparts (Fig. 4.8c).

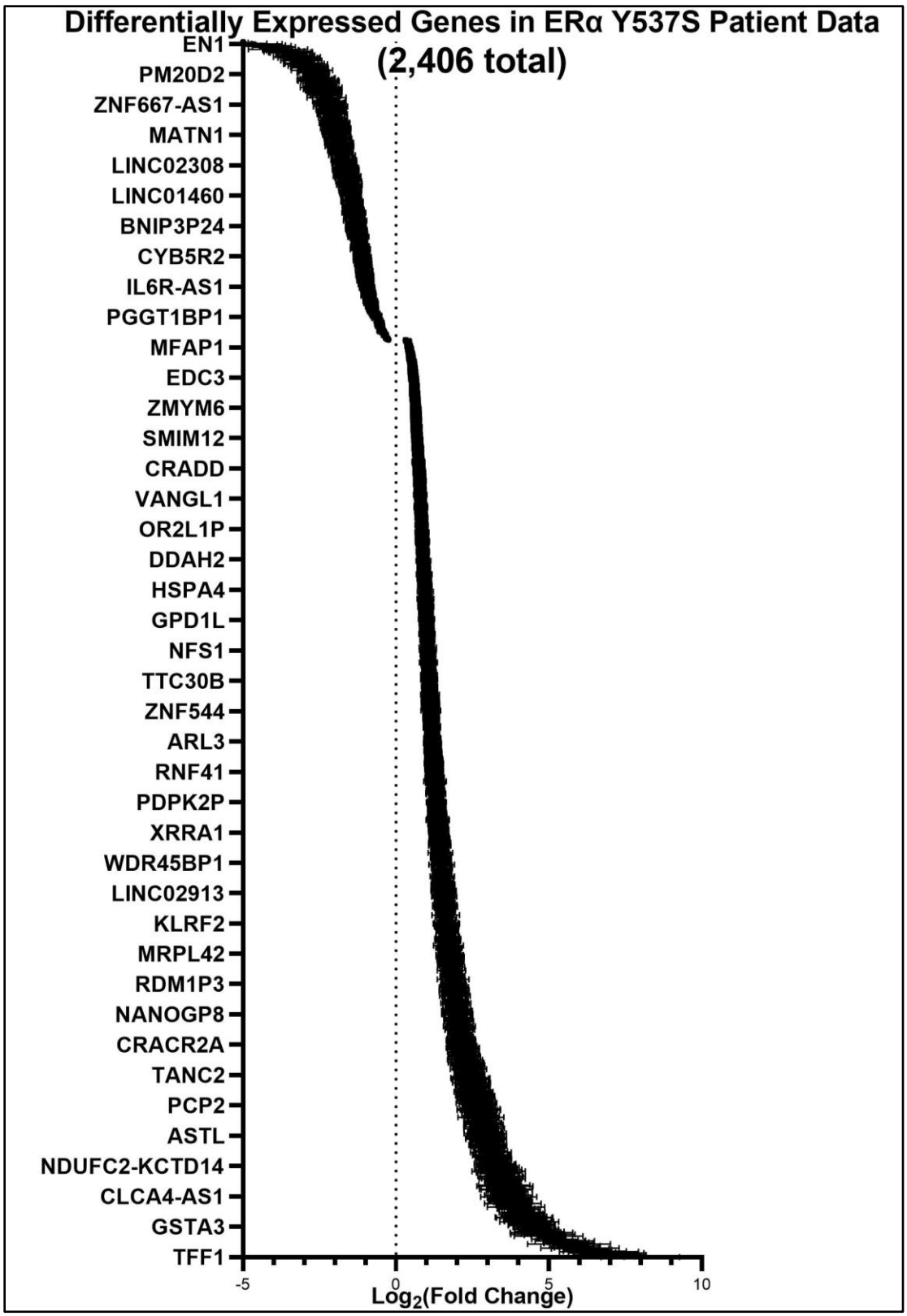

Figure 4.7: 2,406 transcripts are differentially expressed in patient tumors expressing ERα Y537S relative to ERα WT. Plot of log2(fold change) for differentially expressed transcripts (|log2(FC)| > 1, p-adj < 0.05) in patient tumors expressing ERα Y537S relative to ERα WT.

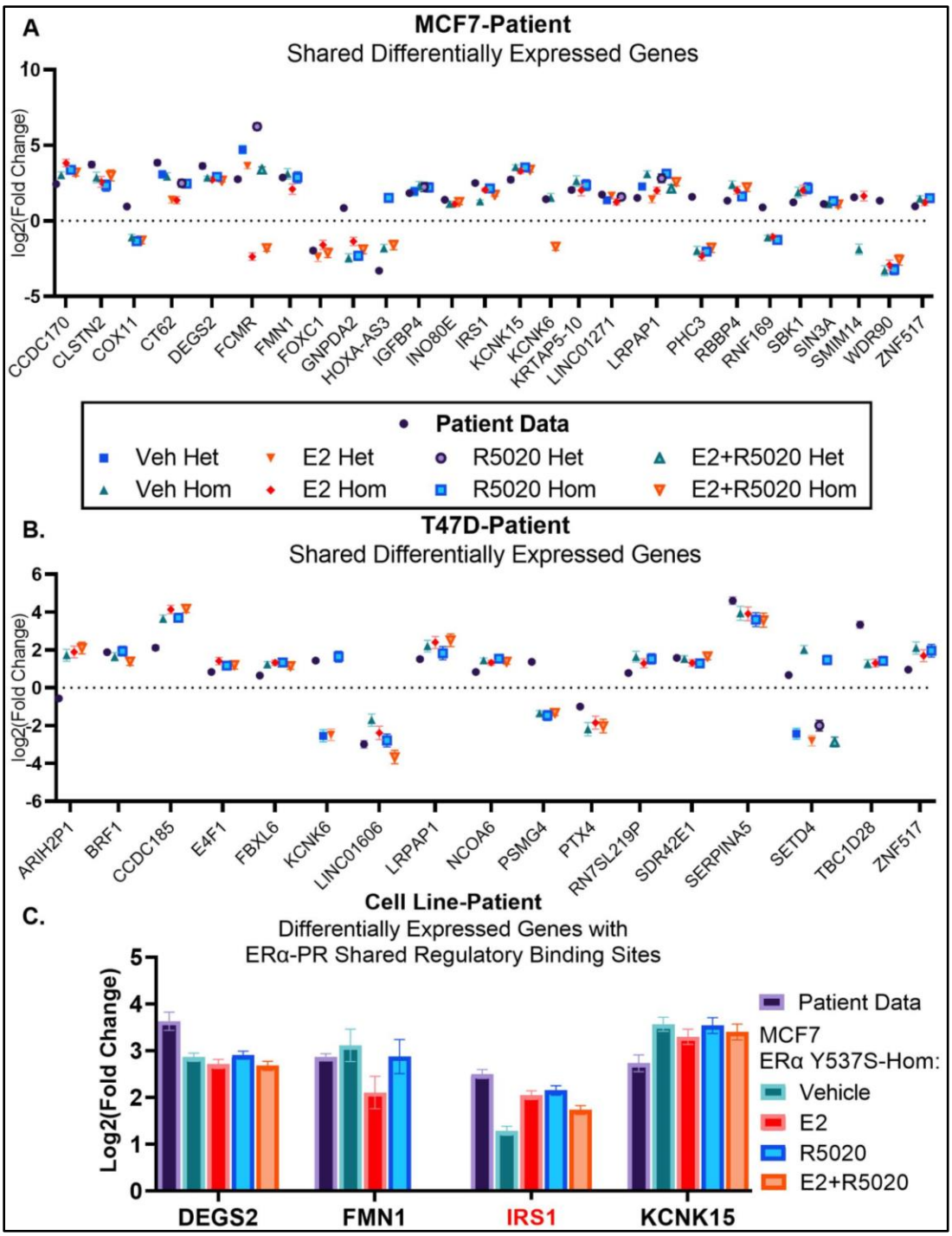

Figure 4.8: Patient breast cancers harboring ERα Y537S mutations share differential expression of several potential shared ERα/PR genes with immortalized cell lines. Log_2(fold change) of differentially expressed genes shared between ERα Y537S-expressing patient tumor transcriptome data and A) MCF7 and B) T47D cell lines. Of those, differential expression of genes with potential shared ERα/PR regulatory binding sites, as defined by Khushi et al. (2014), is depicted in C. Significantly differentially expressed genes are those with $p < 0.05$ and $| \log_2(\text{fold change}) | > 1$, where fold change is relative to matched tumors or cell lines expressing ERα WT. Data represent the average of 3 biological replicates.

To assess the functional significance of upregulated expression of *DEGS2*, *FMN1*, *IRS1*, and *KCNK15* in the context of the ERα Y537S mutation, I conducted a siRNA knockdown screen of each to determine if depletion affected the proliferation of MCF7 and T47D cells expressing ERα WT, ERα Y537S-het, or ERα Y537S-hom. Overall, knockdown of IRS1 resulted in the most significant decrease in proliferation of both MCF7 and T47D cells expressing ERα Y537S, with particularly consistent decreased proliferation in the context of the homozygous mutation (Fig. 4.9). This sensitivity to IRS1 depletion was largely specific to the context of the ERα Y537S mutation; apart from hormone-deprived and E2-stimulated T47D ERα WT cells, knockdown of IRS1 did not affect proliferation of any ERα WT cells (Fig. 4.9). siRNA knockdown of several other shared patient-cell line differentially expressed genes showed ERα Y537S-specific effects on proliferation, which may be of potential future interest (Table 9, Table 10). However, IRS1 was the only candidate gene that 1) is significantly upregulated in terms of RNA expression in both patient tumors and cell lines expressing ERα Y537S, 2) contains potential ERα-PR shared regulatory binding events based on Khushi et al. (2014), and 3) significantly reduces proliferation upon knockdown, specifically in ERα Y537S-expressing cells. Additionally, previous studies implicate IRS1 in crosstalk interactions with both ERα and PR, as well as pro-proliferative signaling in breast cancer [167, 169-172]. Thus, IRS1 became the focus as an ideal target for assessing the effect of ERα Y537S on ERα/PR crosstalk.

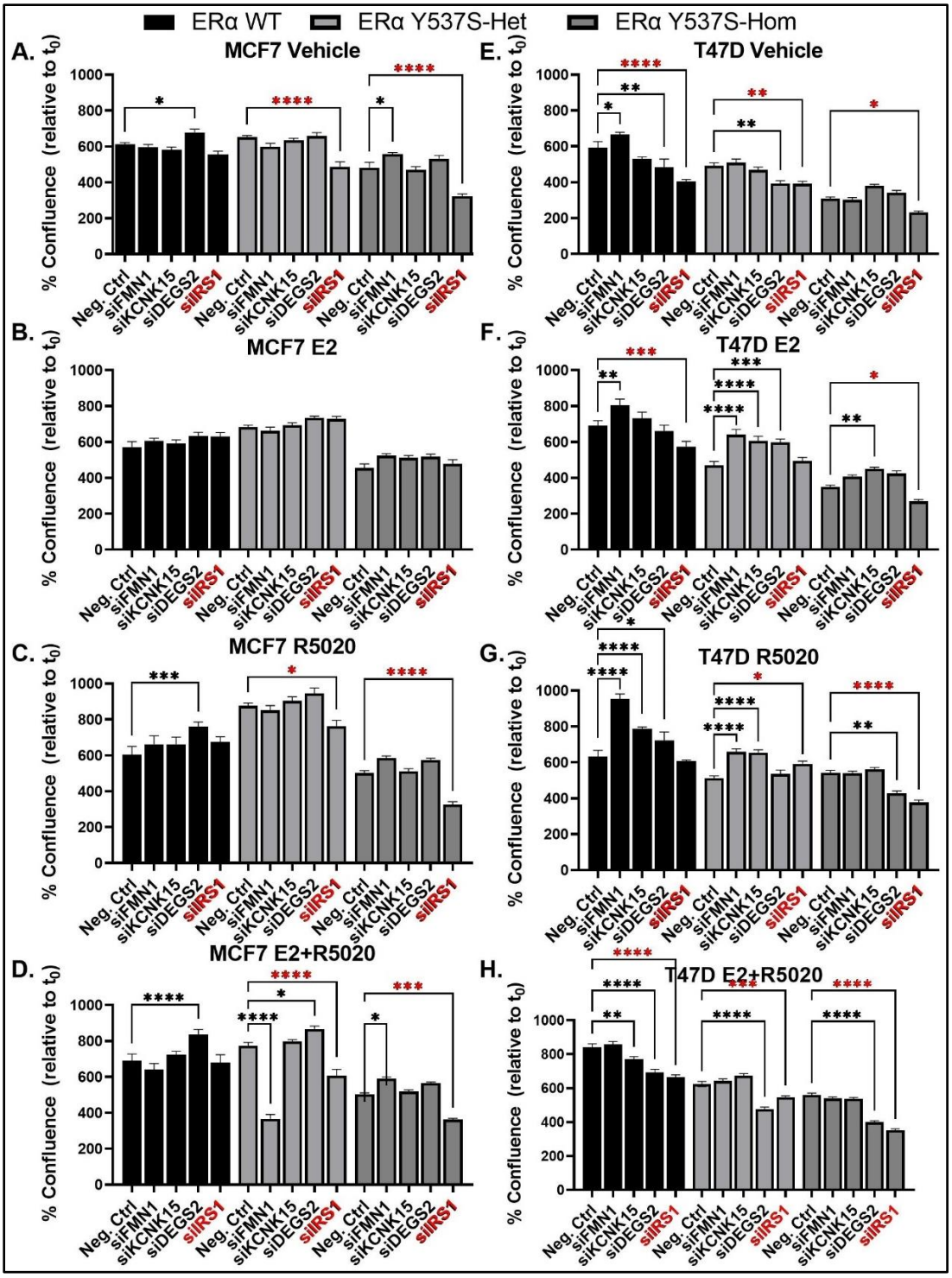

Figure 4.9: IRS1 depletion results in decreased proliferation in cells expressing ERα Y537S. Proliferation, as measured by % cell confluence relative to the initial timepoint (t_0), upon siRNA knockdown of candidate gene expression (*FMN1*, *KCNK15*, *DEGS2*, and *IRS1*) is shown in MCF7 (A-D) and T47D cell lines (E-H). Cell variants were treated with vehicle (hormone-deprived, A,E), 10nM E2 (B,F), 10nM R5020 (C,G), or both (D,H). Significant difference in % confluence relative to negative control is indicated as * $p < 0.05$, ** $p < 0.005$, *** $p < 0.0005$, or **** $p < 0.0001$.

MCF7 siRNA screen											
siRNA Target	Predicted Mean Diff. (NS1 - siRNA)	Adj. P-Value	siRNA Target	Predicted Mean Diff. (NS1 - siRNA)	Adj. P-Value	siRNA Target	Predicted Mean Diff. (NS1 - siRNA)	Adj. P-Value	siRNA Target	Predicted Mean Diff. (NS1 - siRNA)	Adj. P-Value
WT Vehicle			WT E2			WT R5020			WT E2+R5020		
SDR42E1	94.01	0.0043	KCNK6	141.5	0.0002	LRPAP1	310.9	<0.0001	SDR42E1	213.4	<0.0001
LRPAP1	281.3	<0.0001				CCDC170	-125.3	0.0109	CLSTN2	126.2	<0.0001
SETD4	103.8	0.0009				INO80E	-133.5	0.0045	LRPAP1	398.1	<0.0001
KCNK6	283.8	<0.0001				KCNK6	308.1	<0.0001	CCDC170	-138.7	<0.0001
COX11	192.7	<0.0001				NCOA6	-134.8	0.0039	INO80E	-86.99	0.0164
KRTAP5-10	145.9	<0.0001				CCDC185	-125.2	0.011	KCNK6	430.3	<0.0001
RBBP4	214.4	<0.0001				TBC1D28	156.6	0.0003	COX11	424.3	<0.0001
TBC1D28	261	<0.0001				ZNF517	-163.7	0.0001	SMIM14	448.2	<0.0001
SERP1NA5	98.9	0.0019				DEGS2	-156.8	0.0003	PHC3	94.97	0.0051
SIN3A	178.8	<0.0001				WDR90	-150.3	0.0006	E4F1	89.05	0.0123
FCMR	82.65	0.0232				FCMR	125.3	0.0109	RBBP4	179	<0.0001
BRF1	113.2	0.0001				IGFBP4	-135.7	0.0035	CT62	334.4	<0.0001
									TBC1D28	308.4	<0.0001
									FBXC6	152	<0.0001
									SERP1NA5	436.7	<0.0001
									DEGS2	-145.9	<0.0001
									WDR90	-114	0.0002
									FOXC1	242.8	<0.0001
									SIN3A	104.4	0.0011
									FCMR	272.7	<0.0001
									GNPDA2	111.5	0.0003
									BRF1	149	<0.0001
									IGFBP4	-81.9	0.0326
Het Vehicle			Het E2			Het R5020			Het E2+R5020		
SDR42E1	301.1	<0.0001	SMIM14	315.2	<0.0001	SDR42E1	276.1	<0.0001	FMN1	407	<0.0001
LRPAP1	467.1	<0.0001				CLSTN2	171.8	<0.0001	SDR42E1	526.4	<0.0001
KCNK6	412	<0.0001				LRPAP1	525.7	<0.0001	CLSTN2	263.7	<0.0001
COX11	470.4	<0.0001				SETD4	167.1	<0.0001	LRPAP1	514.5	<0.0001
CCDC185	129.3	<0.0001				KCNK6	393.3	<0.0001	CCDC170	124.3	<0.0001
SMIM14	490.2	<0.0001				COX11	380.3	<0.0001	SETD4	375.4	<0.0001
PHC3	94.01	0.0043				CCDC185	312.6	<0.0001	KCNK6	497.2	<0.0001
RBBP4	190.7	<0.0001				SMIM14	709	<0.0001	COX11	578	<0.0001
CT62	360.9	<0.0001				PHC3	212.1	<0.0001	NCOA6	121.9	<0.0001
TBC1D28	200.1	<0.0001				E4F1	177.8	<0.0001	CCDC185	643.6	<0.0001
FBXC6	157.5	<0.0001				RBBP4	397.1	<0.0001	KRTAP5-10	396.9	<0.0001
SERP1NA5	341.8	<0.0001				CT62	607.3	<0.0001	SMIM14	669.5	<0.0001
RNF169	180.6	<0.0001				PTX4	-134.8	0.0039	PHC3	427.1	<0.0001
IRS1	163.9	<0.0001				TBC1D28	287.3	<0.0001	E4F1	175.7	<0.0001
FOXC1	274.3	<0.0001				FBXC6	154.5	0.0004	RBBP4	574.9	<0.0001
SIN3A	293.4	<0.0001				SERP1NA5	650.2	<0.0001	CT62	672.2	<0.0001
FCMR	343.9	<0.0001				RNF169	225.1	<0.0001	PTX4	112.1	0.0003
GNPDA2	210.4	<0.0001				IRS1	113.6	0.0343	TBC1D28	348.3	<0.0001
						FOXC1	336.1	<0.0001	ZNF517	-82.15	0.0315
						SIN3A	336	<0.0001	FBXC6	376.6	<0.0001
						FCMR	436.2	<0.0001	SERP1NA5	668.9	<0.0001
						GNPDA2	214.6	<0.0001	DEGS2	-93.16	0.0067
						BRF1	138.5	0.0025	RNF169	419.9	<0.0001
									IRS1	167	<0.0001
									FOXC1	404.2	<0.0001
									SIN3A	653.3	<0.0001
									FCMR	613.5	<0.0001
									SBK1	166.9	<0.0001
									GNPDA2	551.2	<0.0001
									BRF1	399.4	<0.0001
									IGFBP4	432.8	<0.0001
Hom Vehicle			Hom E2			Hom R5020			Hom E2+R5020		
SETD4	197	<0.0001	SETD4	103.9	0.0252	SDR42E1	-117	0.0249	FMN1	-87.61	0.0151
CCDC185	85.65	0.0153	NCOA6	-102.4	0.0296	SETD4	243.4	<0.0001	SDR42E1	-157.2	<0.0001
E4F1	205.4	<0.0001	BRF1	-118.5	0.0046	E4F1	250.7	<0.0001	LRPAP1	-93.97	0.0059
IRS1	158.9	<0.0001				RBBP4	125.6	0.0106	CCDC170	-92.21	0.0077
						IRS1	176.8	<0.0001	SETD4	247.2	<0.0001
									NCOA6	-127.8	<0.0001
									E4F1	256.9	<0.0001
									RBBP4	102.2	0.0016
									PTX4	-136	<0.0001
									IRS1	141	<0.0001
									BRF1	-103	0.0014

Table 9: Significant changes to MCF7 cell proliferation from siRNA candidate gene screen

T47D siRNA screen												
siRNA Target	Predicted Mean Diff. (NS1 - siRNA)	Adj. P-Value	siRNA Target	Predicted Mean Diff. (NS1 - siRNA)	Adj. P-Value	siRNA Target	Predicted Mean Diff. (NS1 - siRNA)	Adj. P-Value	siRNA Target	Predicted Mean Diff. (NS1 - siRNA)	Adj. P-Value
WT Vehicle			WT E2			WT R5020			WT E2+R5020		
FMN1	-73.79	0.0486	FMN1	-113.8	0.0051	FMN1	-323	<0.0001	SDR42E1	-80.16	0.0021
SDR42E1	-173.1	<0.0001	SDR42E1	-222.3	<0.0001	SDR42E1	-398.1	<0.0001	INO80E	164.7	<0.0001
LRPAP1	-172	<0.0001	CLSTN2	-112.5	0.0061	KCNK15	-157	<0.0001	SETD4	497.4	<0.0001
INO80E	-96.38	0.0015	CCDC170	-179.6	<0.0001	CLSTN2	-300.8	<0.0001	COX11	98.56	<0.0001
SETD4	463.5	<0.0001	SETD4	383.4	<0.0001	LRPAP1	-298.7	<0.0001	NCOA6	-67.98	0.0205
COX11	-92.3	0.003	KCNK6	-139.1	0.0001	CCDC170	-251.3	<0.0001	CCDC185	-128.9	<0.0001
KRTAP5-10	114.4	<0.0001	COX11	112.6	0.0059	INO80E	-145.6	0.0005	KRTAP5-10	182.5	<0.0001
SMIM14	246.7	<0.0001	NCOA6	-101.2	0.0232	SETD4	228	<0.0001	SMIM14	148.8	<0.0001
PHC3	168.5	<0.0001	CCDC185	-203.2	<0.0001	KCNK6	-197.7	<0.0001	PHC3	227.9	<0.0001
E4F1	246	<0.0001	KRTAP5-10	123.3	0.0015	COX11	-196.4	<0.0001	E4F1	353	<0.0001
RBBP4	353.4	<0.0001	SMIM14	130.9	0.0005	NCOA6	-205.1	<0.0001	RBBP4	452.6	<0.0001
PTX4	-139.7	<0.0001	PHC3	178.1	<0.0001	CCDC185	-285.5	<0.0001	PTX4	-146.3	<0.0001
TBC1D28	152.7	<0.0001	E4F1	215.4	<0.0001	E4F1	173.1	<0.0001	TBC1D28	180.1	<0.0001
FBXC6	-150.5	<0.0001	RBBP4	384	<0.0001	RBBP4	327.5	<0.0001	SERP1NA5	191.9	<0.0001
SERP1NA5	114.9	<0.0001	PTX4	-208.1	<0.0001	CT62	-203.5	<0.0001	DEGS2	109.1	<0.0001
DEGS2	108.2	0.0002	TBC1D28	183	<0.0001	PTX4	-348.3	<0.0001	RNF169	290.7	<0.0001
RNF169	315.9	<0.0001	ZNF517	-139	0.0001	ZNF517	-169.3	<0.0001	WDR90	73.96	0.007
IRS1	189.1	<0.0001	SERP1NA5	151.1	<0.0001	FBXC6	-259.7	<0.0001	IRS1	138.3	<0.0001
FOXC1	-139.2	<0.0001	RNF169	285.1	<0.0001	RNF169	122.7	0.0076	FOXC1	-156.8	<0.0001
GNPDA2	-114.2	<0.0001	IRS1	119.2	0.0025	FOXC1	-499.6	<0.0001	SIN3A	269.1	<0.0001
BRF1	-233.1	<0.0001	FOXC1	-239.2	<0.0001	GNPDA2	-205.4	<0.0001	FCMR	64.3	0.0374
IGFBP4	-177	<0.0001	SIN3A	123.6	0.0014	BRF1	-339.4	<0.0001	SBK1	68.7	0.0181
			SBK1	271.9	<0.0001	IGFBP4	-270.8	<0.0001			
			GNPDA2	-95.93	0.0412						
			BRF1	-129.4	0.0006						
			IGFBP4	-96.88	0.0373						
Het Vehicle			Het E2			Het R5020			Het E2+R5020		
SDR42E1	-147.2	<0.0001	FMN1	-170.8	<0.0001	FMN1	-146.3	0.0004	SDR42E1	-94.21	<0.0001
SETD4	343.4	<0.0001	SDR42E1	-338.5	<0.0001	SDR42E1	-320.6	<0.0001	KCNK15	-61.73	0.0494
COX11	126.4	<0.0001	KCNK15	-137.2	0.0002	KCNK15	-142.1	0.0007	CLSTN2	-114.8	<0.0001
KRTAP5-10	151	<0.0001	CLSTN2	-157.5	<0.0001	CLSTN2	-218.4	<0.0001	INO80E	155.8	<0.0001
SMIM14	165	<0.0001	LRPAP1	-145.7	<0.0001	CCDC170	-116.3	0.0151	SETD4	272.4	<0.0001
PHC3	182.7	<0.0001	CCDC170	-215.7	<0.0001	SETD4	180	<0.0001	COX11	137.3	<0.0001
E4F1	210.9	<0.0001	SETD4	235.3	<0.0001	CCDC185	-253.4	<0.0001	CCDC185	-179	<0.0001
RBBP4	279.3	<0.0001	KCNK6	-258.5	<0.0001	E4F1	126.7	0.0048	SMIM14	65.46	0.027
CT62	83.03	0.0132	NCOA6	-135.9	0.0002	RBBP4	223.8	<0.0001	PHC3	158.3	<0.0001
TBC1D28	142.9	<0.0001	CCDC185	-233.2	<0.0001	CT62	-117	0.0141	E4F1	284.3	<0.0001
FBXC6	-124.7	<0.0001	RBBP4	200.1	<0.0001	PTX4	-131.6	0.0027	RBBP4	315.1	<0.0001
SERP1NA5	81.79	0.0159	CT62	-179.9	<0.0001	ZNF517	-117.7	0.0131	CT62	-74.08	0.0056
DEGS2	99.75	0.0008	ZNF517	-177.4	<0.0001	RNF169	141.4	0.0008	PTX4	-112.6	<0.0001
RNF169	274.8	<0.0001	FBXC6	-207.7	<0.0001	FOXC1	-144.4	0.0005	TBC1D28	156.7	<0.0001
IRS1	100	0.0008	DEGS2	-128	0.0008	FCMR	-135.9	0.0016	SERP1NA5	67.3	0.0197
SIN3A	107.4	0.0002	RNF169	188.8	<0.0001	SBK1	-116.9	0.0143	DEGS2	136	<0.0001
IGFBP4	-86.7	0.0075	FOXC1	-258.1	<0.0001	BRF1	-206.9	<0.0001	RNF169	197.3	<0.0001
			GNPDA2	-186.9	<0.0001	IGFBP4	-199	<0.0001	WDR90	94.57	<0.0001
			BRF1	-240.5	<0.0001				IRS1	66.76	0.0216
			IGFBP4	-137.5	0.0002				SIN3A	148.6	<0.0001
									SBK1	-116.6	<0.0001
Hom Vehicle			Hom E2			Hom R5020			Hom E2+R5020		
SDR42E1	-137.2	<0.0001	SDR42E1	-220.6	<0.0001	SDR42E1	-108.2	0.0345	LRPAP1	79.86	0.0022
INO80E	-129.8	<0.0001	KCNK15	-100	0.0266	SETD4	287.1	<0.0001	CCDC170	81.14	0.0017
SETD4	198.7	<0.0001	LRPAP1	-133.7	0.0003	COX11	217	<0.0001	INO80E	95.33	<0.0001
KCNK6	-86.02	0.0083	CCDC170	-103	0.0189	SMIM14	176	<0.0001	SETD4	318.8	<0.0001
CCDC185	-73.62	0.0497	INO80E	-143.1	<0.0001	PHC3	141.1	0.0008	COX11	217.5	<0.0001
SMIM14	115.6	<0.0001	SETD4	163.4	<0.0001	E4F1	342.3	<0.0001	SMIM14	232.1	<0.0001
E4F1	180	<0.0001	KCNK6	-191.4	<0.0001	RBBP4	335.8	<0.0001	PHC3	191.1	<0.0001
RBBP4	132.8	<0.0001	CCDC185	-134.5	0.0003	TBC1D28	275.1	<0.0001	E4F1	342.5	<0.0001
PTX4	-89.42	0.0048	E4F1	144.2	<0.0001	SERP1NA5	168.5	<0.0001	RBBP4	323.6	<0.0001
TBC1D28	130.9	<0.0001	RBBP4	132.1	0.0004	DEGS2	115	0.0175	TBC1D28	294.7	<0.0001
RNF169	82.91	0.0134	PTX4	-105	0.0151	RNF169	180.7	<0.0001	FBXC6	139.6	<0.0001
IRS1	76.44	0.034	FBXC6	-114.9	0.0044	WDR90	130.8	0.0029	SERP1NA5	161.8	<0.0001
SIN3A	93.67	0.0023	FOXC1	-155.6	<0.0001	IRS1	166.3	<0.0001	DEGS2	159.8	<0.0001
SBK1	125.1	<0.0001	SBK1	99.92	0.0268	FOXC1	-123.5	0.0069	RNF169	204.1	<0.0001
BRF1	-136.9	<0.0001	BRF1	-162	<0.0001	SIN3A	252	<0.0001	WDR90	188.2	<0.0001
IGFBP4	-84.22	0.011	IGFBP4	-157	<0.0001	SBK1	126	0.0052	IRS1	206.7	<0.0001
									SIN3A	295.6	<0.0001
									FCMR	102.6	<0.0001
									GNPDA2	117.9	<0.0001
									BRF1	99.63	<0.0001

Table 10: Significant changes to T47D cell proliferation from siRNA candidate gene screen

Occupation of ERα and PR at *IRS1* regulatory binding sites is altered in the context of the ERα Y537S mutation

To determine if differential expression of *IRS1* in the context of the ERα Y537S mutation could be a result of altered ERα/PR crosstalk, I next assessed ERα and PR genomic binding at three chromatin binding sites referred to here as IRS1-3 (distal location, contains both an ERE half site and a PRE half site), IRS1-TSS (proximal location near transcription start site (TSS), contains a PRE half site) and IRS1-Protein (proximal location near protein coding region, contains a PRE half site). In both hormone-deprived MCF7 and T47D cells, ERα and PR chromatin occupancy at IRS1-3 increased significantly in the context of ERα Y537S-hom compared to either ERα WT or Y537S-het (Fig. 4.10a,b, Fig. 4.11a,b). This suggests that the ERα Y537S mutation not only alters the transcription factor activity of ERα but also that of PR. In hormone-deprived conditions, ERα and PR chromatin occupancy at IRS1-TSS and IRS1-Protein was only increased in MCF7 ERα Y537S-het cells, suggesting a more limited role of these binding sites in regulating IRS1 expression through ERα/PR-dependent mechanisms (Fig. 4.10c-f, Fig. 4.11c-f). Importantly, these ERα Y537S-associated increases in PR chromatin occupancy at *IRS1* occur despite the absence of PR ligand, highlighting a role of ERα Y537S in driving hormone-independent PR activity. It should be noted, however, that E2 and/or R5020 treatment (in some cases) facilitates a further increase in ERα and PR chromatin occupancy at *IRS1* (Fig. 4.10, Fig. 4.11).

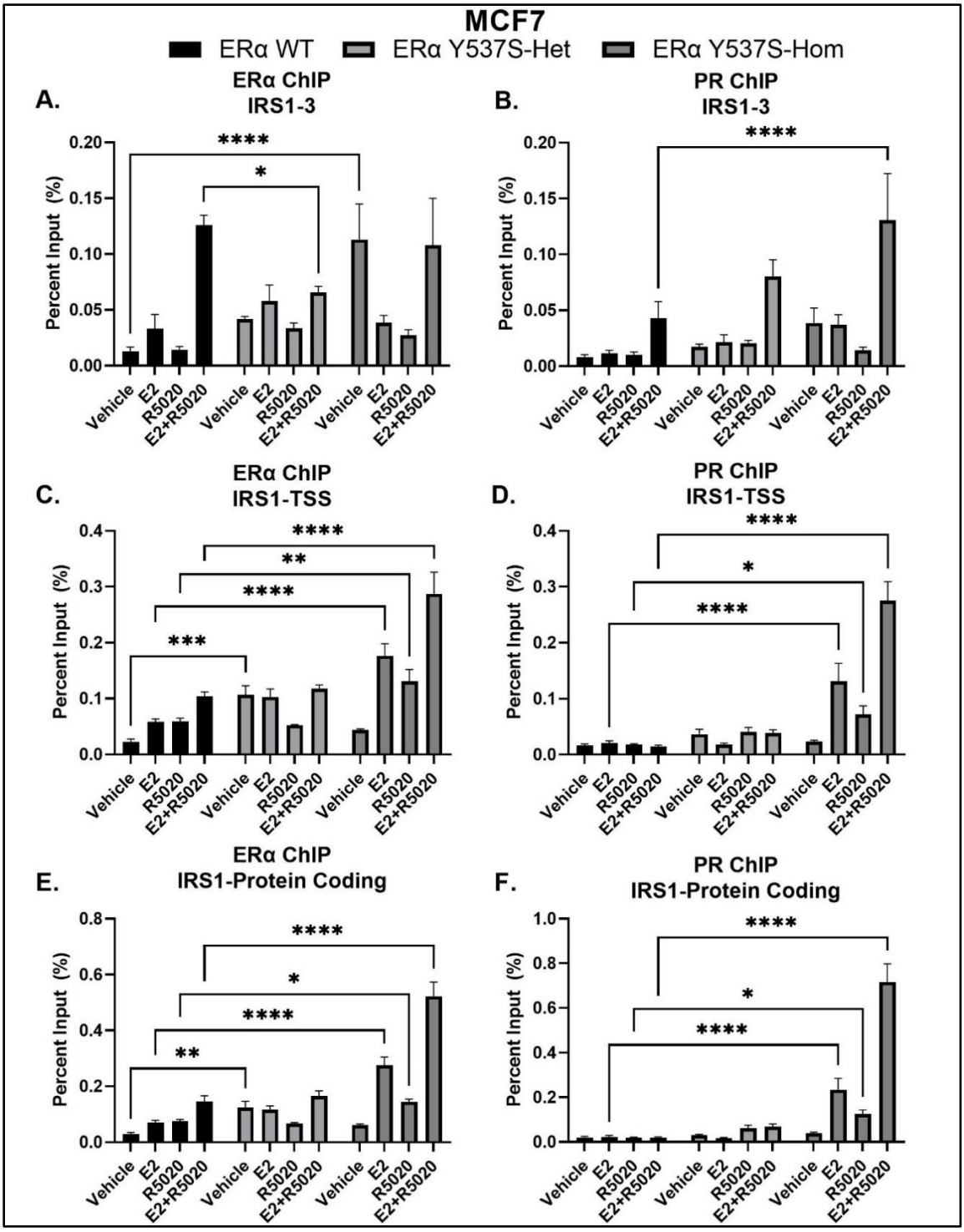

Figure 4.10: ERα and PR chromatin binding at *IRS1* is altered in MCF7 cells expressing ERα Y537S. Chromatin binding of ERα (A, C, and E) and PR (B, D, and F) at three distinct regions of IRS1 in MCF7 cell variants. Chromatin regions include A,B) IRS1-3 (distal location, contains both an ERE half site and a PRE half site), C,D) IRS1-TSS (proximal location near TSS, contains a PRE half site), and E,F) IRS1-Protein (proximal location near protein coding region, contains a PRE half site). Data represents the % of input chromatin analyzed. Significant difference relative to ERα WT is indicated as * $p < 0.05$, ** $p < 0.005$, *** $p < 0.0005$, or **** $p < 0.0001$.

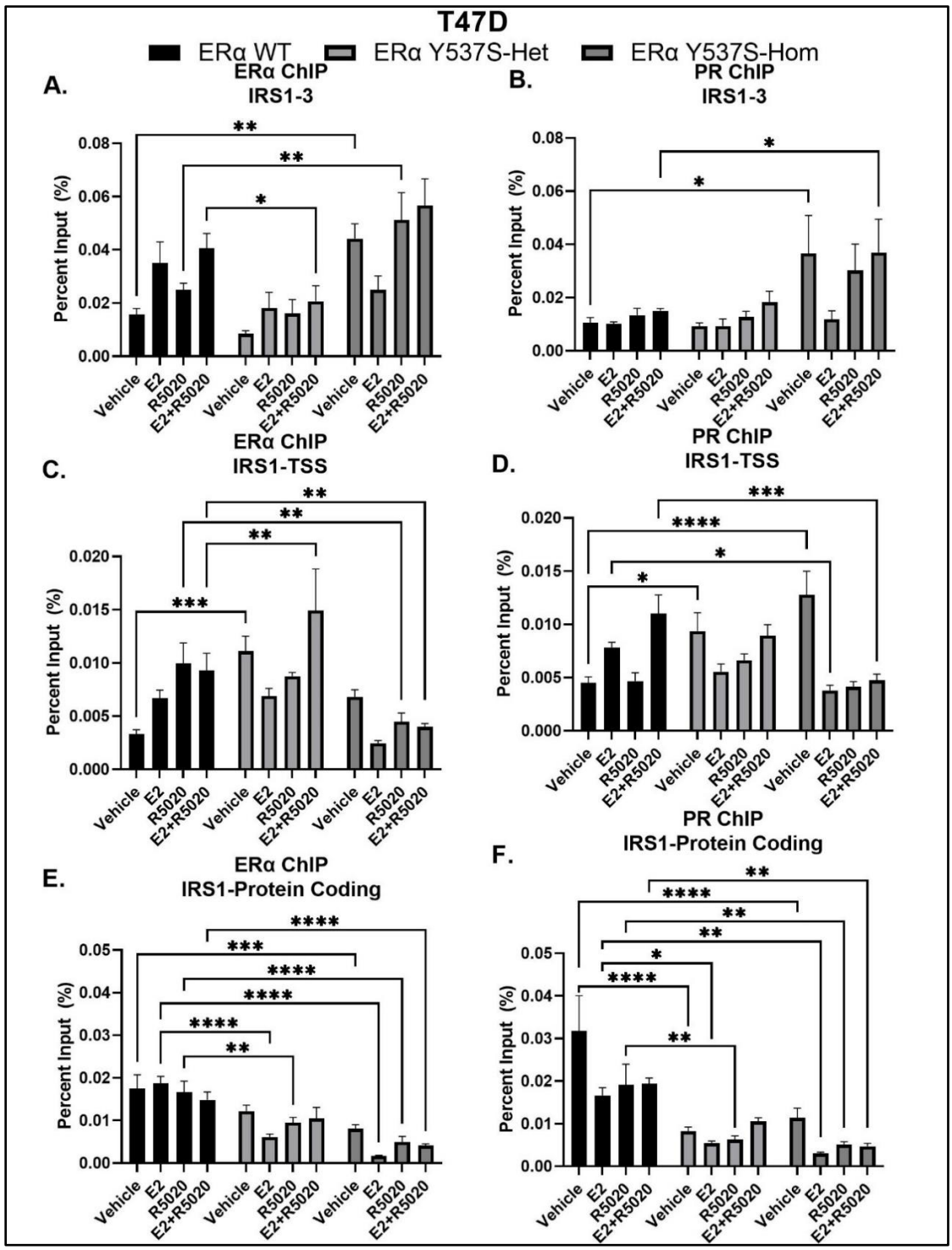

Figure 4.11: ERα and PR chromatin binding at *IRS1* is altered in T47D cells expressing ERα Y537S. Chromatin binding of ERα (A, C, and E) and PR (B, D, and F) at three distinct regions of IRS1 in T47D cell variants. Chromatin regions include A,B) IRS1-3 (distal location, contains both an ERE half site and a PRE half site), C,D) IRS1-TSS (proximal location near TSS, contains a PRE half site), and E,F) IRS1-Protein (proximal location near protein coding region, contains a PRE half site). Data represents the % of input chromatin analyzed. Significant difference relative to ERα WT is indicated as * $p < 0.05$, ** $p < 0.005$, *** $p < 0.0005$, or **** $p < 0.0001$.

While ERα Y537S-associated changes to ERα/PR crosstalk as related to chromatin occupancy of the two transcription factors is novel on its own, I next assessed the expression of IRS1 to determine if these cistromal changes translated to altered RNA and protein expression. As noted previously, *IRS1* mRNA was expressed 2.5- to 4.4-fold higher in MCF7 ERα Y537S-hom cells than MCF7 ERα WT (Fig. 4.8c, *fold change* = 2^y), but was not significantly differentially expressed in T47D cells. Interestingly, at the protein level, IRS1 was significantly increased in T47D ERα Y537S-hom cells relative to ERα WT, but remained stable in MCF7 cell variants, regardless of hormone treatment (Fig. 4.12). This observed stability may be due to an increased rate of protein turnover indicative of high activity, as is also observed with ERα expression in response to E2 in MCF7 cells but not in T47D cells (Fig. 4.13, Fig. 4.14)[173-175].

Phospho-Ser307 IRS1 expression (pIRS1) was also increased in T47D ERα Y537S-hom cells and stable in MCF7 ERα Y537S cells (Fig. 4.12c,f). pIRS1 uncouples IRS1 from the insulin receptor as part of a negative feedback loop to regulate signal duration in an active signaling pathway [172, 176]. In some cases, but not all, this results in ubiquitination and degradation of pIRS1 [172, 176]. The unchanged levels of pIRS1 observed in MCF7 cells correlate with steady IRS1 degradation whereas high pIRS1 levels in T47D ERα Y537S-hom cells suggest accumulation. Both cases indicate a cell-line specific, yet similarly active, ERα Y537S-associated signaling pathway by which IRS1 regulates downstream signaling for the IR/IGF-1R pathway, resulting in increased cell proliferation.

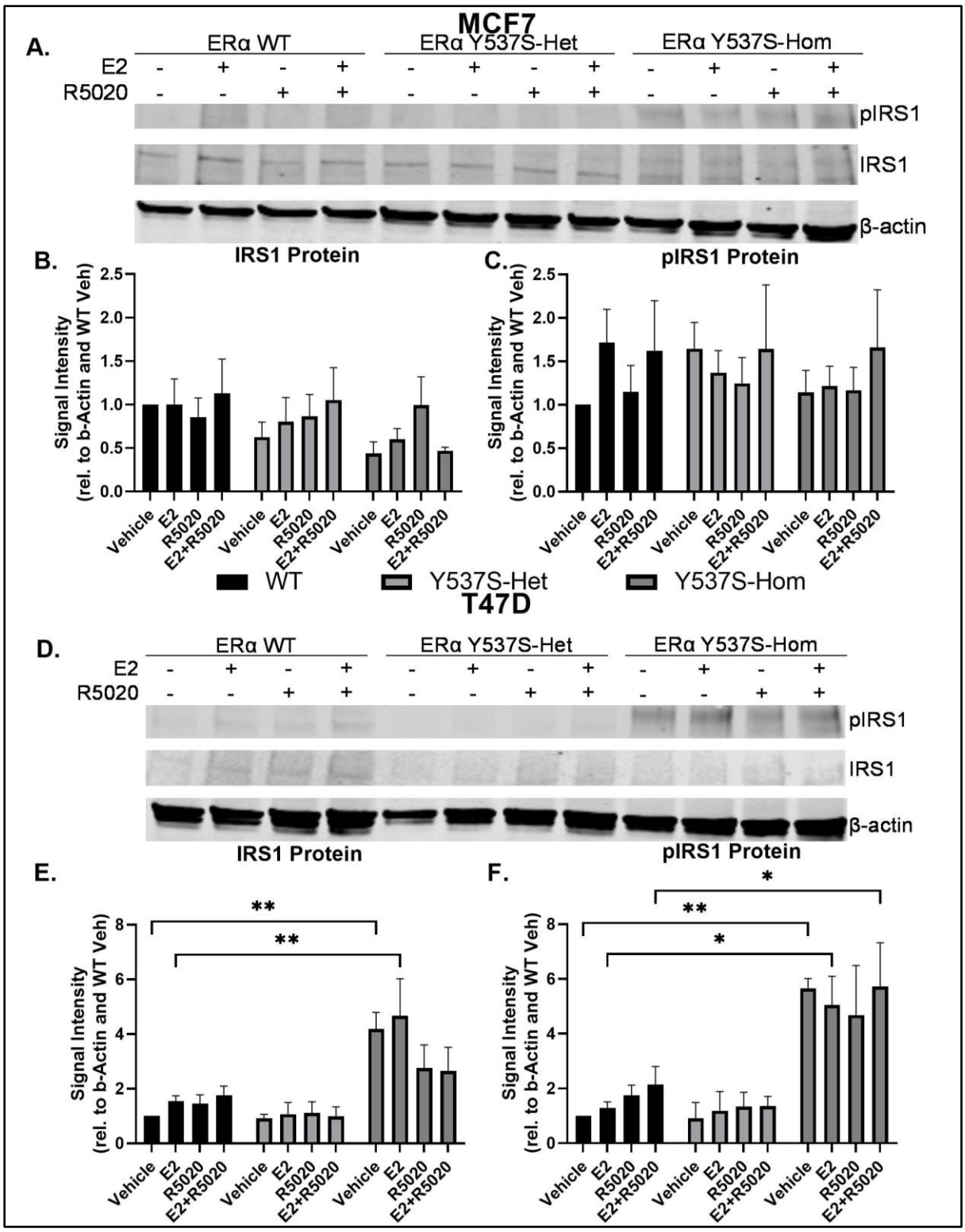

Figure 4.12: IRS1 protein expression is altered in the context of ERα Y537S in T47D cells. Cytoplasmic protein expression of total IRS1 and pIRS1 (phospho-Ser307) normalized to β-actin loading control for A-C) MCF7 and D-F) T47D ERα cell variants. Significant difference in protein expression relative to ERα WT is indicated as * $p < 0.05$, ** $p < 0.005$, *** $p < 0.0005$, or **** $p < 0.0001$.

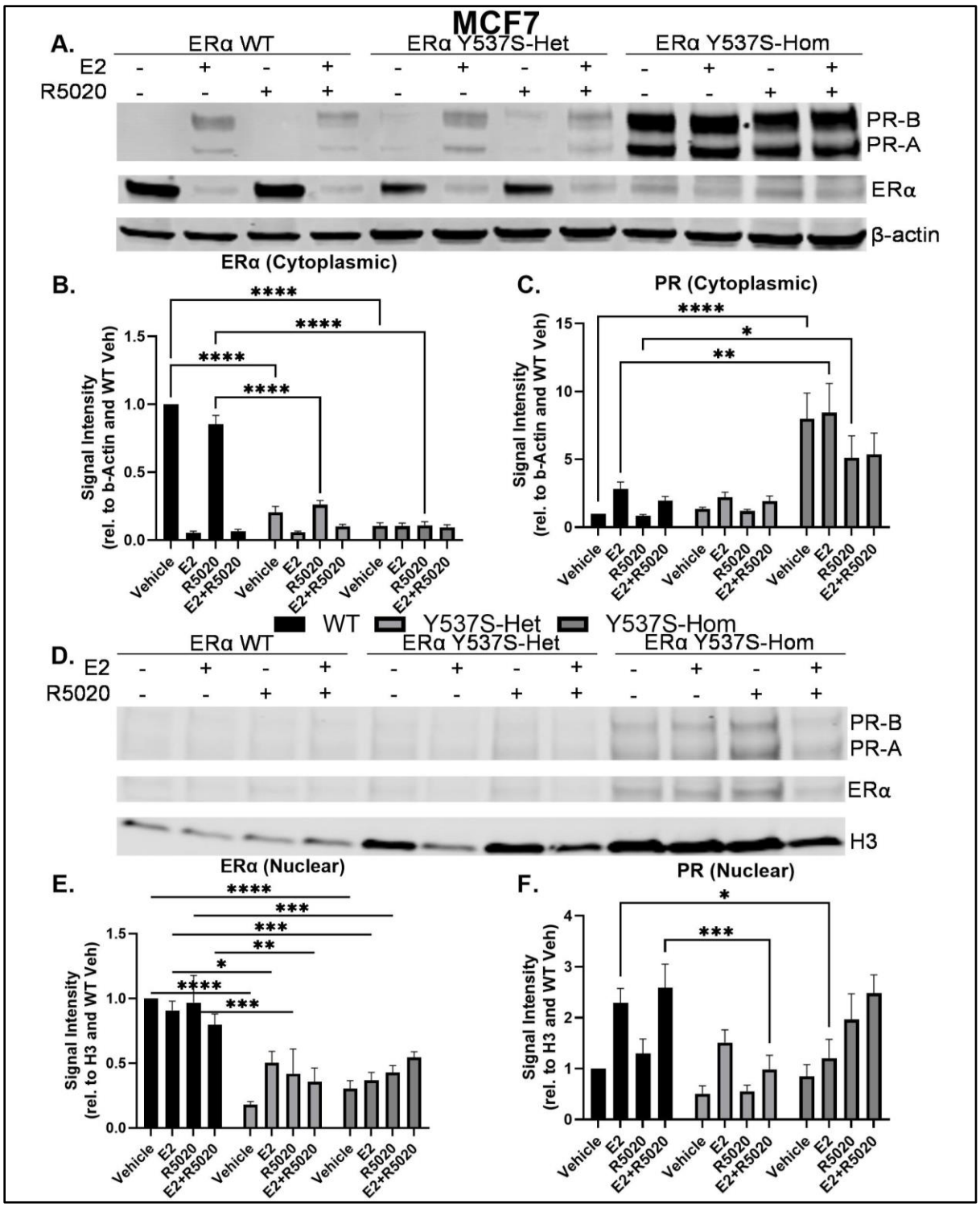

Figure 4.13: ERα and PR protein levels in MCF7 cells indicate high activity and rapid turnover of ERα Y537S. A-C) Cytoplasmic and D-F) nuclear protein expression of ERα (B,E) and PR (C,F) in MCF7 ERα cell variants. Cytoplasmic protein expression is normalized to β-actin loading control and nuclear protein expression is normalized to Histone 3 (H3) loading control. Significant difference in protein expression relative to ERα WT is indicated as * $p < 0.05$, * $p < 0.005$, *** $p < 0.0005$, or **** $p < 0.0001$.

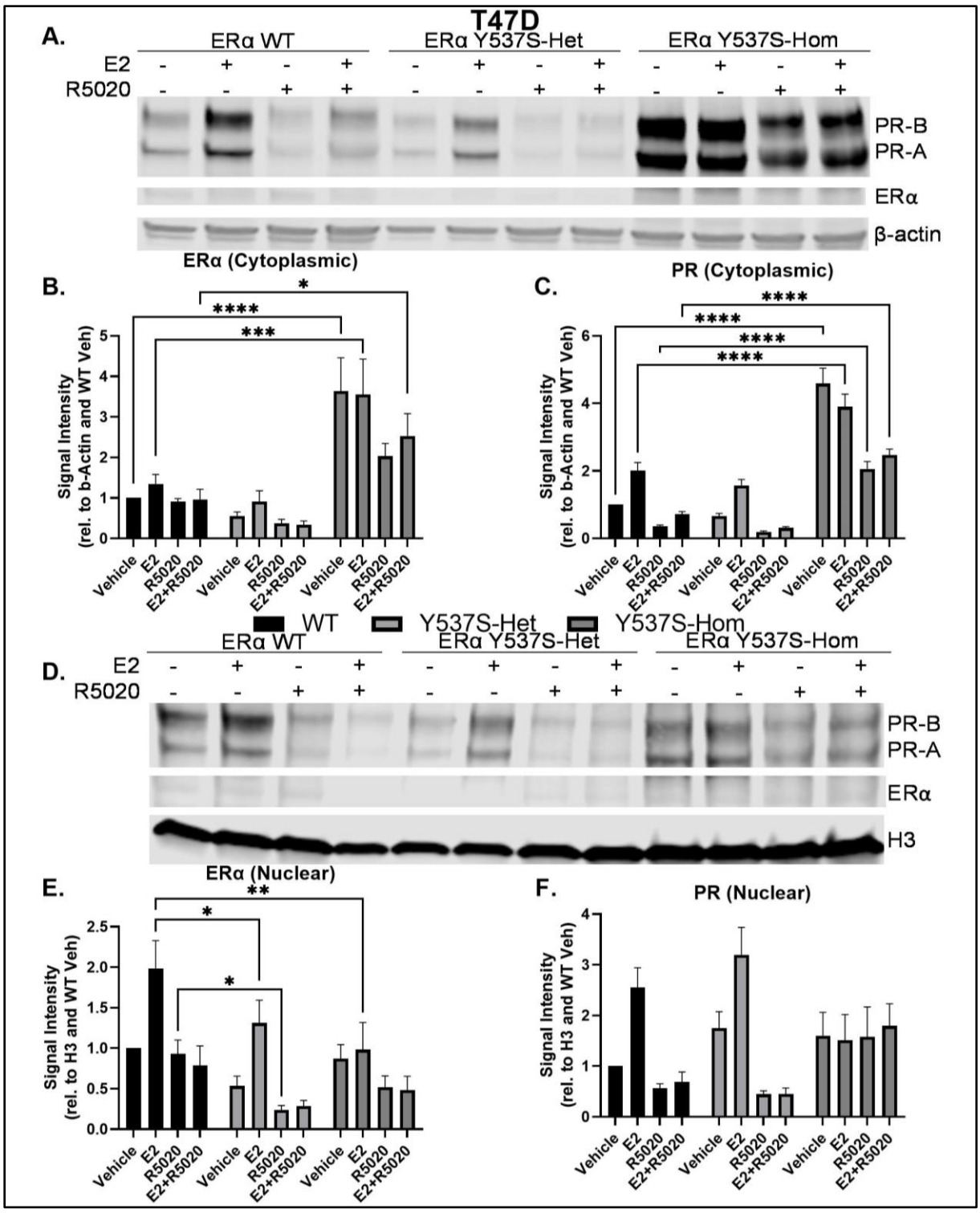

Figure 4.14: ERα and PR protein levels in T47D cells indicate high activity without rapid turnover of ERα Y537S. A-C) Cytoplasmic and D-F) nuclear protein expression of ERα (B,E) and PR (C,F) in T47D ERα cell variants. Cytoplasmic protein expression is normalized to β-actin loading control and nuclear protein expression is normalized to Histone 3 (H3) loading control. Significant difference in protein expression relative to ERα WT is indicated as * $p < 0.05$, * $p < 0.005$, *** $p < 0.0005$, or **** $p < 0.0001$.

Inhibition of IRS1 by NT157 depletes the proliferative effect of the ERα Y537S mutation

Due to the antiproliferative effect of IRS1 knockdown in MCF7 and T47D cells expressing ERα Y537S, I next investigated if NT-157, a small molecule inhibitor of IRS1, would similarly reduce cell growth. NT-157 functions by degrading IRS1/2, leading to the inhibition of IGF-1R/IRS1/2, PI3K, and AXL-mediated signaling pathways [172, 177, 178]. NT-157 reduces *in vitro* cell growth and *in vivo* tumor growth in models of uveal melanoma, chronic myeloid leukemia, myeloproliferative neoplasms, osteosarcoma, and prostate cancer [178-183]. Additionally, preliminary studies have found NT-157 to inhibit proliferation in breast cancer cell lines, including those resistant to tamoxifen [167, 184]. Though NT-157 has yet to be approved for use clinically, several IGF-1R inhibitors, including cixutumumab, have proved to be well-tolerated and effective in stabilizing several advanced cancers including Ewing's sarcoma and adrenocortical carcinoma [185-187].

As a single treatment, 5uM NT-157 effectively reduced the proliferation of all MCF7 and T47D ERα cell variants apart from MCF7 ERα Y537S-hom (Fig. 4.15). 5uM NT-157 falls within the range of effective doses used in preliminary studies in breast and prostate cancer cell lines (37, 38). To determine the efficacy of combining ET with IRS1 inhibition via NT-157, MCF7 and T47D ERα cell variant proliferation was assessed over 5 days of treatment with 100nM 4OHT (a SERM), 100nM Laso (a novel SERM), 1uM Ful (a SERD), 100nM CDB4124 (a SPRM), or 100nM PRA-027 (a SPRM), each alone or in combination with 5uM NT-157.

Across both MCF7 and T47D cell variants, proliferation was largely unaffected by treatment with 4OHT, and combined treatment with 4OHT and NT-157 did not improve inhibition beyond that of single NT-157 treatment (Fig. 4.15). In fact, NT-157 alone effectively reduced the proliferation of MCF7 and T47D ERα WT cells by more than 50%; combined treatment of NT-

157 with all SERMs/SERDs tested did little to enhance this inhibitory effect in the ERα WT context (Fig. 4.15a,b, black). MCF7 and T47D ERα Y537S-het cells were similarly responsive to NT-157 treatment as ERα WT cells and combination treatments did not add to the antiproliferative effect of NT-157 alone (Fig. 4.15a,b, pink). Interestingly, in both MCF7 and T47D ERα Y537S-hom cells, a combination of either lasofoxifene or fulvestrant with NT-157 resulted in additive inhibition beyond that of NT-157 alone (Fig. 4.15a,b, teal). While proliferation in response to CDB4124 and PRA-027 was also assessed, these SPRM compounds produced only a modest inhibitory effect in T47D ERα Y537S-hom cells and did not add to the antiproliferative effects of NT-157 treatment alone (Fig. 4.16). In fact, SPRM treatment increased proliferation somewhat in MCF7 ERα WT and ERα Y537S-hom cells (Fig. 4.16a). Overall, the striking effect of inhibition of IRS1 via NT-157, alone or in combination with lasofoxifene or fulvestrant, may offer a treatment avenue for ET-resistant breast cancers.

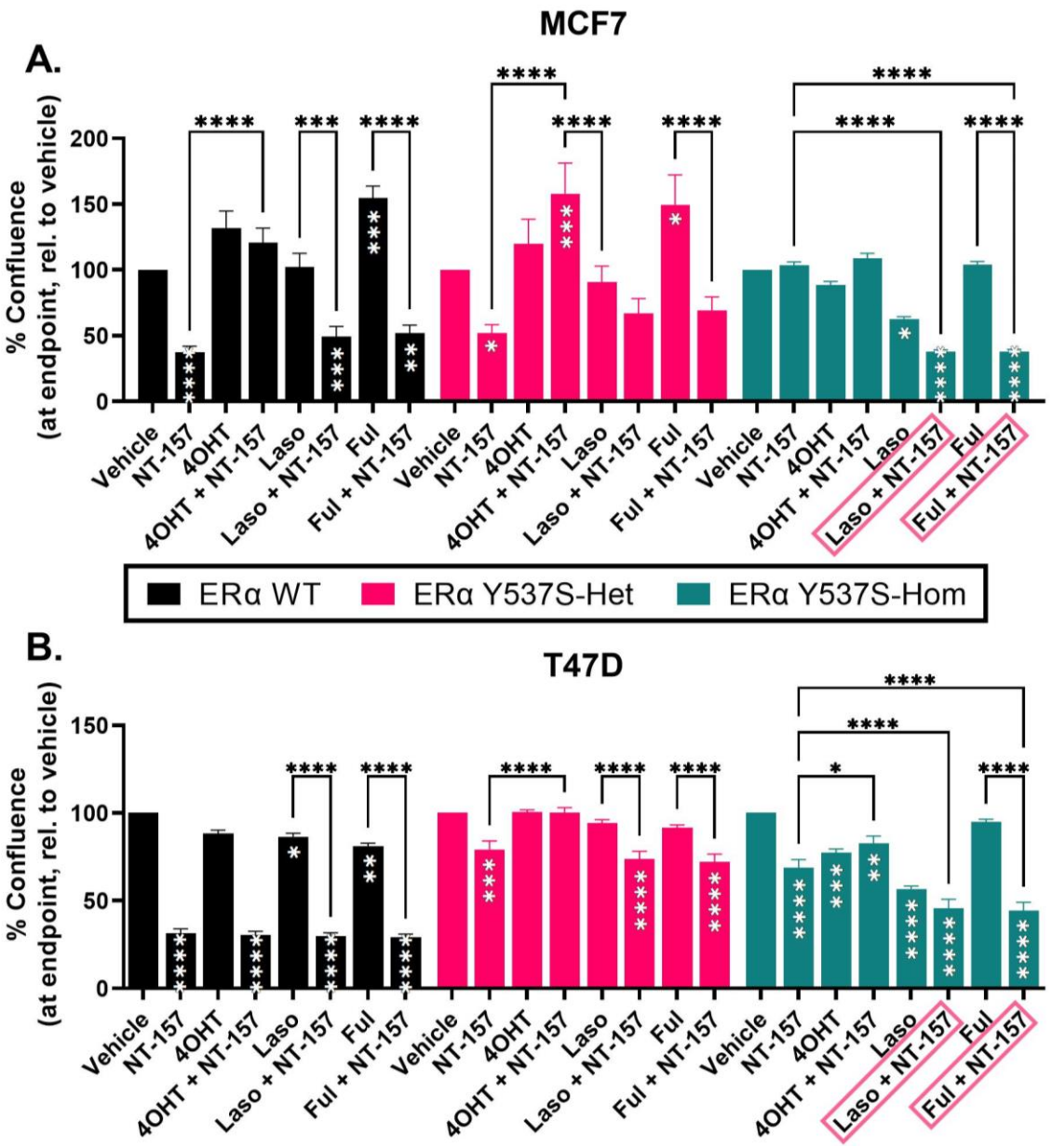

Figure 4.15: The IRS1 inhibitor NT-157, alone or in combination with ET, effectively inhibits cell proliferation in MCF7 and T47D ERα Y537S cells. Proliferation of A) MCF7 and B) T47D ERα WT (black), ERα Y537S-het (pink), and ERα Y537S-hom (teal) cells treated with Vehicle, 4OHT, laso, or ful, alone or in combination with NT-157. Graphs show % confluence after 5 days of treatment, normalized to vehicle. White asterisks indicate a significant change in proliferation compared to vehicle treatment; black asterisks indicate a significant change in proliferation compared to each respective single drug treatment (NT-157, 4OHT, laso, or ful alone). Significance is indicated as * $p < 0.05$, ** $p < 0.005$, *** $p < 0.0005$, or **** $p < 0.0001$.

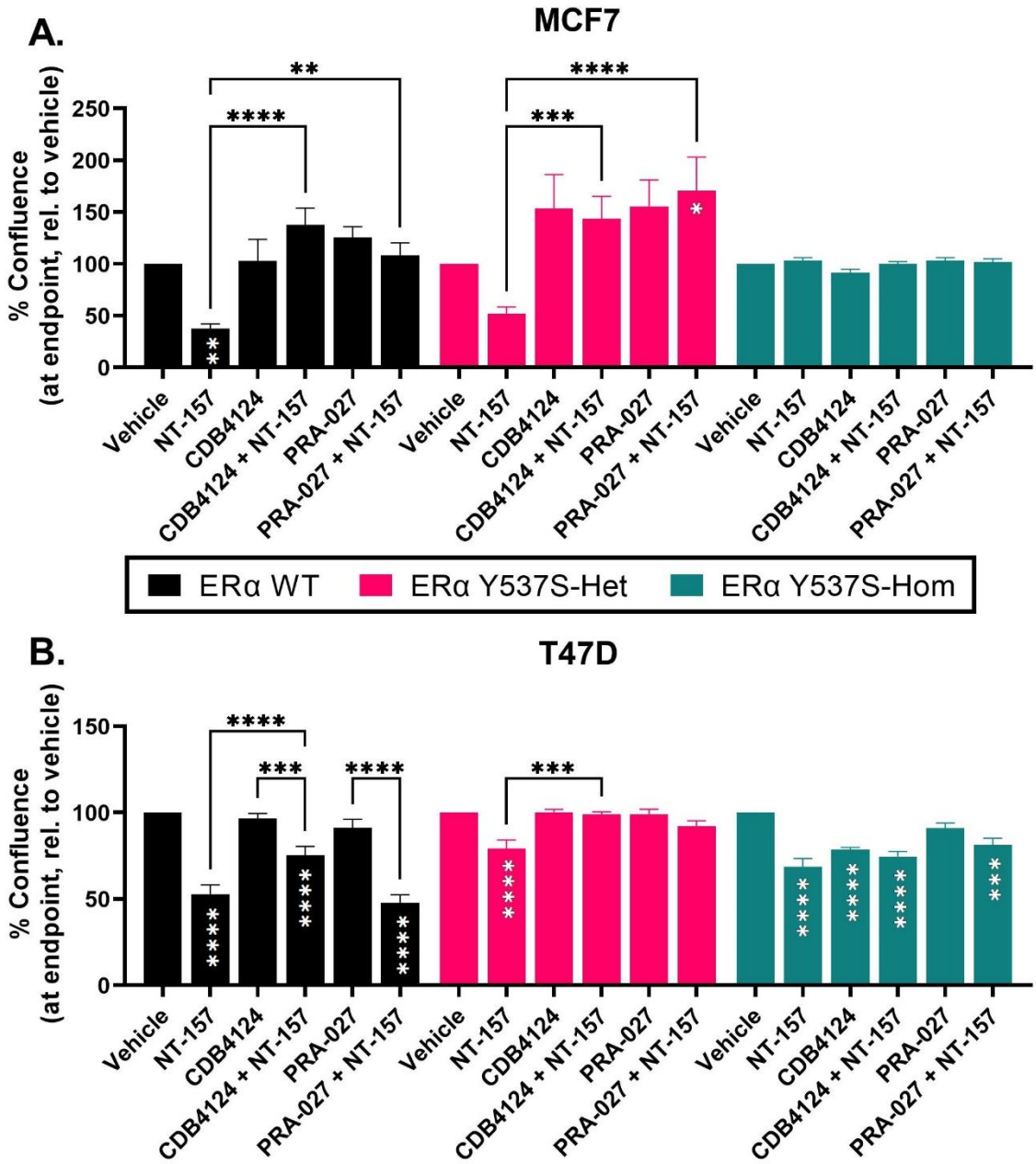

Figure 4.16: SPRM compounds have a limited effect on cell proliferation in MCF7 and T47D ERα Y537S cells. Proliferation of A) MCF7 and B) T47D ERα WT (black), ERα Y537S-het (pink), and ERα Y537S-hom (teal) cells treated with Vehicle, CDB4124, or PRA-027, alone or in combination with NT-157. Graphs show % confluence after 5 days of treatment, normalized to vehicle. White asterisks indicate a significant change in proliferation compared to vehicle treatment; black asterisks indicate a significant change in proliferation compared to each respective single drug treatment (NT-157, CDB4124, or PRA-027 alone). Significance is indicated as * $p < 0.05$, ** $p < 0.005$, *** $p < 0.0005$, or **** $p < 0.0001$.

Discussion

Prior research on the constitutively activating ERα Y537S mutation has understandably focused on ERα function, vastly advancing our knowledge of the mutation's contribution to ET resistance [123, 162, 163, 174, 188, 189]. However, the effect of ERα Y537S on the complex relationship known as ERα/PR crosstalk has previously not been thoroughly investigated. In this study, I aimed to determine the effects of the ERα Y537S mutation on ERα/PR crosstalk and resulting transcriptional activity and to elucidate how this unique interaction contributes to ET resistance in ERα-positive breast cancer.

A comparison of transcriptomes between MCF7 and T47D cell variants supports previous studies highlighting the two cell lines' vastly different expression profiles [190-192]. However, both MCF7 and T47D cells expressing homozygous ERα Y537S differentially expressed hundreds of genes when each was compared to ERα WT. Notably, far fewer genes are differentially expressed when comparing ERα Y537S-het cell variants to ERα WT cell variants (Fig. 4.6b,c). This highlights the importance of including heterozygous and homozygous models when studying a mutation such as ERα Y537S, which is clinically observed as mosaic expression within a patient's cancer.

Given the imperfect cell line model systems described above, I then compared these findings to publicly available patient data and identified four gene expression changes aligned with potential ERα-PR shared regulatory binding sites [152, 154, 155]. Of these, IRS1 proved most notable due to 1) increased mRNA expression in MCF7 ERα Y537S-hom cells (Fig. 4.8c), 2) increased protein expression in T47D ERα Y537S-hom cells (Fig. 4.12d-f), and 3) increased effect of IRS1 knockdown resulting in decreased proliferation of MCF7 and T47D cells expressing either heterozygous or homozygous ERα Y537S, compared to ERα WT (Fig. 4.9). This information

alone would not confirm that ERα Y537S impacts ERα/PR crosstalk, as these effects on IRS1 expression and dependence could be driven solely by the constitutive activity of ERα resulting from the Y537S mutation. However, ERα and PR chromatin occupancy at IRS1 shared ERα/PR binding sites (IRS1-3) increased significantly in the context of ERα Y537S-hom, highlighting that the ERα Y537S mutation not only alters the transcription factor activity of ERα but also that of PR (Fig. 4.10a,b, Fig. 4.11a,b). Interestingly, both ERα Y537S and PR chromatin occupancy is present at sites with only PRE half sites and no ERE, indicating the presence of ERα-PR regulatory complexes in which ERα Y537S may act as a co-regulator for PR [137, 144, 145].

To further confirm the role of IRS1 in maintaining cell proliferation in the context of ERα Y537S, I assessed the small molecule IRS1 inhibitor, NT-157 in MCF7 and T47D ERα cell variant drug screens. To further confirm the role of IRS1 in maintaining cell proliferation in the context of ERα Y537S, we assessed the small molecule IRS1 inhibitor NT-157 in MCF7 and T47D ERα cell variant drug screens. NT-157 effectively reduced cell proliferation in MCF7 and T47D cells expressing ERα WT or ERα Y537S (Fig. 4.15). Co-targeting ERα via SERM or SERD treatment and IRS1 via NT-157 had an additive antiproliferative effect on cells expressing homozygous ERα Y537S, indicating a potential treatment avenue for restoring ET sensitivity to resistant breast cancers expressing ERα Y537S. Combination SERM/SERD and NT-157 treatments did not have a similar additive effect on proliferation of ERα WT or ERα Y537S-het cells. The explanation for the difference in compound sensitivity between heterozygous and homozygous ERα Y537S cells is three-fold:

1. The ERα Y537S-het and -hom cell lines were derived separately (Chapter II, *Cell Lines and Growth Conditions*).

2. Heterozygous and homozygous ERα Y537S phenotypes are characteristically unique (Fig. 3.7, Fig. 4.1, Fig. 4.2, Fig. 4.4, Fig. 4.5).
3. Single NT-157 treatment has a consequentially anti-proliferative effect on ERα Y537S-het cells, which seemingly cannot be improved upon.

Overall, these findings highlight a treatment sensitivity that is particularly strong in the context of the ERα Y537S mutation, which supports our proposed mechanism by which IRS1 upregulation drives cell proliferation in the context of the ERα Y537S mutation in response to increased ERα/PR crosstalk. Importantly, the antiproliferative effect of IRS1 inhibition by NT-157 is further enhanced by combined treatment with the novel SERM lasofoxifene or the SERD fulvestrant, highlighting that ET sensitivity is restored by co-targeting this pathway in resistant ERα Y537S cells (Fig. 4.15a,b, teal).

CHAPTER V

DISCUSSION, FUTURE DIRECTIONS, AND CONCLUSIONS

Discussion

Despite advances in diagnosis and treatment, breast cancer remains the most frequently occurring cancer among females in the United States and results in over half a million deaths per year worldwide [1-4]. Though endocrine therapy (ET) has improved post-surgical outcomes and relapse-free survival in patients with ERα-positive breast cancer, 15-20% of tumors are intrinsically ET-resistant and 30-40% acquire resistance over time [62, 104, 105]. One of the most frequent drivers of acquired ET resistance is *ESR1* point mutations, of which the Y537S LBD mutation is detected most often [116-122]. ERα Y537S results in constitutive activity of ERα and reduced affinity for antagonists, contributing to resistant and aggressive metastatic disease [119, 123]. Previous research has focused on the effects of the Y537S mutation on ERα function, but ERα does not function in a vacuum. Here, I investigated the complex relationship between ERα and PR known as ERα/PR crosstalk to elucidate how ERα Y537S affects the overlapping transcriptional activities of these two hormone receptors. As described in chapter I, ERα/PR crosstalk can be categorized into four mechanisms, which are also depicted in figure 5.1:

1) Liganded ERα regulating *PGR* gene transcription [137-141]
2) Liganded PR increasing ERα target gene regulation through ERα phosphorylation [137]
3) PR-dependent chromatin remodeling to facilitate ERα binding [142, 143]
4) ERα/PR physical interaction via regulatory complexes contributing to ligand-independent target gene expression [137, 144, 145]

Given the impact of ERα Y537S on ERα function and response to endocrine therapy, I hypothesized that ERα Y537S alters ERα/PR crosstalk through 1) increased physical interaction

of the two receptors and 2) increased ERα/PR coregulation of pro-proliferative gene expression contributing to endocrine therapy resistance.

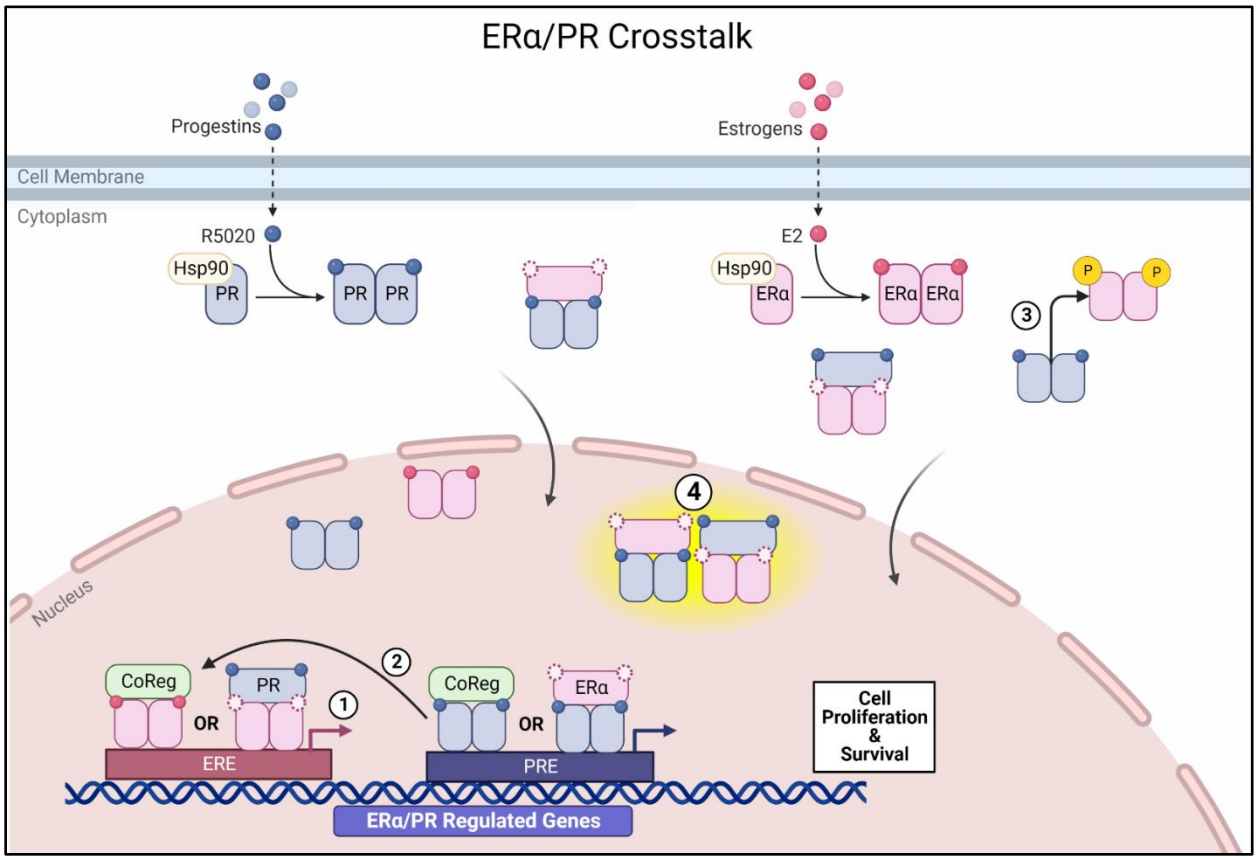

Figure 5.1: Diagram representing mechanisms through which ERα/PR crosstalk can occur. Both ERα and PR are classically activated by steroid hormone binding (progestins [R5020] for PR, estrogens [E2] for ERα), leading to receptor dimerization. Upon activation and dimerization, ERα and PR enter the nucleus, binding to their respective response elements (PREs for PR, EREs for ERα) to regulate target gene expression. In addition to their independent transcription factor activities, 1) ERα regulates the expression of PR by binding to an ERE within the PGR gene. 2) PR-dependent chromatin remodeling facilitates ERα binding at EREs. 3) Activated PR also regulates ERα phosphorylation, leading to ligand-independent ERα activity. The least understood mechanism (and predominant focus of my work) by which ERα/PR crosstalk occurs is through 4) ERα/PR physical interaction via regulatory complexes that control target gene expression. As indicated by the presence of R5020 but a potential absence of E2, my findings suggest that ERα/PR crosstalk via regulatory complex interactions is largely independent of ERα ligand binding but requires liganded PR. Created with BioRender.com

Through NanoBRET, PLA, and CoIP assays, I identified an increased physical interaction between ERα and PR in the context of the ERα Y537S mutation in MCF7 and T47D cell lines (Fig. 3.4c, Fig. 3.7, Fig. 3.8). Physical interaction of PR with either ERα WT or ERα Y537S was

significantly enhanced by PR stimulation with R5020, suggesting that active PR is a key driver of ERα/PR crosstalk through ERα/PR physical interaction. Interestingly, ERα Y537S/PR physical interaction seems to occur whether or not E2 is present, which supports the ligand-independent activity of ERα Y537S. PLA images and CoIP analyses of cytoplasmic and nuclear extracts clarified an important distinction about these observed ERα/PR physical interactions – increased ERα Y537S/PR interactions are not limited to the cytoplasm, but also occur in the nucleus (Fig. 3.7, Fig. 3.8). Taken alone, nuclear ERα Y537S/PR interaction does not conclusively indicate pro-tumorigenic gene regulatory functions associated with altered ERα/PR crosstalk in the context of the ERα Y537S mutation. However, ChIP-reChIP qPCR identified increased ERα/PR co-occupancy in the context of ERα Y537S at chromatin binding sites within genes consequential to breast cancer progression (Fig. 3.9). While ERα/PR cistromal changes associated with the ERα Y537S mutation varied somewhat between MCF7 and T47D cell lines, the overall pattern indicates a reprogramming of ERα/PR crosstalk through receptor physical interaction and genomic co-occupancy in the context of the ERα Y537S mutation.

Overall, these findings highlighted the effects of ERα Y537S on mechanism 4 of ERα/PR crosstalk – ERα Y537S increases ERα/PR physical interaction via regulatory complexes (Fig. 5.1, mechanism 4). The next objective was to determine if and how these ERα Y537S/PR regulatory complexes contribute to endocrine therapy resistance via regulation of gene expression. Through RNA-seq analysis comparing MCF7 and T47D cell lines expressing ERα Y537S with patient tumors expressing ERα Y537S, I identified four gene expression changes (relative to corresponding ERα WT samples) that were shared across cell line models and patient tumor transcriptomes. Of note, these four differentially expressed genes each contained potential ERα-PR shared regulatory binding sites, as characterized by Khushi et al. (2014). Included in this small

subset of differentially expressed genes was *IRS1*, which was one of the genes at which ERα/PR co-occupancy was found to be increased in the context of ERα Y537S (Fig. 3.9). IRS1 is a component of the insulin receptor tyrosine kinase signaling pathway and contributes to ET resistance in ERα-positive breast cancers [167].

Further investigation of ERα and PR chromatin binding through single ChIP supported the previous findings from ChIP-reChIP of increased ERα/PR co-occupancy at a shared ERα/PR regulatory region of IRS1 (Fig. 4.10a,b, Fig. 4.11a,b). These results highlight the fact that the ERα Y537S mutation alters the transcription factor activity of both ERα and PR. Furthermore, ERα Y537S and PR chromatin occupancy is present at sites with only PRE half sites and no ERE, indicating the presence of ERα-PR regulatory complexes in which ERα Y537S may act as a co-regulator for PR [137, 144, 145]. Here, I propose a mechanism by which ERα Y537S results in constitutive activity of ERα, even in the presence of SERMs, leading to increased ERα-PR regulatory complexes driving increased IRS1 expression and ET-resistant cell proliferation (Fig. 5.2).

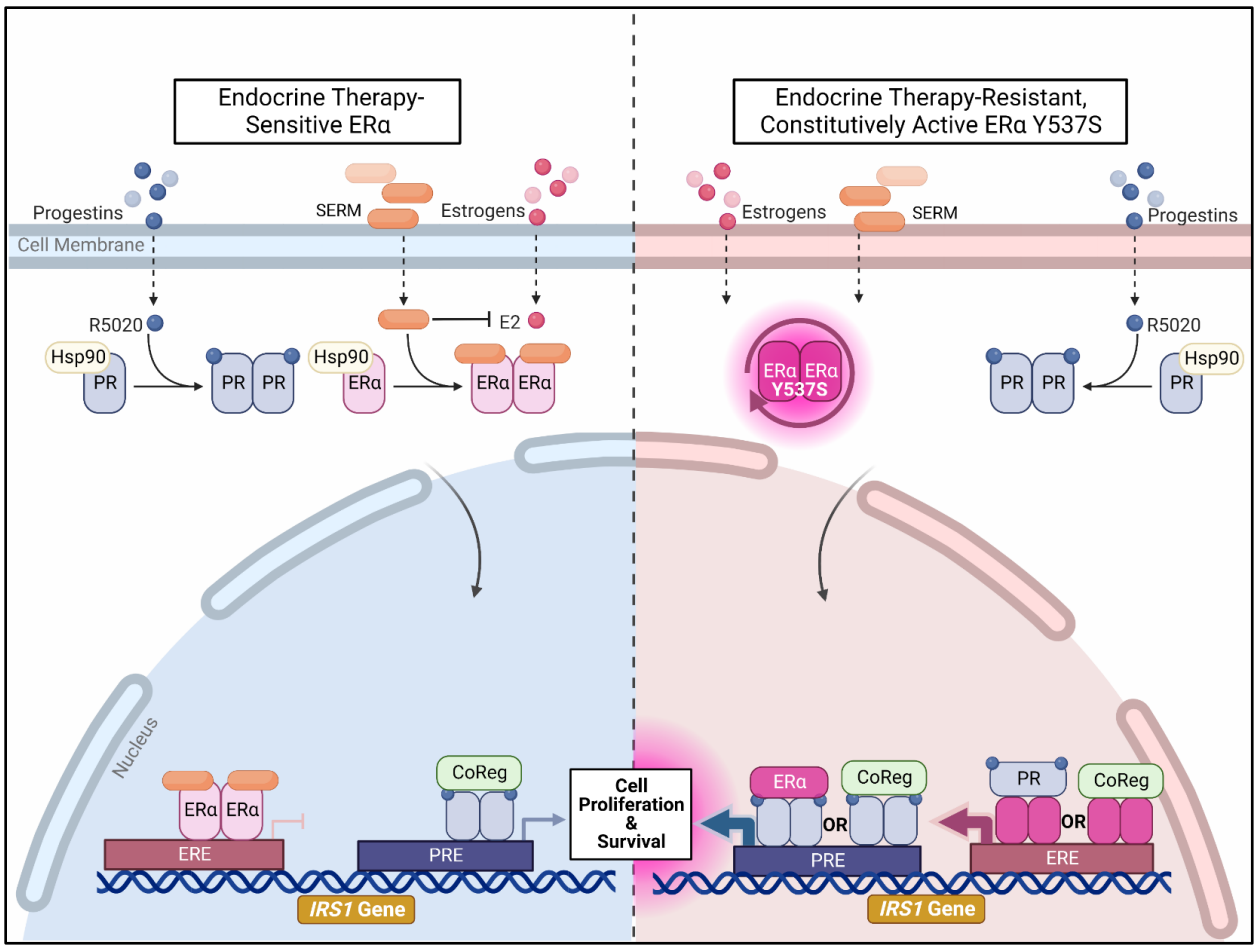

Figure 5.2: Proposed mechanism for IRS1-dependent cell proliferation in the context of the ERα Y537S mutation. *Left panel*: In ET-sensitive (ERα WT) cells, selective estrogen receptor modulators (SERMs) competitively bind to ERα, blocking estradiol. SERM-bound ERα is still able to dimerize and bind to chromatin sites, but the antagonistic functions of SERMs prevent recruitment of co-activators required to drive transcription of target genes, including *IRS1*. Some transcription of *IRS1* occurs through PR-dependent transcription. *Right panel*: In ET-resistant (ERα Y537S) cells, ERα is constitutively active and has reduced affinity for SERM binding. *IRS1* transcription is high due to activity at both EREs and PREs, both by independent ERα and PR transcription factor activity as well as by the two receptors physically interacting as coregulators. This overdrive of *IRS1* expression contributes to a reliance on the expression of this signaling pathway component for continued cell proliferation and survival in ET-resistant cells. Created with BioRender.com

Supporting the role of IRS1 as a driver of proliferation in the context of elevated ERα Y537S/PR crosstalk is the striking effect of knockdown or inhibition of IRS1 in the context of ERα Y537S (Fig. 4.9, 4.15). Interestingly, sensitivity to IRS1 depletion by siRNA knockdown was largely specific to the context of the ERα Y537S mutation (Fig. 4.9) while IRS1 inhibition by NT-

157 effectively reduced proliferation in ERα WT, ERα Y537S-het, and ERα Y537S-hom cells (Fig. 4.15). This may be due to the fact that NT-157 degrades both IRS1 and IRS2, which likely leads to a more potent inhibition of the pro-proliferative IGF-1R/IRS1/2, PI3K, and AXL-mediated signaling pathways [172, 177, 178]. Overall, these findings highlight a treatment sensitivity that is particularly strong in the context of the ERα Y537S mutation, which supports our proposed mechanism by which IRS1 upregulation drives cell proliferation in the context of the ERα Y537S mutation in response to increased ERα/PR crosstalk (Fig. 5.2). Importantly, the antiproliferative effect of IRS1 inhibition by NT-157 is further enhanced by combined treatment with the novel SERM lasofoxifene or the SERD fulvestrant, highlighting that ET sensitivity is restored by co-targeting this pathway in resistant ERα Y537S cells (Fig. 4.15a,b, teal).

Future Directions

Considering the antiproliferative effect of the IRS1 inhibitor NT-157 on two-dimensional (2D) cell lines expressing ERα Y537S, the next objective is to assess this compound in three-dimensional (3D) patient-derived organoid models (PDxOs) and paired xenograft mice (PDXs). Our lab has developed PDxOs from dozens of patient tumors, with additional established PDxOs obtained from the Welm laboratory at the Huntsman Cancer Institute [193]. PDxOs provide a method of cell culture that is more representative of the diversity and complexity of tumor heterogeneity and morphology than 2D cell culture while allowing for more time-efficient experimentation than PDX models. Using ET-resistant patient-derived tumors, including those with ERα Y537S mutations, one may assess various combinations of NT-157 with SERMs, and SERDs in PDxO 3D culture drug screens to identify particular combinations that show promise in both 2D and 3D model systems. Such treatments can be further assessed for efficacy and toxicity in the *in vivo* setting of PDX mice, monitoring tumor growth in response to promising NT-157

drug combinations.

An additional future direction of interest is the role of other genes, besides *IRS1*, that are differentially regulated in the context of the ERα Y537S mutation based on my findings, such as *DEGS2* (Delta-4-Desaturase, Sphingolipid 2). ERα and PR co-occupancy at shared regulatory sites was significantly altered within *DEGS2* (Fig. 3.9), and *DEGS2* mRNA was expressed ~8-fold higher in MCF7 ERα Y537S-hom cells and nearly 16-fold in patient tumors expressing ERα Y537S relative to their respective ERα WT counterparts (Fig. 4.8c, *fold change* = 2^y). Though the effect of *DEGS2* knockdown on the proliferation of MCF7 and T47D cells expressing ERα Y537S was not as consistent or significant as knockdown of *IRS1* (Fig. 4.9), the regulatory and expression changes of *DEGS2* in the context of ERα Y537S warrant further investigation. Interestingly, recent research identified that upregulated DEGS2 expression correlates with increased proliferation, migration, and invasion in both TNBC and colorectal cancer, likely due to dysregulated ceramide synthesis [194, 195]. A recent study by the Frasor laboratory at the University of Illinois at Chicago (with collaborative contributions from myself in the Greene laboratory) has shown that NVP-231, a ceramide kinase inhibitor, restores sensitivity to ET-resistant cells [196]. Further investigation may characterize a mechanistic link between altered DEGS2 expression in the context of the ET-resistant ERα Y537S mutation and sensitivity to ceramide kinase inhibition.

In addition to its effects on ERα/PR crosstalk, it is possible that the ERα Y537S mutation also alters the relationship of ERα with other hormone receptors such as the androgen receptor (AR) and glucocorticoid receptor (GR). AR, known most for its role in the development of prostate cancer, is also co-expressed in 60-80% of ERα-positive breast cancers and is generally an indicator of good prognosis [197-200]. Previous research suggests that AR may regulate chromatin binding of ERα, and that treatment with the antiandrogen enzalutamide inhibits both AR and ERα

chromatin binding [201, 202]. In ERα/GR crosstalk, the two hormone receptors engage in reciprocal chromatin remodeling to facilitate the binding of one another to chromatin binding sites [203-206]. In both instances of hormone receptor crosstalk, AR and GR inhibit ERα Y537S chromatin binding, suggesting further potential therapeutic avenues through which treatment resistance associated with the ERα Y537S mutation may be targeted [197, 207, 208]. Thus, ERα/AR and ERα/GR crosstalk in the context of the ERα Y537S mutation should be further investigated in depth.

Conclusions

Though it was previously known that ERα Y537S alters the activity and transcriptome of ERα, the effect of the mutation on PR-associated transcription was heretofore unknown. I hypothesized that ERα Y537S alters ERα/PR crosstalk through increased ERα/PR physical interaction and increased ERα/PR coregulation of pro-proliferative gene expression contributing to endocrine therapy resistance. I characterized the physical interaction of ERα and PR and identified increased formation of regulatory complexes containing ERα and PR in the context of ERα Y537S. I identified differential expression of ERα-PR shared regulatory genes in the context of the ERα Y537S mutation, corresponding with altered occupancy of both ERα and PR at chromatin binding sites. Of particular consequence is increased chromatin occupancy of ERα and PR at regulatory binding sites for *IRS1*, leading to increased expression of this pro-proliferative signaling pathway component in the context of the ET resistance-associated ERα Y537S mutation. Furthermore, knockdown or inhibition of IRS1 decreases proliferation in the context of ERα Y537S, indicating a potential therapeutic avenue through which treatment sensitivity may be restored in ET-resistant breast cancers. In summary, ERα/PR crosstalk is altered in the context of ERα Y537S through increased physical interaction of the two receptors in transcription regulatory

complexes, contributing to the expression of a pro-proliferative transcriptome that contributes to endocrine therapy resistance in breast cancer.

REFERENCES

1. Siegel, R.L., et al., *Cancer statistics, 2022.* CA Cancer J Clin, 2022. **72**(1): p. 7-33.

2. Arnold, M., et al., *Current and future burden of breast cancer: Global statistics for 2020 and 2040.* Breast, 2022. **66**: p. 15-23.

3. Ben-Dror, J., M. Shalamov, and A. Sonnenblick, *The History of Early Breast Cancer Treatment.* Genes (Basel), 2022. **13**(6).

4. Sung, H., et al., *Global Cancer Statistics 2020: GLOBOCAN Estimates of Incidence and Mortality Worldwide for 36 Cancers in 185 Countries.* CA Cancer J Clin, 2021. **71**(3): p. 209-249.

5. Hong, R. and B. Xu, *Breast cancer: an up-to-date review and future perspectives.* Cancer Commun (Lond), 2022. **42**(10): p. 913-936.

6. McPherson, K., C.M. Steel, and J.M. Dixon, *ABC of breast diseases. Breast cancer-epidemiology, risk factors, and genetics.* BMJ, 2000. **321**(7261): p. 624-8.

7. McPherson, K. and R. Mant, *Dose and duration of hormone use: understanding the effects of combined menopausal hormones on breast cancer better, 1976-2004.* J Epidemiol Community Health, 2005. **59**(12): p. 1078-9.

8. McTiernan, A., *Behavioral risk factors in breast cancer: can risk be modified?* Oncologist, 2003. **8**(4): p. 326-34.

9. Gonzalo-Encabo, P., et al., *Dose-response effects of aerobic exercise on adiposity markers in postmenopausal women: pooled analyses from two randomized controlled trials.* Int J Obes (Lond), 2021. **45**(6): p. 1298-1309.

10. Anderson, G.L. and M.L. Neuhouser, *Obesity and the risk for premenopausal and postmenopausal breast cancer.* Cancer Prev Res (Phila), 2012. **5**(4): p. 515-21.

11. Neuhouser, M.L., et al., *Overweight, Obesity, and Postmenopausal Invasive Breast Cancer Risk: A Secondary Analysis of the Women's Health Initiative Randomized Clinical Trials.* JAMA Oncol, 2015. **1**(5): p. 611-21.

12. Lichtenstein, P., et al., *Environmental and heritable factors in the causation of cancer--analyses of cohorts of twins from Sweden, Denmark, and Finland.* N Engl J Med, 2000. **343**(2): p. 78-85.

13. Smith, S.A., et al., *Allele losses in the region 17q12-21 in familial breast and ovarian cancer involve the wild-type chromosome.* Nat Genet, 1992. **2**(2): p. 128-31.

14. *Hereditary Cancer Syndromes and Risk Assessment: ACOG COMMITTEE OPINION, Number 793.* Obstet Gynecol, 2019. **134**(6): p. e143-e149.

15. Sinn, H.P. and H. Kreipe, *A Brief Overview of the WHO Classification of Breast Tumors, 4th Edition, Focusing on Issues and Updates from the 3rd Edition.* Breast Care (Basel), 2013. **8**(2): p. 149-54.

16. Zubair, M., S. Wang, and N. Ali, *Advanced Approaches to Breast Cancer Classification and Diagnosis.* Front Pharmacol, 2020. **11**: p. 632079.

17. Makki, J., *Diversity of Breast Carcinoma: Histological Subtypes and Clinical Relevance.* Clin Med Insights Pathol, 2015. **8**: p. 23-31.

18. Barroso-Sousa, R. and O. Metzger-Filho, *Differences between invasive lobular and invasive ductal carcinoma of the breast: results and therapeutic implications.* Ther Adv Med Oncol, 2016. **8**(4): p. 261-6.

19. Rakha, E.A. and I.O. Ellis, *Lobular breast carcinoma and its variants.* Semin Diagn Pathol, 2010. **27**(1): p. 49-61.

20. Li, C.I., et al., *Trends in incidence rates of invasive lobular and ductal breast carcinoma.* JAMA, 2003. **289**(11): p. 1421-4.

21. Tan, P.H., et al., *The 2019 World Health Organization classification of tumours of the breast.* Histopathology, 2020. **77(**2): p. 181-185.

22. Amin, M.B., et al., *The Eighth Edition AJCC Cancer Staging Manual: Continuing to build a bridge from a population-based to a more "personalized" approach to cancer staging.* CA Cancer J Clin, 2017. **67**(2): p. 93-99.

23. Bloom, H.J. and W.W. Richardson, *Histological grading and prognosis in breast cancer; a study of 1409 cases of which 359 have been followed for 15 years.* Br J Cancer, 1957. **11**(3): p. 359-77.

24. Elston, C.W. and I.O. Ellis, *Pathological prognostic factors in breast cancer. I. The value of histological grade in breast cancer: experience from a large study with long-term follow-up.* Histopathology, 1991. **19**(5): p. 403-10.

25. Rakha, E.A., et al., *Breast cancer prognostic classification in the molecular era: the role of histological grade.* Breast Cancer Res, 2010. **12**(4): p. 207.

26. Rakha, E.A. and F.G. Pareja, *New Advances in Molecular Breast Cancer Pathology.* Semin Cancer Biol, 2021. **72**: p. 102-113.

27. Dai, X., et al., *Breast cancer intrinsic subtype classification, clinical use and future trends.* Am J Cancer Res, 2015. **5**(10): p. 2929-43.

28. Anderson, W.F., et al., *Estrogen receptor breast cancer phenotypes in the Surveillance, Epidemiology, and End Results database.* Breast Cancer Res Treat, 2002. **76(**1): p. 27-36.

29. Vuong, D., et al., *Molecular classification of breast cancer.* Virchows Arch, 2014. **465**(1): p. 1-14.

30. Rakha, E.A., J.S. Reis-Filho, and I.O. Ellis, *Combinatorial biomarker expression in breast cancer.* Breast Cancer Res Treat, 2010. **120**(2): p. 293-308.

31. Slamon, D.J., et al., *Human breast cancer: correlation of relapse and survival with amplification of the HER-2/neu oncogene.* Science, 1987. **235**(4785): p. 177-82.

32. Cameron, D., et al., *11 years' follow-up of trastuzumab after adjuvant chemotherapy in HER2-positive early breast cancer: final analysis of the HERceptin Adjuvant (HERA) trial.* Lancet, 2017. **389**(10075): p. 1195-1205.

33. Filipits, M., et al., *Association of p27 and Cyclin D1 Expression and Benefit from Adjuvant Trastuzumab Treatment in HER2-Positive Early Breast Cancer: A TransHERA Study.* Clin Cancer Res, 2018. **24**(13): p. 3079-3086.

34. Piccart-Gebhart, M.J., et al., *Trastuzumab after adjuvant chemotherapy in HER2-positive breast cancer.* N Engl J Med, 2005. **353**(16): p. 1659-72.

35. Bardou, V.J., et al., *Progesterone receptor status significantly improves outcome prediction over estrogen receptor status alone for adjuvant endocrine therapy in two large breast cancer databases.* J Clin Oncol, 2003. **21**(10): p. 1973-9.

36. Fisher, B., et al., *Twenty-five-year follow-up of a randomized trial comparing radical mastectomy, total mastectomy, and total mastectomy followed by irradiation.* N Engl J Med, 2002. **347**(8): p. 567-75.

37. Veronesi, U., et al., *Intraoperative radiotherapy versus external radiotherapy for early breast cancer (ELIOT): a randomised controlled equivalence trial.* Lancet Oncol, 2013. **14**(13): p. 1269-77.

38. Clarke, M., et al., *Effects of radiotherapy and of differences in the extent of surgery for early breast cancer on local recurrence and 15-year survival: an overview of the randomised trials.* Lancet, 2005. **366**(9503): p. 2087-106.

39. Lagendijk, M., et al., *Breast conserving therapy and mastectomy revisited: Breast cancer-specific survival and the influence of prognostic factors in 129,692 patients.* Int J Cancer, 2018. **142**(1): p. 165-175.

40. Litière, S., et al., *Breast conserving therapy versus mastectomy for stage I-II breast cancer: 20 year follow-up of the EORTC 10801 phase 3 randomised trial.* Lancet Oncol, 2012. **13**(4): p. 412-9.

41. Bonadonna, G., et al., *Combination chemotherapy as an adjuvant treatment in operable breast cancer.* N Engl J Med, 1976. **294**(8): p. 405-10.

42. Bonadonna, G., et al., *Combination chemotherapy and combined treatment modality in disseminated and locally advanced breast cancer.* Prog Clin Biol Res, 1977. **12**: p. 437-58.

43. Rossi, A., P. Valagussa, and G. Bonadonna, *Surgery and adjuvant chemotherapy in the treatment of operable breast cancer.* Prog Clin Biol Res, 1977. **12**: p. 391-404.

44. (EBCTCG), E.B.C.T.C.G., *Effects of chemotherapy and hormonal therapy for early breast cancer on recurrence and 15-year survival: an overview of the randomised trials.* Lancet, 2005. **365**(9472): p. 1687-717.

45. Peto, R., et al., *Comparisons between different polychemotherapy regimens for early breast cancer: meta-analyses of long-term outcome among 100,000 women in 123 randomised trials.* Lancet, 2012. **379**(9814): p. 432-44.

46. Fisher, B., et al., *Effect of preoperative chemotherapy on local-regional disease in women with operable breast cancer: findings from National Surgical Adjuvant Breast and Bowel Project B-18.* J Clin Oncol, 1997. **15**(7): p. 2483-93.

47. van der Hage, J.A., et al., *Preoperative chemotherapy in primary operable breast cancer: results from the European Organization for Research and Treatment of Cancer trial 10902.* J Clin Oncol, 2001. **19**(22): p. 4224-37.

48. Jacquillat, C., et al., *Results of neoadjuvant chemotherapy and radiation therapy in the breast-conserving treatment of 250 patients with all stages of infiltrative breast cancer.* Cancer, 1990. **66**(1): p. 119-29.

49. Hurley, J., et al., *The use of neoadjuvant platinum-based chemotherapy in locally advanced breast cancer that is triple negative: retrospective analysis of 144 patients.* Breast Cancer Res Treat, 2013. **138**(3): p. 783-94.

50. von Minckwitz, G., et al., *Neoadjuvant carboplatin in patients with triple-negative and HER2-positive early breast cancer (GeparSixto; GBG 66): a randomised phase 2 trial.* Lancet Oncol, 2014. **15**(7): p. 747-56.

51. Huggins, C. and D.M. Bergenstal, *Inhibition of human mammary and prostatic cancers by adrenalectomy.* Cancer Res, 1952. **12**(2): p. 134-41.

52. Greene, G.L., F.W. Fitch, and E.V. Jensen, *Monoclonal antibodies to estrophilin: probes for the study of estrogen receptors.* Proc Natl Acad Sci U S A, 1980. **77**(1): p. 157-61.

53. Jensen, E.V., et al., *Estrogen receptors and breast cancer response to adrenalectomy.* Natl Cancer Inst Monogr, 1971. **34**: p. 55-70.

54. Huggins, C. and E.V. Jensen, *The depression of estrone-induced uterine growth by phenolic estrogens with oxygenated functions at positions 6 or 16: the impeded estrogens.* J Exp Med, 1955. **102**(3): p. 335-46.

55. Jensen, E.V., *On the mechanism of estrogen action.* Perspect Biol Med, 1962. **6**: p. 47-59.

56. Jensen, E.V., *Mechanism of estrogen action in relation to carcinogenesis.* Proc Can Cancer Conf, 1966. **6**: p. 143-65.

57. Jensen, E.V., et al., *Estrogen-receptor interactions in target tissues.* Arch Anat Microsc Morphol Exp, 1967. **56**(3): p. 547-69.

58. Jensen, E.V. and E.R. DeSombre, *Effects of ovarian hormones at the subcellular level.* Curr Top Exp Endocrinol, 1971. **1**: p. 229-69.

59. Jensen, E.V., *Estrogen receptors in hormone-dependent breast cancers.* Cancer Res, 1975. **35**(11 Pt. 2): p. 3362-4.

60. Davies, C., et al., *Long-term effects of continuing adjuvant tamoxifen to 10 years versus stopping at 5 years after diagnosis of oestrogen receptor-positive breast cancer: ATLAS, a randomised trial.* Lancet, 2013. **381**(9869): p. 805-16.

61. Fisher, B., et al., *Treatment of lymph-node-negative, oestrogen-receptor-positive breast cancer: long-term findings from National Surgical Adjuvant Breast and Bowel Project randomised clinical trials.* Lancet, 2004. **364**(9437): p. 858-68.

62. Lumachi, F., et al., *Treatment of estrogen receptor-positive breast cancer.* Curr Med Chem, 2013. **20**(5): p. 596-604.

63. Ward, H.W., *Anti-oestrogen therapy for breast cancer: a trial of tamoxifen at two dose levels.* Br Med J, 1973. **1**(5844): p. 13-4.

64. Ward, R.L., et al., *Tamoxifen reduces bone turnover and prevents lumbar spine and proximal femoral bone loss in early postmenopausal women.* Bone Miner, 1993. **22**(2): p. 87-94.

65. Mocellin, S., et al., *Breast Cancer Chemoprevention: A Network Meta-Analysis of Randomized Controlled Trials.* J Natl Cancer Inst, 2016. **108**(2).

66. Fisher, B., et al., *A randomized clinical trial evaluating tamoxifen in the treatment of patients with node-negative breast cancer who have estrogen-receptor-positive tumors.* N Engl J Med, 1989. **320**(8): p. 479-84.

67. Fisher, B., et al., *Five versus more than five years of tamoxifen therapy for breast cancer patients with negative lymph nodes and estrogen receptor-positive tumors.* J Natl Cancer Inst, 1996. **88**(21): p. 1529-42.

68. Davies, C., et al., *Relevance of breast cancer hormone receptors and other factors to the efficacy of adjuvant tamoxifen: patient-level meta-analysis of randomised trials.* Lancet, 2011. **378**(9793): p. 771-84.

69. Cuzick, J., et al., *Tamoxifen for prevention of breast cancer: extended long-term follow-up of the IBIS-I breast cancer prevention trial.* Lancet Oncol, 2015. **16**(1): p. 67-75.

70. Powles, T.J., et al., *Twenty-year follow-up of the Royal Marsden randomized, double-blinded tamoxifen breast cancer prevention trial.* J Natl Cancer Inst, 2007. **99**(4): p. 283-90.

71. Veronesi, U., et al., *Tamoxifen for the prevention of breast cancer: late results of the Italian Randomized Tamoxifen Prevention Trial among women with hysterectomy.* J Natl Cancer Inst, 2007. **99**(9): p. 727-37.

72. Sella, T., et al., *Neoadjuvant Endocrine Therapy in Clinical Practice: A Review.* JAMA Oncol, 2021. **7**(11): p. 1700-1708.

73. Smith, I.E., et al., *Neoadjuvant treatment of postmenopausal breast cancer with anastrozole, tamoxifen, or both in combination: the Immediate Preoperative Anastrozole, Tamoxifen, or Combined with Tamoxifen (IMPACT) multicenter double-blind randomized trial.* J Clin Oncol, 2005. **23**(22): p. 5108-16.

74. Fisher, B., et al., *Tamoxifen for the prevention of breast cancer: current status of the National Surgical Adjuvant Breast and Bowel Project P-1 study.* J Natl Cancer Inst, 2005. **97**(22): p. 1652-62.

75. Iqbal, J., et al., *Endometrial cancer and venous thromboembolism in women under age 50 who take tamoxifen for prevention of breast cancer: a systematic review.* Cancer Treat Rev, 2012. **38**(4): p. 318-28.

76. Heldring, N., et al., *Identification of tamoxifen-induced coregulator interaction surfaces within the ligand-binding domain of estrogen receptors.* Mol Cell Biol, 2004. **24**(8): p. 3445-59.

77. Heldring, N., et al., *Estrogen receptors: how do they signal and what are their targets.* Physiol Rev, 2007. **87**(3): p. 905-31.

78. Katzenellenbogen, J.A., B.W. O'Malley, and B.S. Katzenellenbogen, *Tripartite steroid hormone receptor pharmacology: interaction with multiple effector sites as a basis for the cell- and promoter-specific action of these hormones.* Mol Endocrinol, 1996. **10**(2): p. 119-31.

79. Shang, Y. and M. Brown, *Molecular determinants for the tissue specificity of SERMs.* Science, 2002. **295**(5564): p. 2465-8.

80. Lainé, M., et al., *Lasofoxifene as a potential treatment for therapy-resistant ER-positive metastatic breast cancer.* Breast Cancer Res, 2021. **23**(1): p. 54.

81. Howell, A., et al., *Results of the ATAC (Arimidex, Tamoxifen, Alone or in Combination) trial after completion of 5 years' adjuvant treatment for breast cancer.* Lancet, 2005. **365**(9453): p. 60-2.

82. Thürlimann, B., et al., *A comparison of letrozole and tamoxifen in postmenopausal women with early breast cancer.* N Engl J Med, 2005. **353**(26): p. 2747-57.

83. Smith, I., et al., *Comparative Efficacy and Safety of Adjuvant Letrozole Versus Anastrozole in Postmenopausal Patients With Hormone Receptor-Positive, Node-Positive Early Breast Cancer: Final Results of the Randomized Phase III Femara Versus Anastrozole Clinical Evaluation (FACE) Trial.* J Clin Oncol, 2017. **35**(10): p. 1041-1048.

84. (EBCTCG), E.B.C.T.C.G., *Aromatase inhibitors versus tamoxifen in early breast cancer: patient-level meta-analysis of the randomised trials.* Lancet, 2015. **386**(10001): p. 1341-1352.

85. Fan, M., R.M. Bigsby, and K.P. Nephew, *The NEDD8 pathway is required for proteasome-mediated degradation of human estrogen receptor (ER)-alpha and essential for the antiproliferative activity of ICI 182,780 in ERalpha-positive breast cancer cells.* Mol Endocrinol, 2003. **17**(3): p. 356-65.

86. Marsaud, V., et al., *Various phosphorylation pathways, depending on agonist and antagonist binding to endogenous estrogen receptor alpha (ERalpha), differentially affect ERalpha extractability, proteasome-mediated stability, and transcriptional activity in human breast cancer cells.* Mol Endocrinol, 2003. **17**(10): p. 2013-27.

87. Osborne, C.K., A. Wakeling, and R.I. Nicholson, *Fulvestrant: an oestrogen receptor antagonist with a novel mechanism of action.* Br J Cancer, 2004. **90 Suppl 1**(Suppl 1): p. S2-6.

88. Di Leo, A., et al., *Results of the CONFIRM phase III trial comparing fulvestrant 250 mg with fulvestrant 500 mg in postmenopausal women with estrogen receptor-positive advanced breast cancer.* J Clin Oncol, 2010. **28**(30): p. 4594-600.

89. Di Leo, A., et al., *Final overall survival: fulvestrant 500 mg vs 250 mg in the randomized CONFIRM trial.* J Natl Cancer Inst, 2014. **106**(1): p. djt337.

90. Boér, K., *Fulvestrant in advanced breast cancer: evidence to date and place in therapy.* Ther Adv Med Oncol, 2017. **9**(7): p. 465-479.

91. Ellis, M.J., et al., *Fulvestrant 500 mg Versus Anastrozole 1 mg for the First-Line Treatment of Advanced Breast Cancer: Overall Survival Analysis From the Phase II FIRST Study.* J Clin Oncol, 2015. **33**(32): p. 3781-7.

92. Robertson, J.F., et al., *Fulvestrant 500 mg versus anastrozole 1 mg for the first-line treatment of advanced breast cancer: follow-up analysis from the randomized 'FIRST' study.* Breast Cancer Res Treat, 2012. **136**(2): p. 503-11.

93. Robertson, J.F.R., et al., *Fulvestrant 500 mg versus anastrozole 1 mg for hormone receptor-positive advanced breast cancer (FALCON): an international, randomised, double-blind, phase 3 trial.* Lancet, 2016. **388**(10063): p. 2997-3005.

94. Davaadelger, B., et al., *Mechanism of Telapristone Acetate (CDB4124) on Progesterone Receptor Action in Breast Cancer Cells.* Endocrinology, 2018. **159**(10): p. 3581-3595.

95. Lee, O., et al., *Selective Progesterone Receptor Modulators in Early-Stage Breast Cancer: A Randomized, Placebo-Controlled Phase II Window-of-Opportunity Trial Using Telapristone Acetate.* Clin Cancer Res, 2020. **26**(1): p. 25-34.

96. Attardi, B.J., et al., *CDB-4124 and its putative monodemethylated metabolite, CDB-4453, are potent antiprogestins with reduced antiglucocorticoid activity: in vitro comparison to mifepristone and CDB-2914.* Mol Cell Endocrinol, 2002. **188**(1-2): p. 111-23.

97. Berrodin, T.J., et al., *Novel progesterone receptor modulators with gene selective and context-dependent partial agonism.* Biochem Pharmacol, 2009. **77**(2): p. 204-15.

98. Research, W., *WAY-257027: Progesterone receptor antagonist (PRA) program*. 2009, Meeting with Oncorion and Essex Woodlands in Malvern, PA.

99. Cottu, P.H., et al., *Phase I study of onapristone, a type I antiprogestin, in female patients with previously treated recurrent or metastatic progesterone receptor-expressing cancers.* PLoS One, 2018. **13**(10): p. e0204973.

100. Lewis, J.H., et al., *Onapristone Extended Release: Safety Evaluation from Phase I-II Studies with an Emphasis on Hepatotoxicity.* Drug Saf, 2020. **43**(10): p. 1045-1055.

101. Robertson, J.F., et al., *Onapristone, a progesterone receptor antagonist, as first-line therapy in primary breast cancer.* Eur J Cancer, 1999. **35**(2): p. 214-8.

102. Hagan, C.R., et al., *Role of phosphorylation in progesterone receptor signaling and specificity.* Mol Cell Endocrinol, 2012. **357**(1-2): p. 43-9.

103. Wiehle, R., et al., *CDB-4124, a progesterone receptor modulator, inhibits mammary carcinogenesis by suppressing cell proliferation and inducing apoptosis.* Cancer Prev Res (Phila), 2011. **4**(3): p. 414-24.

104. Anurag, M., M.J. Ellis, and S. Haricharan, *DNA damage repair defects as a new class of endocrine treatment resistance driver.* Oncotarget, 2018. **9**(91): p. 36252-36253.

105. Lei, J.T., et al., *Endocrine therapy resistance: new insights.* Breast, 2019. **48 Suppl 1**(Suppl 1): p. S26-S30.

106. Bray, F., et al., *Global cancer statistics 2018: GLOBOCAN estimates of incidence and mortality worldwide for 36 cancers in 185 countries.* CA Cancer J Clin, 2018. **68**(6): p. 394-424.

107. Giaquinto, A.N., et al., *Breast Cancer Statistics, 2022.* CA Cancer J Clin, 2022.

108. Anurag, M., et al., *Comprehensive Profiling of DNA Repair Defects in Breast Cancer Identifies a Novel Class of Endocrine Therapy Resistance Drivers.* Clin Cancer Res, 2018. **24**(19): p. 4887-4899.

109. Miller, C.A., et al., *Aromatase inhibition remodels the clonal architecture of estrogen-receptor-positive breast cancers.* Nat Commun, 2016. **7**: p. 12498.

110. Haricharan, S., et al., *Somatic mutation load of estrogen receptor-positive breast tumors predicts overall survival: an analysis of genome sequence data.* Breast Cancer Res Treat, 2014. **146**(1): p. 211-20.

111. Haricharan, S., et al., *Loss of MutL Disrupts CHK2-Dependent Cell-Cycle Control through CDK4/6 to Promote Intrinsic Endocrine Therapy Resistance in Primary Breast Cancer.* Cancer Discov, 2017. **7**(10): p. 1168-1183.

112. Ma, C.X., et al., *A Phase II Trial of Neoadjuvant MK-2206, an AKT Inhibitor, with Anastrozole in Clinical Stage II or III.* Clin Cancer Res, 2017. **23**(22): p. 6823-6832.

113. Ma, C.X., et al., *NeoPalAna: Neoadjuvant Palbociclib, a Cyclin-Dependent Kinase 4/6 Inhibitor, and Anastrozole for Clinical Stage 2 or 3 Estrogen Receptor-Positive Breast Cancer.* Clin Cancer Res, 2017. **23**(15): p. 4055-4065.

114. Hartmaier, R.J., et al., *Recurrent hyperactive ESR1 fusion proteins in endocrine therapy-resistant breast cancer.* Ann Oncol, 2018. **29**(4): p. 872-880.

115. Lei, J.T., et al., *Functional Annotation of ESR1 Gene Fusions in Estrogen Receptor-Positive Breast Cancer.* Cell Rep, 2018. **24**(6): p. 1434-1444.e7.

116. Li, S., et al., *Endocrine-therapy-resistant ESR1 variants revealed by genomic characterization of breast-cancer-derived xenografts.* Cell Rep, 2013. **4**(6): p. 1116-30.

117. Pejerrey, S.M., et al., *The Impact of ESR1 Mutations on the Treatment of Metastatic Breast Cancer.* Horm Cancer, 2018. **9**(4): p. 215-228.

118. Jeselsohn, R., et al., *Emergence of constitutively active estrogen receptor-α mutations in pretreated advanced estrogen receptor-positive breast cancer.* Clin Cancer Res, 2014. **20**(7): p. 1757-1767.

119. Jeselsohn, R., et al., *Allele-Specific Chromatin Recruitment and Therapeutic Vulnerabilities of ESR1 Activating Mutations.* Cancer Cell, 2018. **33**(2): p. 173-186.e5.

120. Toy, W., et al., *ESR1 ligand-binding domain mutations in hormone-resistant breast cancer.* Nat Genet, 2013. **45**(12): p. 1439-45.

121. Robinson, D.R., et al., *Activating ESR1 mutations in hormone-resistant metastatic breast cancer.* Nat Genet, 2013. **45**(12): p. 1446-51.

122. Angus, L., et al., *ESR1 mutations: Moving towards guiding treatment decision-making in metastatic breast cancer patients.* Cancer Treat Rev, 2017. **52**: p. 33-40.

123. Fanning, S.W., et al., *Estrogen receptor alpha somatic mutations Y537S and D538G confer breast cancer endocrine resistance by stabilizing the activating function-2 binding conformation.* Elife, 2016. **5**.

124. Greene, G.L., et al., *Sequence and expression of human estrogen receptor complementary DNA.* Science, 1986. **231**(4742): p. 1150-4.

125. Greene, G.L. and M.F. Press, *Structure and dynamics of the estrogen receptor.* J Steroid Biochem, 1986. **24**(1): p. 1-7.

126. Green, S., et al., *Human oestrogen receptor cDNA: sequence, expression and homology to v-erb-A.* Nature, 1986. **320**(6058): p. 134-9.

127. Kuiper, G.G., et al., *Cloning of a novel receptor expressed in rat prostate and ovary.* Proc Natl Acad Sci U S A, 1996. **93**(12): p. 5925-30.

128. Paterni, I., et al., *Estrogen receptors alpha (ERα) and beta (ERβ): subtype-selective ligands and clinical potential.* Steroids, 2014. **90**: p. 13-29.

129. Fuentes, N. and P. Silveyra, *Estrogen receptor signaling mechanisms.* Adv Protein Chem Struct Biol, 2019. **116**: p. 135-170.

130. Chang, E.C., et al., *Impact of estrogen receptor beta on gene networks regulated by estrogen receptor alpha in breast cancer cells.* Endocrinology, 2006. **147**(10): p. 4831-42.

131. AlFakeeh, A. and C. Brezden-Masley, *Overcoming endocrine resistance in hormone receptor-positive breast cancer.* Curr Oncol, 2018. **25**(Suppl 1): p. S18-S27.

132. Jeltsch, J.M., et al., *Cloning of the chicken progesterone receptor.* Proc Natl Acad Sci U S A, 1986. **83**(15): p. 5424-8.

133. Conneely, O.M., et al., *Molecular cloning of the chicken progesterone receptor.* Science, 1986. **233**(4765): p. 767-70.

134. Loosfelt, H., et al., *Cloning and sequence analysis of rabbit progesterone-receptor complementary DNA.* Proc Natl Acad Sci U S A, 1986. **83**(23): p. 9045-9.

135. Scarpin, K.M., et al., *Progesterone action in human tissues: regulation by progesterone receptor (PR) isoform expression, nuclear positioning and coregulator expression.* Nucl Recept Signal, 2009. **7**: p. e009.

136. Azeez, J.M., et al., *New insights into the functions of progesterone receptor (PR) isoforms and progesterone signaling.* Am J Cancer Res, 2021. **11**(11): p. 5214-5232.

137. Diep, C.H., H. Ahrendt, and C.A. Lange, *Progesterone induces progesterone receptor gene (PGR) expression via rapid activation of protein kinase pathways required for cooperative estrogen receptor alpha (ER) and progesterone receptor (PR) genomic action at ER/PR target genes.* Steroids, 2016. **114**: p. 48-58.

138. Petz, L.N., et al., *Estrogen receptor alpha and activating protein-1 mediate estrogen responsiveness of the progesterone receptor gene in MCF-7 breast cancer cells.* Endocrinology, 2002. **143**(12): p. 4583-91.

139. Petz, L.N., et al., *Differential regulation of the human progesterone receptor gene through an estrogen response element half site and Sp1 sites.* J Steroid Biochem Mol Biol, 2004. **88**(2): p. 113-22.

140. Kastner, P., et al., *Two distinct estrogen-regulated promoters generate transcripts encoding the two functionally different human progesterone receptor forms A and B.* EMBO J, 1990. **9**(5): p. 1603-14.

141. Graham, J.D., et al., *Preferential stimulation of human progesterone receptor B expression by estrogen in T-47D human breast cancer cells.* J Biol Chem, 1995. **270**(51): p. 30693-700.

142. Singhal, H., et al., *Progesterone receptor isoforms, agonists and antagonists differentially reprogram estrogen signaling.* Oncotarget, 2018. **9**(4): p. 4282-4300.

143. Mohammed, H., et al., *Progesterone receptor modulates ERα action in breast cancer.* Nature, 2015. **523**(7560): p. 313-7.

144. Knutson, T.P., et al., *Posttranslationally modified progesterone receptors direct ligand-specific expression of breast cancer stem cell-associated gene programs.* J Hematol Oncol, 2017. **10**(1): p. 89.

145. Daniel, A.R., et al., *Progesterone receptor-B enhances estrogen responsiveness of breast cancer cells via scaffolding PELP1- and estrogen receptor-containing transcription complexes.* Oncogene, 2015. **34**(4): p. 506-15.

146. Singhal, H., et al., *Genomic agonism and phenotypic antagonism between estrogen and progesterone receptors in breast cancer.* Sci Adv, 2016. **2**(6): p. e1501924.

147. Giulianelli, S., et al., *Estrogen receptor alpha mediates progestin-induced mammary tumor growth by interacting with progesterone receptors at the cyclin D1/MYC promoters.* Cancer Res, 2012. **72**(9): p. 2416-27.

148. Sflomos, G., et al., *A Preclinical Model for ERα-Positive Breast Cancer Points to the Epithelial Microenvironment as Determinant of Luminal Phenotype and Hormone Response.* Cancer Cell, 2016. **29**(3): p. 407-422.

149. Greene, G.L., et al., *Purification of T47D human progesterone receptor and immunochemical characterization with monoclonal antibodies.* Mol Endocrinol, 1988. **2**(8): p. 714-26.

150. Machleidt, T., et al., *NanoBRET--A Novel BRET Platform for the Analysis of Protein-Protein Interactions.* ACS Chem Biol, 2015. **10**(8): p. 1797-804.

151. Furlan-Magaril, M., H. Rincon-Arano, and F. Recillas-Targa, *Sequential Chromatin Immunoprecipitation Protocol: ChIP-reChIP*, in *DNA-Protein Interactions*, T. Moss and B. Leblanc, Editors. 2009, Springer Protocols.

152. Khushi, M., C.L. Clarke, and J.D. Graham, *Bioinformatic analysis of cis-regulatory interactions between progesterone and estrogen receptors in breast cancer.* PeerJ, 2014. **2**: p. e654.

153. Afgan, E., et al., *The Galaxy platform for accessible, reproducible and collaborative biomedical analyses: 2018 update.* Nucleic Acids Res, 2018. **46**(W1): p. W537-W544.

154. Leiserson, M.D., et al., *MAGI: visualization and collaborative annotation of genomic aberrations.* Nat Methods, 2015. **12**(6): p. 483-4.

155. Pleasance, E., et al., *Pan-cancer analysis of advanced patient tumors reveals interactions between therapy and genomic landscapes.* Nat Cancer, 2020. **1**(4): p. 452-468.

156. Selli, C., J.M. Dixon, and A.H. Sims, *Accurate prediction of response to endocrine therapy in breast cancer patients: current and future biomarkers.* Breast Cancer Res, 2016. **18**(1): p. 118.

157. Jiménez-Panizo, A., et al., *Non-canonical dimerization of the androgen receptor and other nuclear receptors: implications for human disease.* Endocr Relat Cancer, 2019. **26**(8): p. R479-R497.

158. Fuentes-Prior, P., et al., *Diversity of Quaternary Structures Regulates Nuclear Receptor Activities.* Trends Biochem Sci, 2019. **44**(1): p. 2-6.

159. Liu, W., et al., *Steroid receptor heterodimerization demonstrated in vitro and in vivo.* Proc Natl Acad Sci U S A, 1995. **92**(26): p. 12480-4.

160. Chandra, V., et al., *Structure of the intact PPAR-gamma-RXR- nuclear receptor complex on DNA.* Nature, 2008. **456**(7220): p. 350-6.

161. Barrett Mueller, K., et al., *Estrogen receptor inhibits mineralocorticoid receptor transcriptional regulatory function.* Endocrinology, 2014. **155**(11): p. 4461-72.

162. Chandarlapaty, S., et al., *Prevalence of ESR1 Mutations in Cell-Free DNA and Outcomes in Metastatic Breast Cancer: A Secondary Analysis of the BOLERO-2 Clinical Trial.* JAMA Oncol, 2016. **2**(10): p. 1310-1315.

163. Bahreini, A., et al., *Mutation site and context dependent effects of ESR1 mutation in genome-edited breast cancer cell models.* Breast Cancer Res, 2017. **19**(1): p. 60.

164. De Bosscher, K., et al., *Nuclear receptor crosstalk - defining the mechanisms for therapeutic innovation.* Nat Rev Endocrinol, 2020. **16**(7): p. 363-377.

165. Elian, F.A., E. Yan, and M.A. Walter, *FOXC1, the new player in the cancer sandbox.* Oncotarget, 2018. **9**(8): p. 8165-8178.

166. Zheng, X.J., et al., *EZH2 regulates expression of FOXC1 by mediating H3K27me3 in breast cancers.* Acta Pharmacol Sin, 2021. **42**(7): p. 1171-1179.

167. Dwyer, A.R., et al., *Insulin receptor substrate-1 (IRS-1) mediates progesterone receptor-driven stemness and endocrine resistance in oestrogen receptor+ breast cancer.* Br J Cancer, 2021. **124**(1): p. 217-227.

168. Zhang, Y., et al., *Estrogen induces dynamic ERα and RING1B recruitment to control gene and enhancer activities in luminal breast cancer.* Sci Adv, 2020. **6**(23): p. eaaz7249.

169. Osborne, C.K., et al., *Crosstalk between estrogen receptor and growth factor receptor pathways as a cause for endocrine therapy resistance in breast cancer.* Clin Cancer Res, 2005. **11**(2 Pt 2): p. 865s-70s.

170. Schiff, R., et al., *Breast cancer endocrine resistance: how growth factor signaling and estrogen receptor coregulators modulate response.* Clin Cancer Res, 2003. **9**(1 Pt 2): p. 447S-54S.

171. Lee, A.V., et al., *Enhancement of insulin-like growth factor signaling in human breast cancer: estrogen regulation of insulin receptor substrate-1 expression in vitro and in vivo.* Mol Endocrinol, 1999. **13**(5): p. 787-96.

172. Lero, M.W. and L.M. Shaw, *Diversity of insulin and IGF signaling in breast cancer: Implications for therapy.* Mol Cell Endocrinol, 2021. **527**: p. 111213.

173. Eckert, R.L., et al., *Estrogen receptor synthesis and turnover in MCF-7 breast cancer cells measured by a density shift technique.* Endocrinology, 1984. **114**(2): p. 629-37.

174. Zhao, Y., et al., *Structurally Novel Antiestrogens Elicit Differential Responses from Constitutively Active Mutant Estrogen Receptors in Breast Cancer Cells and Tumors.* Cancer Res, 2017. **77**(20): p. 5602-5613.

175. Horwitz, K.B., M.B. Mockus, and B.A. Lessey, *Variant T47D human breast cancer cells with high progesterone-receptor levels despite estrogen and antiestrogen resistance.* Cell, 1982. **28**(3): p. 633-42.

176. Gual, P., Y. Le Marchand-Brustel, and J.F. Tanti, *Positive and negative regulation of insulin signaling through IRS-1 phosphorylation.* Biochimie, 2005. **87**(1): p. 99-109.

177. Su, S.P., et al., *Impact of the Anticancer Drug NT157 on Tyrosine Kinase Signaling Networks.* Mol Cancer Ther, 2018. **17**(5): p. 931-942.

178. de Miranda, L.B.L., et al., *NT157 exerts antineoplastic activity by targeting JNK and AXL signaling in lung cancer cells.* Sci Rep, 2022. **12**(1): p. 17092.

179. Chattopadhyay, C., et al., *Targeting IRS-1/2 in Uveal Melanoma Inhibits In Vitro Cell Growth, Survival and Migration, and In Vivo Tumor Growth.* Cancers (Basel), 2022. **14**(24).

180. Fenerich, B.A., et al., *NT157 has antineoplastic effects and inhibits IRS1/2 and STAT3/5 in JAK2.* Signal Transduct Target Ther, 2020. **5**(1): p. 5.

181. Scopim-Ribeiro, R., et al., *NT157, an IGF1R-IRS1/2 inhibitor, exhibits antineoplastic effects in pre-clinical models of chronic myeloid leukemia.* Invest New Drugs, 2021. **39**(3): p. 736-746.

182. Garofalo, C., et al., *Preclinical Effectiveness of Selective Inhibitor of IRS-1/2 NT157 in Osteosarcoma Cell Lines.* Front Endocrinol (Lausanne), 2015. **6**: p. 74.

183. Ibuki, N., et al., *The tyrphostin NT157 suppresses insulin receptor substrates and augments therapeutic response of prostate cancer.* Mol Cancer Ther, 2014. **13**(12): p. 2827-39.

184. Yang, Y., et al., *Insulin Receptor Substrate Suppression by the Tyrphostin NT157 Inhibits Responses to Insulin-Like Growth Factor-I and Insulin in Breast Cancer Cells.* Horm Cancer, 2018. **9**(6): p. 371-382.

185. Naing, A., et al., *Phase I trial of cixutumumab combined with temsirolimus in patients with advanced cancer.* Clin Cancer Res, 2011. **17**(18): p. 6052-60.

186. Naing, A., et al., *Insulin growth factor-receptor (IGF-1R) antibody cixutumumab combined with the mTOR inhibitor temsirolimus in patients with refractory Ewing's sarcoma family tumors.* Clin Cancer Res, 2012. **18**(9): p. 2625-31.

187. Naing, A., et al., *Insulin growth factor receptor (IGF-1R) antibody cixutumumab combined with the mTOR inhibitor temsirolimus in patients with metastatic adrenocortical carcinoma.* Br J Cancer, 2013. **108**(4): p. 826-30.

188. Harrod, A., et al., *Genomic modelling of the ESR1 Y537S mutation for evaluating function and new therapeutic approaches for metastatic breast cancer.* Oncogene, 2017. **36**(16): p. 2286-2296.

189. Zhong, L. and D.F. Skafar, *Mutations of tyrosine 537 in the human estrogen receptor-alpha selectively alter the receptor's affinity for estradiol and the kinetics of the interaction.* Biochemistry, 2002. **41**(13): p. 4209-17.

190. Aka, J.A. and S.X. Lin, *Comparison of functional proteomic analyses of human breast cancer cell lines T47D and MCF7.* PLoS One, 2012. **7**(2): p. e31532.

191. Radde, B.N., et al., *Bioenergetic differences between MCF-7 and T47D breast cancer cells and their regulation by oestradiol and tamoxifen.* Biochem J, 2015. **465**(1): p. 49-61.

192. Yu, S., et al., *The T47D cell line is an ideal experimental model to elucidate the progesterone-specific effects of a luminal A subtype of breast cancer.* Biochem Biophys Res Commun, 2017. **486**(3): p. 752-758.

193. DeRose, Y.S., et al., *Patient-derived models of human breast cancer: protocols for in vitro and in vivo applications in tumor biology and translational medicine.* Curr Protoc Pharmacol, 2013. **Chapter 14**: p. Unit14.23.

194. Guo, W., et al., *M6A methylation of DEGS2, a key ceramide-synthesizing enzyme, is involved in colorectal cancer progression through ceramide synthesis.* Oncogene, 2021. **40**(40): p. 5913-5924.

195. Rajput, K., et al., *Ceramide Kinase (CERK) Emerges as a Common Therapeutic Target for Triple Positive and Triple Negative Breast Cancer Cells.* Cancers (Basel), 2022. **14**(18).

196. Pal, P., et al., *Endocrine Therapy-Resistant Breast Cancer Cells Are More Sensitive to Ceramide Kinase Inhibition and Elevated Ceramide Levels Than Therapy-Sensitive Breast Cancer Cells.* Cancers (Basel), 2022. **14**(10).

197. Hickey, T.E., et al., *The androgen receptor is a tumor suppressor in estrogen receptor-positive breast cancer.* Nat Med, 2021. **27**(2): p. 310-320.

198. Giovannelli, P., et al., *The Androgen Receptor in Breast Cancer*. Front Endocrinol (Lausanne), 2018. **9**: p. 492.

199. Iacopetta, D., Y. Rechoum, and S.A. Fuqua, *The Role of Androgen Receptor in Breast Cancer.* Drug Discov Today Dis Mech, 2012. **9**(1-2): p. e19-e27.

200. Rechoum, Y., et al., *AR collaborates with ERα in aromatase inhibitor-resistant breast cancer.* Breast Cancer Res Treat, 2014. **147**(3): p. 473-85.

201. Paakinaho, V. and J.J. Palvimo, *Genome-wide crosstalk between steroid receptors in breast and prostate cancers.* Endocr Relat Cancer, 2021. **28**(9): p. R231-R250.

202. D'Amato, N.C., et al., *Cooperative Dynamics of AR and ER Activity in Breast Cancer.* Mol Cancer Res, 2016. **14**(11): p. 1054-1067.

203. Miranda, T.B., et al., *Reprogramming the chromatin landscape: interplay of the estrogen and glucocorticoid receptors at the genomic level.* Cancer Res, 2013. **73**(16): p. 5130-9.

204. Paakinaho, V., et al., *Single-molecule analysis of steroid receptor and cofactor action in living cells.* Nat Commun, 2017. **8**: p. 15896.

205. Swinstead, E.E., V. Paakinaho, and G.L. Hager, *Chromatin reprogramming in breast cancer.* Endocr Relat Cancer, 2018. **25**(7): p. R385-R404.

206. Voss, T.C., et al., *Dynamic exchange at regulatory elements during chromatin remodeling underlies assisted loading mechanism.* Cell, 2011. **146**(4): p. 544-54.

207. Ponnusamy, S., et al., *Androgen Receptor Is a Non-canonical Inhibitor of Wild-Type and Mutant Estrogen Receptors in Hormone Receptor-Positive Breast Cancers.* iScience, 2019. **21**: p. 341-358.

208. Tonsing-Carter, E., et al., *Glucocorticoid receptor modulation decreases ER-positive breast cancer cell proliferation and suppresses wild-type and mutant ER chromatin association.* Breast Cancer Res, 2019. **21**(1): p. 82.